Comprehensive Multidimensional Separations of Biological Samples using Capillary Electrophoresis coupled with Micro Free Flow Electrophoresis

A Dissertation
SUBMITTED TO THE FACULTY OF
UNIVERSITY OF MINNESOTA
BY

Alexander C. Johnson

IN PARTIAL FULFILLMENT OF THE REQUIREMENTS
FOR THE DEGREE OF
DOCTOR OF PHILOSOPHY

Michael T. Bowser, Advisor

December 2017

Acknowledgements

My tale in chemistry starts at Shanley High School in Fargo, ND. As a Junior, my chemistry teacher, Barry Pemberton, noticed my love for the subject. He offered me a job working for his Ph.D. advisor at North Dakota State University. The summer before I entered college, I worked under the tutelage of Jayaraman Sivaguru (Siva), and Barry in the Siva group. I started undergrad at Concordia College in Moorhead, MN in the fall of 2008 pursuing a pre-pharmacy degree. I struggled academically my first year, and without the extra tutoring sessions from Barry and Siva, I would not have succeeded. From that point on, I changed my degree to ACS Chemistry, and was on the Dean's list every semester until I graduated. I owe Siva and Barry everything in my academic life, and they shaped me into the scientist I am today. For that, I am eternally grateful. Of course everyone in the Siva group helped me in one way or another, but I want to extend a special thank you to Elango, Ramya, Nandini, and Anoklase. Thank you for teaching me how to be scientifically curious, and instilling a love of learning that I carry with me today.

I would also like to thank my undergraduate advisor, Mark Jensen, who changed the way I look at analytical chemistry with his advanced instrumental methods course. Thank you also to Darin Ulness and Chopper Krogstad, your doors were always open to me even if I wasn't taking a class with you. Without all of your encouragement and help at Concordia, I would have never dreamed of pursuing a Ph.D. in chemistry.

I want to extend a special thank you to my Ph.D. advisor, Mike Bowser. I made a great decision in my graduate school career by joining your research group. Your guidance and insight shaped my work ethic and skills that will be with me the rest of my life. The road was not always smooth, but I would not change a thing. To the Bowser

Group, Dr. Nic Frost, Thane Taylor, Dr. Megan Weisenberger, Dr. Amy Stading, Dr. Matt Geiger, Dr. Rachel Harstad, Dr. Sarah Anciaux, Dr. Kailey Soller, Sean Dembowski, Matt LeMon, and Nic Brinza, thank you for the always entertaining conversations and keeping me sane through my graduate school career.

I would also like to thank Professor Pete Carr. I learned the most I have ever learned in your separations class. I would not have my understanding and curiosity of separation science and 2D separations without you. Your advice on my career and life after my Ph.D. has been, and will continue to be invaluable.

Thank you to the Minnesota Nano Center for use of the cleanroom facilities, especially Terry Brough, and Paul Kimani for their valuable insight on fabricating µFFE devices. Also, thank you to the Mechanical Engineering machine shop staff, for all their services throughout the years. Thank you to Prof. Edgar Arriaga, for the gracious use of his laboratory space, and Heather Brown for her help with preparing the BSA digest samples.

For my friends at the University of Minnesota, especially Megan, Kailey, and Victoria, this journey has been rough at times, but your friendship, conversation, and humor brought joy to this Ph.D. I cannot comprehend this journey without all of you, and I cannot wait to see where our lives lead next.

To my parents and brother, a simple thank you would not suffice. I love you all. Mom and Dad, you have always supported me. When I aimed for the sky, you encouraged me to aim for the starts. When I questioned my choices in life, you were always there to back me up. I would not be half the man I am today without you. I know you will be great grandparents, and my child will be lucky to have you. To my brother, Aaron, you have always been my role model. You recognized when your life was not going down a path you wanted, and made decisions to correct them. You are never

afraid to tackle tough tasks. You have an incredible work ethic. The hard work I put into my academic career and this Ph.D. were inspired by you. Maybe one day I will be able to best you in basketball, but for now, I've got you in chemistry.

Last, but certainly not least, the love of my life, Crystal. I would not be able to function without you. I cannot put into words how much you complete me. I am so excited to see the next chapter of our lives. I am thrilled to meet our soon-to-be-born child. Our future is bright, and our love conquers all. You kept me sane throughout my Ph.D. You were the reason I kept going, the reason I followed my dreams. I love you.

Dedicated to my wife, Crystal, our soon-to-be born child, my parents, Curt and Gail Johnson, and my brother, Aaron Johnson.

Abstract

Micro free-flow electrophoresis (μFFE) is a continuous separation technique in which analytes are streamed through a perpendicularly applied electric field in a planar separation channel. Analyte streams are deflected laterally based on their electrophoretic mobilities as they flow through the separation channel. The continuous nature of μFFE separations makes it uniquely suitable as the second dimension for multidimensional separations. The focus of this work is the development of coupling capillary electrophoresis (CE) to μFFE as a high speed two-dimensional (2D) separation platform, followed by an investigation of orthogonality of the two techniques, and finally a novel label-free detection method for μFFE separations. A new μFFE device was fabricated and coupled to CE via capillary inserted directly into the μFFE separation channel. High peak capacity separations of trypsin digested BSA and small molecule bioamines demonstrated the power of CE × μFFE. Since both methods rely on electrophoretic mobility to separate, an investigation on the orthogonality of the two techniques was carried out. μFFE can operate in many different separation modes to increase the orthogonality CE × μFFE. Lastly, fluorescent labeling of the analytes can cause the sample to lose its dimensionality affecting 2D separation peak capacity and coverage. A novel absorption detector was studied to demonstrate the first ever label free absorption detection on a μFFE device. A separation was performed on visible dyes and their detection limits quantified.

Table of Contents

List of Figures

List of Tables

List of Abbreviations

1D	One-Dimensional
2D	Two-Dimensional
2D-GE	Two-Dimensional Gel Electrophoresis
2D-LC	Two-Dimensional Liquid Chromatography
^{1}D	First Dimension Separation
^{2}D	Second Dimension Separation
µFFE	Micro Free Flow Electrophoresis
µFFIEF	Micro Free Flow Isoelectric Focusing
µFFMEKC	Micro Free Flow Micellar Electrokinetic Chromatography
ABS	Acrylonitrile Butadiene Styrene
ACE	Affinity Capillary Electrophoresis
ATP	Adenosine Triphosphate
CAPS	N-Cyclohexyl-3-Aminopropanesulfonic Acid
CE	Capillary Electrophoresis
CGE	Capillary Gel Electrophoresis
cLC	Capillary Liquid Chromatography
CSE	Capillary Sieving Electrophoresis
CTAB	Cetrimonium Bromide
CZE	Capillary Zone Electrophoresis
DNA	Deoxyribonucleic Acid
FFE	Free Flow Electrophoresis
GC	Gas Chromatography
GC-GC	Hyphenated Gas Chromatography

HEK	Human Embryonic Kidney
HEPES	4-(2-Hydroxyethyl)-1-Piperazineethanesulfonic Acid
IEF	Isoelectric Focusing
ITP	Isotachophoresis
LC	Liquid Chromatography
LC×LC	Comprehensive Two-Dimensional Liquid Chromatography
LC-LC	Hyphenated Liquid Chromatography
LOD	Limit of Detection
MEKC	Micellar Electrokinetic Chromatography
MES	2-(N-Morpholino)-Ethanesulfonic Acid
NBD-F	4-Fluoro-7-Nitro-2,1,3-Benzoxadiazole
nLC	Nano Liquid Chromatography
PAGE	Polyacrylamide Gel Electrophoresis
PCR	Polymerase Chain Reaction
PDMS	Polydimethylsiloxane
PEO	Polyethylene Oxide
RPLC	Reverse Phase Liquid Chromatography
SDS	Sodium Dodecyl Sulfate

Chapter 1

Introduction

Johnson, A.C., Bowser, M.T., *Lab Chip.* **2017** DOI: 10.1039/C7LC01105A

1.1 The Importance of High Analyte Count Separations and Analysis

One-dimensional (1D) separation techniques such as gas chromatography (GC), liquid chromatography (LC), and capillary electrophoresis (CE) have been the work horses in chemical analysis in academic and industrial settings. Over the past several decades, GC, LC, and CE have been responsible for many analyses in the fields of pharmaceuticals, forensics, industrial quality control, agricultural, and food sciences. Recently, with the advent of the "–omics" fields of study, research has shifted toward analysis of early disease identification biomarkers, detection of peptide fragments in protein digests, cell lysate quantitation, and analysis of other biological samples with analyte counts numbering the hundreds to thousands. Unfortunately, the achievable separation abilities of these traditional 1D techniques are overpowered by the complexity of these samples. This section will describe the importance of these complex analyses, the limitations of 1D techniques, and the promising solution to these limitations.

1.1.1 The Increasing Complexity of Biological Analyses

With the emergence of the "–omics" field of analysis, genomics, proteomics, metabolomics, for example, the analyte count of interest can number hundreds to thousands. These analyses are necessary to understand the complex interactions of biological systems and identify causes of diseases and birth defects. The human genome contains more than 2.85 billion nucleotides across greater than 33,000 genes.[1] While quantitative PCR, microarrays, and other commercial instrumentation have been developed to make identifying and sequencing the human genome possible, the process involved many bright minds and several years to complete. These genes are responsible for encoding several thousand unique proteins. Take into account the majority of proteins are built in large sequences from 21 different amino acids building blocks as

opposed to the 4 nucleic acids for DNA sequences, and it becomes an arduous task to identify proteins in human cells.[2] One human cell can contain anywhere from 20,000-50,000 proteins.[3] In addition, cells contain a wide dynamic range of proteins at any given time. This has yet to be quantified in human cells, but for example in a yeast cell the abundance of a single protein can range from 60 to more than 10^6 replicates.[4] Current methods of analysis involve breaking up the proteins into peptide fragments, known as shotgun proteomics, further amplifying the number of analytes.[5-9] In forensic science, metabolites of illicit substances found in urine or blood can be paramount for achieving conviction in a trial, but those metabolites must first be separated from the other biological metabolites found in the sample. Confirmed metabolite counts for human urine have been estimated to be greater than 2,500 while greater than 4,000 have been identified in human blood.[10,11] The large number of analytes contained in these samples, more than overpower the separation ability of GC, LC, and CE.

1.1.2 Peak Capacity and the Limitations of One-Dimensional Separation Methods

Considering the length of time required to sequence the majority of the human genome, and the increased complexity of protein analysis, there is still a need for high throughput, high peak capacity methods for this analysis. The idea of peak capacity was first mentioned by Horvath and Lipsky in 1967.[12] In that same year, Giddings proposed a practical definition and coined the term.[13] Peak capacity (n_c) is simply defined as number of baseline resolved peaks that can fit within a given separation time. For example, the peak capacity for the ideal separation in Figure 1.1 would be 16.

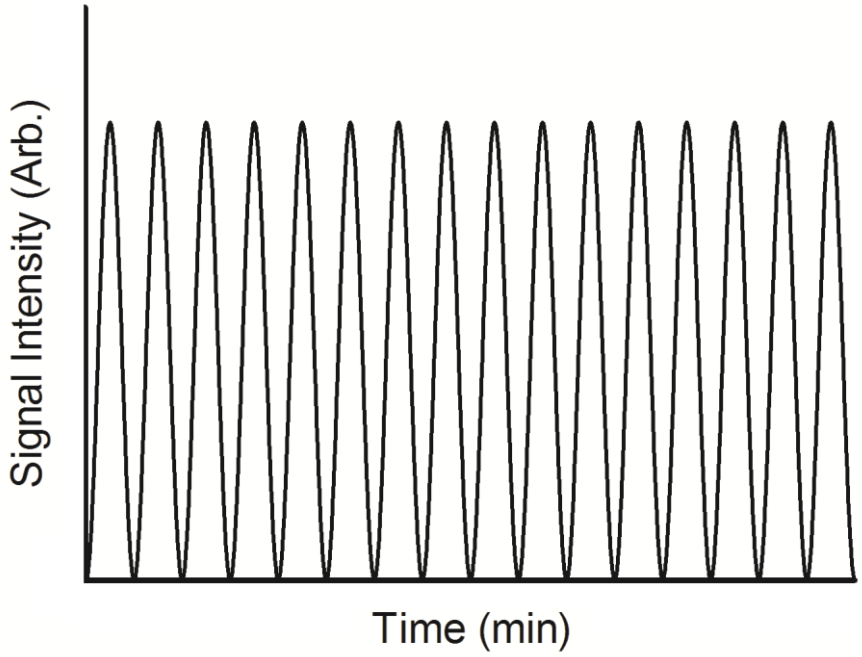

Figure 1.1 Ideal separation of 16 analytes within a given analysis time where all the peaks are baseline resolved and evenly spaced. The peak capacity of this separation would be 16.

The equation for calculating peak capacity for nonideal separations consists of the total time of the separation window (t_s) and the average 4σ peak width ($w_{4\sigma}$) of the peaks used for analysis , where m is the number of peaks chosen (Equation 1.1).[14]

$$n_c = 1 + \frac{t_s}{\frac{1}{m}\sum_1^m w_{4\sigma}} \tag{1.1}$$

In many chromatographic methods, the 4σ widths of well-retained peaks tend to be larger than those that are poorly retained. Care must be taken to select peaks that are representative of the entire separation and not only the narrowest peaks. A selection of peak widths from the entire separation window is necessary to gain an accurate estimation of peak capacity. Peak capacity is regularly used as a metric for measuring the separation power of a given method. The larger the peak capacity the better chance a method has at separation for a certain number of analytes. This is best visualized with peak overlap analysis. Martin et al. used this to characterize the probability that all

analytes in a sample will be baseline resolved for a defined peak capacity (n_c) and number of analytes (m).[15]

$$P_{m,n_c}(m) = (1 - \frac{m-n_c}{n_c-1})^{m-2} \quad (1.2)$$

As illustrated in Figure 1.2, as the peak capacity increases, there is a greater chance for comprehensive separation at a given number of analytes. For example, with a sample of

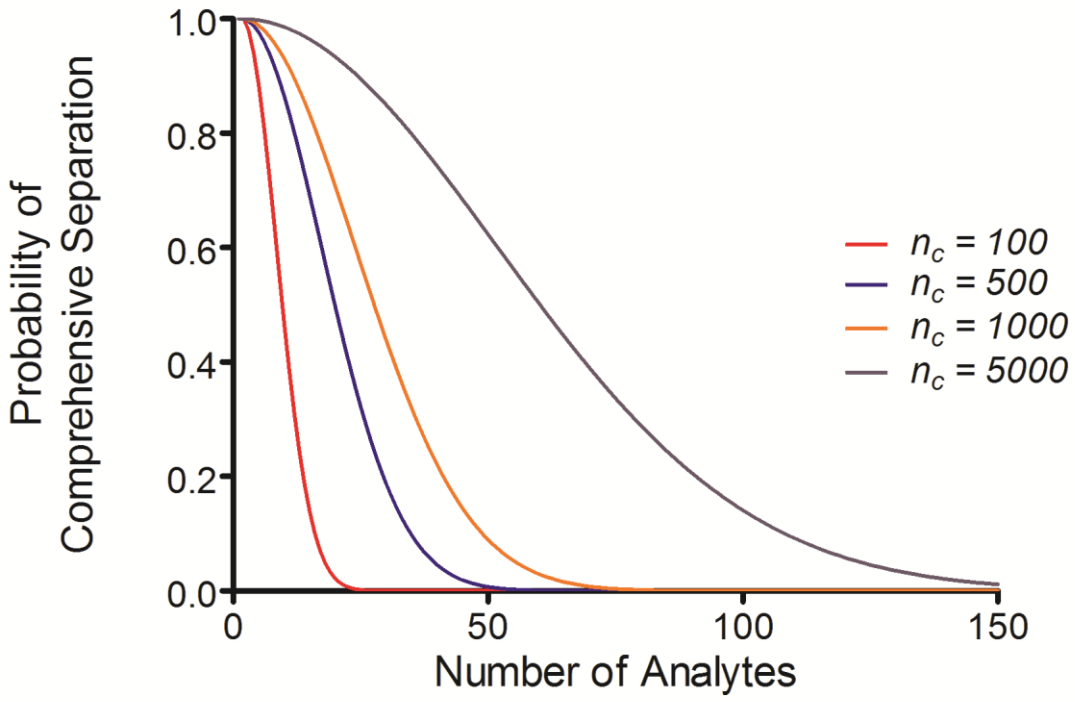

Figure 1.2 A plot of the probability of a comprehensive separation versus the number of analytes in the sample at peak capacities of 100, 500, 1000, and 5000. As the samples get more complex a higher peak capacity is needed to achieve separation in a random distribution of peaks.

25 analytes, a separation with a peak capacity of 100 has very little chance (0.1%) of complete separation without any optimization of the method. However, at a peak capacity of 500, that probability becomes 32%, at 1000 it becomes 57% and at 5000 it becomes 90%. It is important to highlight that this does not mean a 25 analyte separation is not possible with a peak capacity of 100. It simply illustrates the fact that it will require more optimization than a method with a peak capacity of 5000. Increasing a

method to its maximum peak capacity will provide a shortened time optimizing separation parameters and ultimately save time and resources in academic and industrial settings.

Typical peak capacities for gradient reversed phase liquid chromatography (RPLC) on a sample of peptides can range from 300-600 in a 30-60 minute separation time (10 peaks/min).[3,16] Recently capillary liquid chromatography (cLC), also known as nano liquid chromatography (nLC), has given peak capacities of 800 on a separation of peptides, however, the separation took 10 hours to complete (1.33 peaks/min).[17] Capillary zone electrophoresis (CZE), while capable of very high efficiencies often in the one million theoretical plates per meter range, also produces peak capacities of 400-500 in one hour for a peptide separation (~8.33 peaks/min).[18] Even in an article published this year, a 1D CZE method was reported on a separation of peptides that had a peak capacity of 380 in 140 minutes (2.74 peaks/min).[19] These methods are simply overwhelmed by the high analyte samples generated for proteomic, metabolomic, and genomic analysis. Manipulating equation 1.2 to output the minimum peak capacity necessary ($n_{c,min}$) to achieve a given probability (P_x) of comprehensive separation for various analyte counts gives rise to equation 1.3. A plot of equation 1.3 illustrates the

$$n_{c,min} = 1 + \frac{m-1}{1-P_x^{\frac{1}{m-2}}} \tag{1.3}$$

drastic increase in peak capacity necessary to keep probability constant as the number of analytes increases (Figure 1.3).

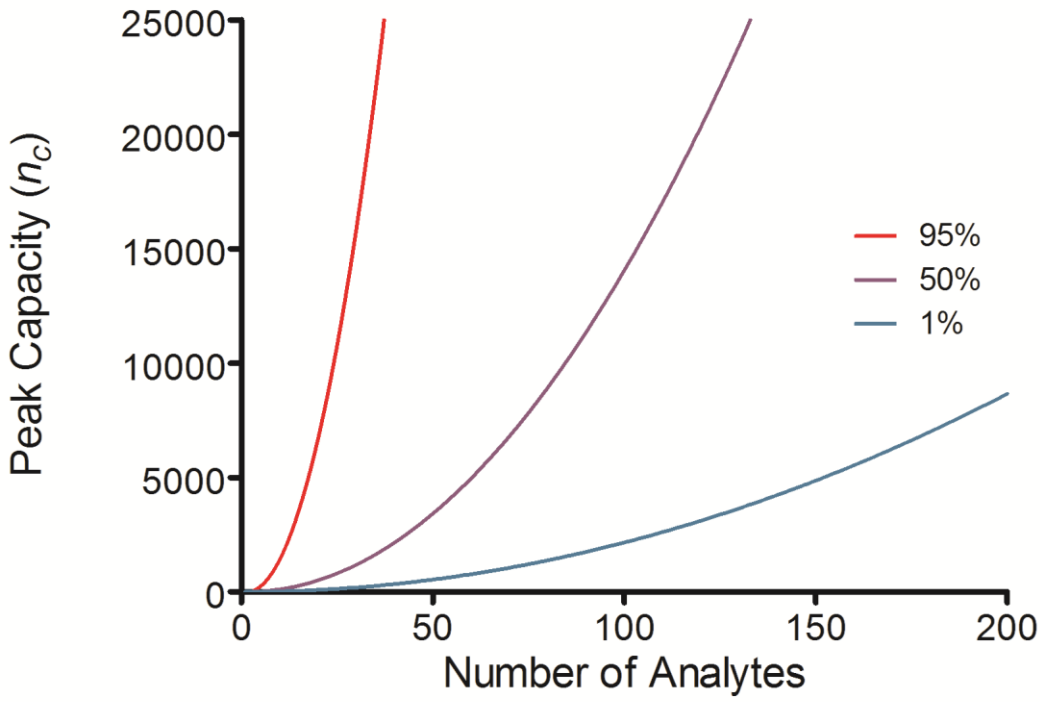

Figure 1.3 A plot of the peak capacity necessary to separate a sample with increasing numbers of analytes at probabilities of comprehensive separation of 95%, 50%, and 1%.

To achieve a 95% probability that all components of a 25 analyte sample will be completely resolved requires a peak capacity of 10,775. To achieve a comprehensive separation of 200 analytes at a meager 1% probability even requires a large peak capacity of 8,657! 1D separation methods simply cannot keep up with the high analyte counts generated by complex bioanalysis. The models in Figures 1.2 and 1.3 both assume constant peak width and a random distribution of peaks throughout the separation space. Optimized separation parameters can lead to better separations than these models predict, however the driving factor behind high peak capacity separations remains the same. Faster, higher peak capacity separations should correlate with less time spent optimizing separation conditions, and therefore higher throughput. There is a pressing need for new high-speed, high peak capacity methods to even come close to achieving separation on these samples.

1.2 Two-Dimensional Separations

Current research has shifted from optimizing 1D separations and instead is focusing on two-dimensional (2D) separations. Karger, Snyder, and Horvath were the first to introduce the large peak capacity potential of a hyphenated 2D separation.[20] In a 2D separation, one separation technique is coupled with a different technique to effectively separate the analytes based on properties of two different methods rather than one.

Perhaps the most widely used and well recognized 2D separation would be 2D-gel electrophoresis (2D-GE). The first description of 2D-GE in literature was by Macgillivray and Wood in 1974,[21] but it was later optimized by O'Farrell in 1975[22] into the technique widely used today. In 2D-GE, analytes, usually proteins or peptides, are first separated via isoelectric points, called isoelectric focusing (IEF), and then the peaks are deposited on a slab gel for sodium dodecyl sulfate polyacrylamide gel electrophoresis (SDS-PAGE) in which the analytes are separated by their molecular weights (Figure 1.4). 2D-GE is capable of generating peak capacities of 10,000 and achieving separation of 2,000 proteins is typical.[23,24] However, this technique is not without its own drawbacks. 2D-GE suffers from a low dynamic range of detection (roughly 4 orders of magnitude), long preparation, run and analysis times (2-3 days), low reproducibility, inability to analyze hydrophobic or alkaline analytes, and difficulty in quantitation.[24]

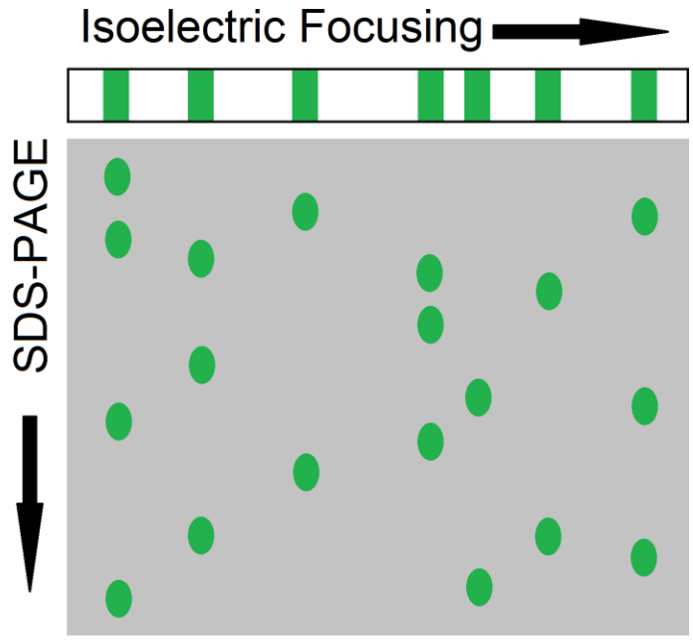

Figure 1.4 A schematic of a Two-Dimensional Gel Electrophoresis separation. A sample, typically a cell lysate or protein digest, is loaded on a strip with an immobilized pH gradient to perform isoelectric focusing IEF in which the sample is separated by their isoelectric points (pI). The analytes on the strip are then transferred to a slab gel to perform sodium dodecyl sulfate polyacrylamide gel electrophoresis (SDS-PAGE) in which the analytes are separated by molecular weight. The analyte spots are then visualized with a post separation modification step like a visual dye or radiography.

1.2.1 Off-line and On-line Two-Dimensional Separations

Due to the drawbacks of 2D-GE, research has shifted toward the coupling of time-based separation techniques such as GC, LC, and CE. There are two main categories of methods for 2D analysis using the above methods, namely, off-line and on-line. Off-line methods collect fractions from the first dimension and are then analyzed by the second dimension separately. Most commonly, this technique is used in “heart-cutting” methods such as LC-LC or GC-GC, in which only a specific fraction or peak is collected and later analyzed by the second dimension.[25,26] The ability to independently optimize the first dimension (^{1}D) and second dimension (^{2}D) separations, as well as the ability to pick and choose which fractions to collect offer unique benefits. However, these benefits become drawbacks if the ^{1}D separation is unknown, or if the entire ^{1}D

separation must be sampled. This drastically increases the time required for complete analysis.

On-line methods, are those in which the ^{1}D and ^{2}D separations are coupled directly together via some interface (Figure 1.5). In other words, no fractions are collected and injected separately at a later time. Comprehensive 2D separations such as LC×LC subject the entirety of the ^{1}D separation to the ^{2}D separation for two-dimensional analysis of the sample. However, this requires the ^{2}D separation to be completed and fully equilibrated before the next sample can be injected. This in turn affects the sampling rate of the ^{1}D separation and limits the number of samples taken. This negatively affects the obtainable peak capacity for the 2D separation.

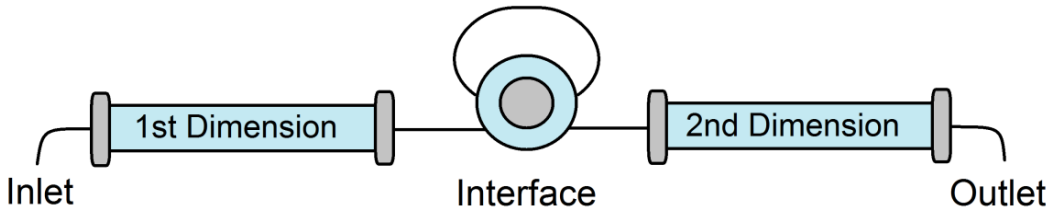

Figure 1.5 Example schematic of an on-line 2D separation method. The sample and eluent run through the inlet. It is then collected and injected via the interface into the second separation. The outlet is then connected to the detection method of choice for analysis of the injected sample.

1.2.2 Two-Dimensional Peak Capacities

As first introduced by Karger et. al.,[20] and later expanded upon by Guichon,[27] and Giddings,[28] the maximum achievable, or ideal, peak capacity of a 2D separation ($n_{c,2D}$) can be defined as the product of the peak capacity from the first separation ($^{1}n_c$) and the second separation ($^{2}n_c$).

$$n_{c,2D} = {}^{1}n_c \times {}^{2}n_c \tag{1.4}$$

The multiplicative nature of 2D separations as shown in Equation 1.4 highlights an important advantage of 2D separations versus their 1D counterparts. It would be easier to generate 2 separations in tandem that achieve an ideal peak capacity of 10,000 (i.e. ${}^{1}n_c = {}^{2}n_c = 100$) which are obtainable peak capacities for two separate 1D separations rather than a 1D separation that has a peak capacity of 10,000, which is currently unobtainable within reasonable analysis times. However, achieving the ideal peak capacity of a 2D separation is not straightforward. In fact, Equation 1.3 only holds true if there is no resolution lost at the interface between the two separations, and the separation mechanisms of the two separations must be orthogonal.[28]

1.2.3 The Under Sampling Correction Factor

Resolution is typically lost between the ^{1}D and ^{2}D separation when sample is allowed to remix, or the ^{1}D separation is under sampled. Under sampling was first described by Murphy, Schure, and Foley,[29] and later elaborated on by Davis, Stoll and Carr.[30] The sampling rate of a 2D separation is defined as the number of fractions which are taken from ^{1}D and injected on the ^{2}D separation per unit of time. The amount of time required to run the ^{2}D separation and prepare it for another injection is commonly referred to as the cycle time. In LC×LC, for example, this would be the time required to run a separation method and re-equilibrate the column. Murphy et al. proposed a sampling rate of at least 3-4 times across the 8σ peak width as adequate sampling of the ^{1}D separation.[29] For example, with an 8σ peak width of 2 minutes, a cycle time of at least 40 seconds would be required. In comprehensive 2D separations, a faster cycle time would be desirable since the initial fraction is not always collected at the beginning of the 8σ peak width. Often in 2D separations, the cycle time is not fast enough to achieve this guideline, which in turn causes negative effects on the peak capacity. Davis, Stoll, and

Carr quantified this loss in peak capacity (β) caused by under sampling (Equation 1.5). The fraction of ${}^1n_c$ retained is defined as ${}^1/_\beta$ (Equation 1.6).[30]

$$\beta = \sqrt{1 + \alpha \times \left(\frac{t_s}{{}^1w}\right)^2} \tag{1.5}$$

$${}^1n_c' = \frac{{}^1n_c}{\beta} \tag{1.6}$$

The corrected ^{1}D peak capacity (${}^1n_c'$) is inversely proportional to the root of the ratio of cycling time (t_s), and the average 4σ peak width (${}^1w$) as measured from the ^{1}D separation peaks. The under sampling correction factor (α) was quantified as 3.35 by Davis et al. by simulations in which peaks are randomly assigned retention times, random peak heights assigned from an exponential distribution, and a resolution between peaks of 1.[30,31] Figure 1.6 visualizes the effect of under sampling for various ^{1}D separation times and ^{2}D cycle times. For a ^{1}D separation time of 5 minutes, assuming an efficiency of 100,000 plates, a cycle time of 1 second is necessary to retain 90% of the ^{1}D peak capacity. On a 120 minute ^{1}D separation, a cycle time of 23 seconds is necessary to retain 90% of the ^{1}D peak capacity. The fastest LC×LC cycle times reported to date are 12-21 seconds.[32,33] At these cycle times, roughly 49% of peak capacity is lost on a ^{1}D separation time of 30 minutes, and 24% is lost on a 60 minute separation. An improvement in cycle time speed would be necessary, however, in LC a faster cycle time comes at the cost of ^{2}D peak capacity.[34]

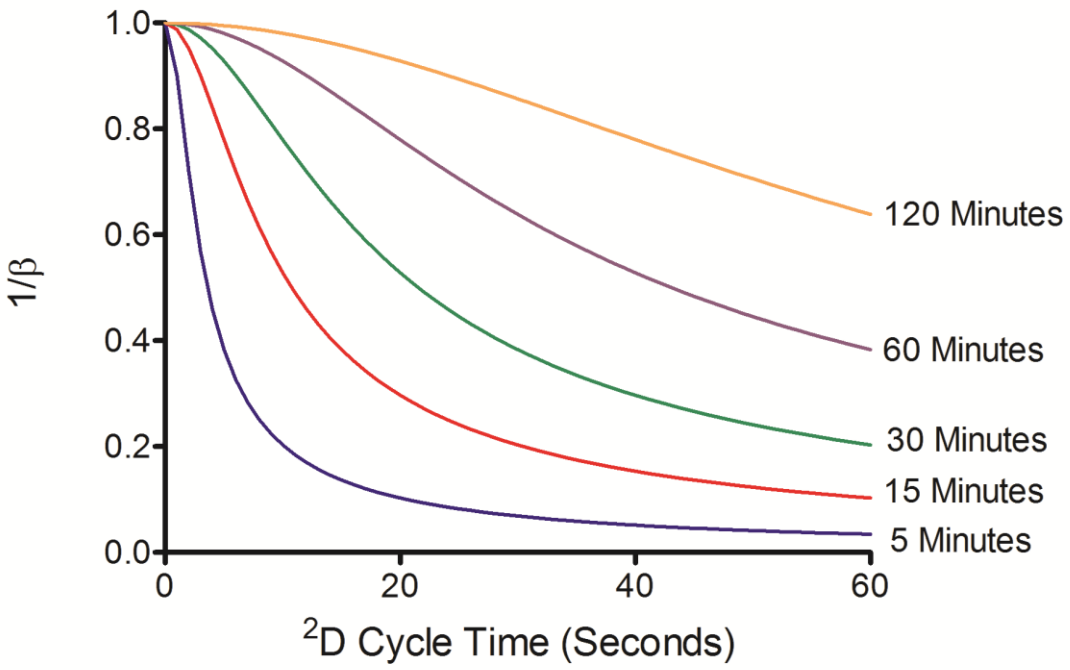

Figure 1.6 A plot of the fraction of ^{1}D peak capacity retained (1/β) versus the ^{2}D cycle time ($\boldsymbol{t_s}$) from equation 1.4 is shown for ^{1}D separation times of 5, 15, 30, 60, and 120 minutes. This calculation assumes a ^{1}D theoretical plate count of 100,000.

Performing CE as the second separation would be a better candidate for faster cycle times. The faster separation ability of CE has resulted in faster cycle times. Ramsey et al. reported a cycle time of 1 second on a ^{1}D CE separation of 15 minutes using a 1.3 cm long microfluidic channel.[35] However, this still results in ~2% loss in peak capacity, and it is unclear how further improvement can be achieved. Alternate methods for eliminating under sampling are required for optimal 2D peak capacity.

1.2.4 Orthogonality

The other factor influencing the effective 2D separation peak capacity ($n'_{c,2D}$) is the orthogonality, or the ability of the two dimensions to separate the analytes based on different properties. For example, in 2D-GE, IEF is used to separate the sample based on analyte pIs, and then SDS-PAGE is performed to separate the sample again based

on molecular weight. These two techniques separate analytes based on different mechanisms, and should give a large coverage of the separation space (i.e. orthogonal) as shown in figure 1.7B. However, if the two techniques are not sufficiently different, for example LC × LC with two C18 columns, the peaks will be distributed along a diagonal line across the separation space (i.e. non-orthogonal) as shown in figure 1.7A.

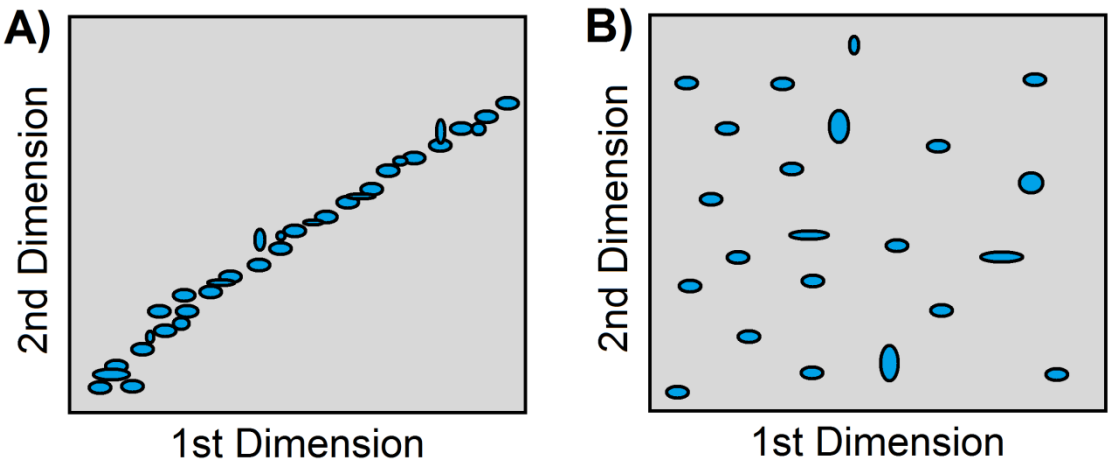

Figure 1.7 A) A highly correlated distribution of peaks in a 2D separation space where the 1st and 2nd dimension separations are represented as non-orthogonal. B) A random distribution of peaks in a 2D separation space where the 1st and 2nd dimension separations are represented as orthogonal.

The orthogonality of a separation does not only depend on the separation mechanisms chosen, it also depends on the sample dimensionality. As stated by Giddings, the sample must have a dimensionality of at least two or more to observe orthogonality.[36] In other words, the sample must have at least two independent characteristics such as charge, size, hydrophobicity, etc., for orthogonal separation to be possible. This in turn will determine the methods for separation chosen. For example, if a sample consists only of analytes with like size to charge ratios, CZE would not be a good choice for separation of these analytes. Common sense prevails here, but it is not so simple when the sample analytes are unknown. In which case, a way to estimate orthogonality and a systematic approach to separation method coupling is necessary.

Fractional coverage (f) refers to the fraction of 2D separation space that are accessible to peaks in a 2D separation. This is the current mathematical representation of the orthogonality of the ^{1}D and ^{2}D separations. There are many proposed methods for calculating f including correlation coefficients,[37,38] fan area,[39] peak counting,[40] fractal dimensionality,[41] box counting,[42,43] asterisk,[44] and nearest neighboring peak.[45,46] Rutan et al. reviewed various methods based on ecological home range calculations, and determined the minimum convex hull method has important advantages over previously reported methods.[47]

In the minimum convex hull method, a polygon with interior angles less than 180^o is drawn connecting the outermost points in a normalized 2D separation space.[48,49] This is best visualized by imagining the peaks on the 2D separation space are pegs in a pegboard (Figure 1.8). A rubber band is then stretched around the outermost pegs. The area of the rubber band is then calculated as a percentage of the total normalized separation space, thus calculating the value for fractional coverage. The advantages of this method for calculating f are the lack of user adjustable parameters, it is easily implemented with computer programs, and it can be easily scaled to different retention time normalizations.

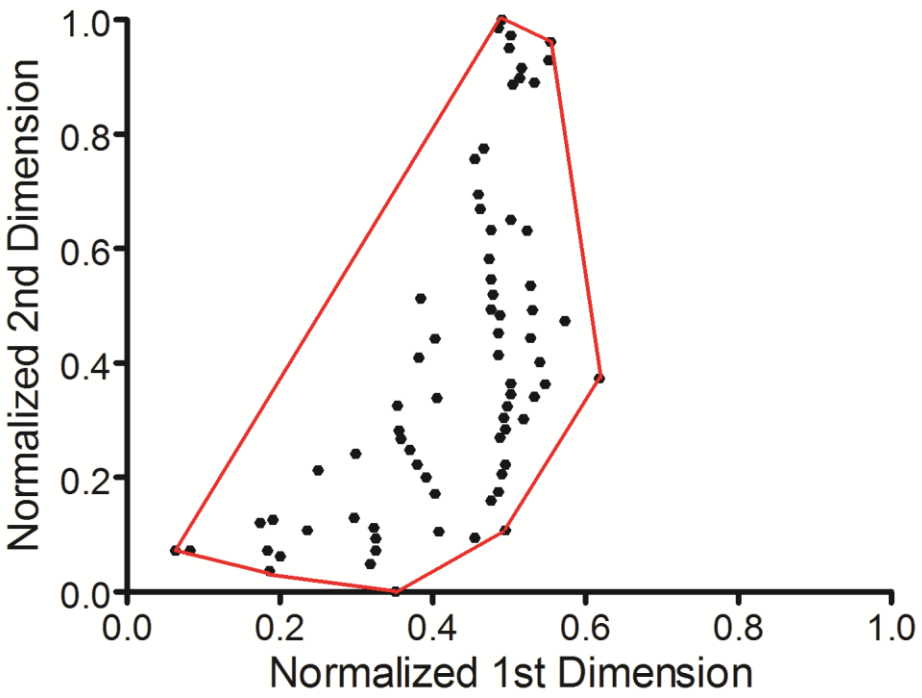

Figure 1.8 An example of a minimum convex hull plot. The peaks are denoted by the black dots, and the red line represents the smallest polygon connecting the outer most peaks with interior angles <180°. The fractional coverage is then calculated by dividing the area of the polygon by the total normalized separation area. In this case $\boldsymbol{f}$ = 0.29.

Combining fractional coverage and the under sampling correction factor with equation 1.3 gives the effective 2D peak capacity of a 2D separation (Equation 1.7).

$$n'_{c,2D} = {}^{1}n_c \times {}^{2}n_c \times \frac{1}{\beta} \times f \qquad (1.7)$$

It is important to note that these correction factors are still not widely used in reporting of 2D peak capacities in literature. Therefore, in following chapters, when reporting and comparing values from literature, the 2D peak capacity will be denoted as either ideal, or effective with which correction factors were used. In the case of fractional coverage, since there is no universal method for calculation, the method used will also be included.

1.3 Micro Free Flow Electrophoresis

Free flow electrophoresis (FFE) was introduced by Barriollier *et al.*, and later Hannig, almost 60 years ago.[50,51] A continuous sample stream is introduced into buffer flowing through a planar separation channel.[52-54] An electric field is applied perpendicularly to the buffer flow, separating streams in space according to analyte size and charge (Figure 1.9).

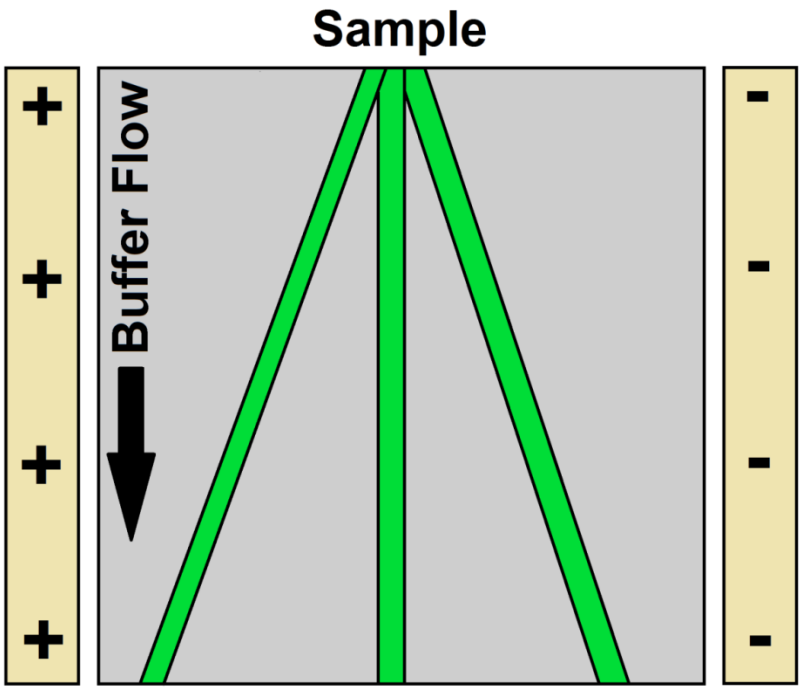

Figure 1.9 FFE separation mechanism. A sample is continuously introduced into the planar separation channel where it is exposed to a perpendicular electric field. Analyte streams are driven through the channel with buffer, and are deflected according to their total electrophoretic mobility.

Electrodes are isolated from the separation channel using ion-permeable membranes to prevent electrolysis bubbles from interfering with the separation. Analytes are separated in space rather than time. Sample introduction, separation and collection are performed continuously. The continuous nature of FFE makes the separation technique particularly well suited for preparative scale fractionation and purification of

biomolecules.[54] FFE has been demonstrated using a number of electrophoresis modes including zone electrophoresis (ZE), isotachophoresis (ITP), isoelectric focusing (IEF), and micellar electrokinetic chromatography (MEKC).[53,55,56]

Preparative scale FFE does present a number of significant challenges. The relatively large dimensions of the separation channel often generates significant current, which in turn leads to Joule heating and electrolysis products at even low potentials.[53,57] Laminar flow must be maintained to achieve predictable analyte steams. Careful control of separation channel depth and buffer flow is therefore necessary. Online detection is challenging, usually requiring offline UV absorbance analysis of collected fractions. This can be time consuming since 90 or more fractions are commonly collected. These challenges make FFE an attractive candidate for miniaturization into a micro free flow electrophoresis (μFFE) system. Operating on the microscale increases surface area to volume ratios which improves heat dissipation, shortens separation times, minimizes volumes of buffers and sample, promotes consistent laminar flow, facilitates on device detection, and lends itself to combination with other microfluidic techniques for a total analysis system.[58]

Raymond *et al.* were the first to successfully fabricate a μFFE device in 1994.[59] The device significantly reduced Joule heating effects while incorporating on device, real time detection of analyte streams. The device was limited to ≤75 V due to the electrical breakdown potential of the silicon substrate used for fabrication.[59] Since then a number of groups have continued to optimize μFFE through improved fabrication methods and instrument designs. The introduction of novel μFFE applications has increased as the performance and reliability of these has improved.

1.3.1 Device Design and Fabrication

Raymond *et al.* fabricated their initial μFFE device in a silicon substrate to leverage existing micromachining techniques developed in the electronics industry.[59] However, silicon is not an ideal substrate for μFFE due to its low electric breakdown potential, which in turn limits the separation potential that can be applied. Silicon substrates were therefore quickly replaced in favor of more suitable materials such as poly(dimethylsiloxane) (PDMS),[60-63] glass,[64-68] polystyrene,[69] and various rigid polymers.[70-73] When choosing a fabrication strategy, it is important to consider challenges that are unique to μFFE. For example, the aspect ratio of the open separation channel is much higher than normally encountered in microfluidic devices. Methods for eliminating electrolysis bubbles generated at electrodes also presents a significant design challenge. Figure 1.10 shows images of a number of μFFE devices reported in the literature, demonstrating interesting design approaches to address these challenges. This section will give a brief overview of methods for fabricating μFFE devices and their design in these materials.

Glass is a rigid material well suited for μFFE fabrication since it can withstand high voltages and pressure, is stable over a wide range of pH, and is relatively chemically inert.[74] Fabrication in glass uses standard photolithography and wet etching techniques to pattern the electrode channel, separation channel, and electrodes in a bottom wafer.[58,64,75]

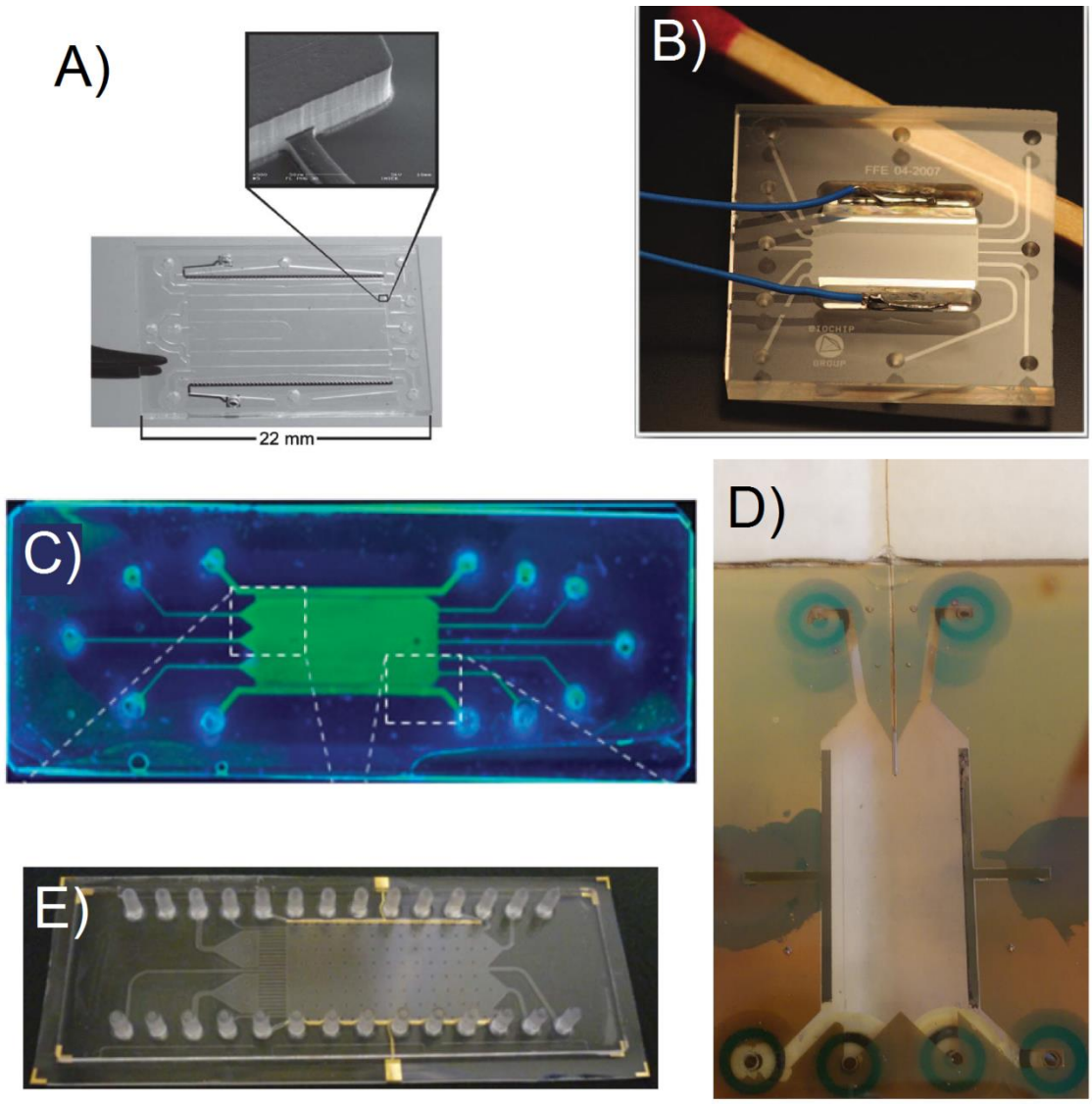

Figure 1.10 A) A Pyrex based µFFE device used for bacteria concentration. B) A Borofloat wafer based µFFE device created for bubble free electrophoresis. C) A glass slide µFFE device for the fluorescent determination of pIs in proteins. D) A Borofloat wafer based µFFE design for high peak capacity separations of peptides. E) An injection molded µFFE device in cycloolefin polymer for low cost fast mass production of devices.

The featured wafer is then bonded to a second unpatterned glass wafer to enclose the channel. Thermal bonding and anodic bonding have be used to bond the two wafers together.[64,76,77] While thermal bonding is much more commonly used in general microfluidics fabrication, the large open channel in µFFE devices makes this approach challenging. Care must be taken during the annealing step to prevent sagging in the

separation channel. Additionally, the low contact area between wafers can lead to significant interfacial stress between the wafers upon cooling, which can make the final devices brittle and prone to fractures. Anodic bonding addresses these issues.[78] In anodic bonding, amorphous silicon is deposited on the featureless wafer. The two wafers are aligned, brought into contact with electrodes, and a voltage is applied through the wafers. Current through the glass oxidizes the amorphous silicon, forming covalent bonds between the oxidized amorphous silicon and the glass.[78,79]

More recently, Jezierski *et al.* reported a method for fabrication of a glass μFFE device using liquid phase photolithography between two glass wafers.[80] They were able to use a spacerless design to achieve channel heights of 25 μm while eliminating bonding steps. Another interesting way to bond glass wafers is through the use of a polymer bonding layer. Ding *et al.* used a photocurable monomer Norland Optical Adhesive 81 (NOA 81) as the bonding layer between two glass wafers in a μFFE device.[81] Interestingly, the layer is dissolvable, making the glass wafers reusable and easier to maintain if the device is clogged.

Since the introduction of soft photolithography by Whitsides *et al.*, PDMS has become a standard substrate for microfluidics fabrication.[73,82-84] PDMS fabrication follows a simple and inexpensive replica molding strategy which is able to quickly produce devices without the need for specialized facilities or instrumentation.[85] However, the inherent flexibility of PDMS is a challenge for fabrication of μFFE devices. Using standard μFFE designs, the large open area of a separation channel fabricated in PDMS would be expected to bow out when under pressure. Zhang and Manz addressed this issue by using vacuum to pull buffer through a PDMS μFFE device.[63] Support pillars were also incorporated to prevent the separation channel from collapsing

under the applied vacuum.[63] While successful, precise fluidic control through an applied vacuum is significantly more challenging than using pressure driven flow. There was also some concern regarding what effect multiple paths around the pillars would have on stream broadening and the homogeneity of the electric field.

More recent μFFE fabrication strategies have aimed to combine the performance of glass devices with the simplicity and cost effectiveness of PDMS devices. Most successful strategies have utilized low-cost, hard polymer substrates. Walowski *et al.* fabricated low-cost μFFE devices using a multistep lamination process in poly(methyl methacrylate) (PMMA).[86] Devices were fabricated in 1 hour using transfer tape as a spacer to generate a separation channel between two PMMA wafers. Devices supported field strengths as high as 422 V cm^{-1} without any degradation. Akagi *et al.* used a computer numerical controlled (CNC) milling machine to fabricate a PMMA device.[70] The two PMMA substrate wafers were sealed using masking tape. Kohler *et al.* were able to mass produce μFFE devices using an injection molding fabrication method.[87] An 80 ton clamping force injection molding machine was used to fabricate devices with a separation channel depth of 20 μm. de Jesus *et al.* used laser printer toner to make raised channels on a glass substrate.[88] Devices with channel depths as small as 8 μm were fabricated in 1 hour. Anciaux *et al.* were able to produce a μFFE device in ABS (acrylonitrile butadiene styrene) using an off the shelf, consumer grade 3D printer.[71] They were able to produce a working μFFE device for less than a quarter in material cost. The two printed wafers were bonded using an acetone vapor bath and platinum wires were inserted as the electrodes. While the fabrication throughput was slower than other approaches, the ease with which design modifications could be implemented suggests that 3D printing would be an excellent strategy for fast prototype development.

1.3.2 Electrolysis Mediation

The relatively large cross sectional area of the separation channel gives rise to significantly higher currents than typically observed in microfluidic systems, even at low potentials. This enhanced current is a consequence of significant electrolysis and bubble formation at the electrodes. Bubble formation is particularly troublesome since they disrupt flow paths and distort the electric field, giving rise to unstable separations. The continuous nature of the separation is one of μFFE's strongest attributes. Being unable to apply a separation potential over extended periods of time without signficant bubble formation largely eliminates this advantage. As such, significant effort has been spent developing design improvements that mediate the effect of electrolysis bubble formation on μFFE stream stability. These designs can be classified as open or closed channel devices (Figure 1.11).

Figure 1.11 (A) Side view of closed style device, where the electrodes (yellow) are segregated from the separation channel (white) by some kind of structure (purple) usually an ion-permeable membrane, insulator, or wall. (B) Side view of an open style device in which the separation channel is not segregated from the electrodes by any kind of structure.

Early devices aimed to replicate the closed channel, ion permeable membranes commonly used in conventional FFE to isolate the electrodes from the separation channel. Microfabricated channels were integrated as a pseudo membrane between the separation channel and electrode channels.[59,63,89] Unfortunately, these side channels proved largely ineffective. Long and narrow side channels are necessary to effectively

isolate flow in the electrode channel from the separation channel. These channels increased electrical resistance, resulting in a significant proportion of the applied potential being realized in the membrane channels, not the separation channel. In some designs it was reported that <5% of applied potential drop occurred across the separation channel.[89] Subsequent closed channel designs have proven more effective. Several groups have used *in situ* polymerization to generate ion permable membranes.[70,80,81] These ion permeable membranes effectively segregate bubbles from the separation channel, but lacked chemical stability and still introduced a resistive barrier that reduces the applied potential realized in the separation channel. Köhler *et al.* took a unique approach by creating a wall between the electrode channel and separation channel with a 20 μm gap at the top of the device allowing voltage to be applied through a liquid bridge.[72] While electric field strength improved, the device acted as a closed system causing electrodynamic broadening. Other closed design devices include electrostatic induction,[90] and salt bridge connections.[91]

Open channel μFFE devices operate without any physical barrier between the electrodes and the separation channel. While open channel devices are simpler to fabricate and do not introduce an electrically resisitive barrier, they are potentially less effective at isolating electrolysis bubbles than closed channel devices. Lu *et al.* prevented the formation of bubbles in an open channel μFFE device by operating below the potential required for water electrolysis.[92] This strategy limited the separation potential to <2 V, greatly increasing the time necessary to achieve reasonable separation power. Kohlheyer *et al.* introduced a completing redox pair to suppress bubble formation.[77] Streaming a mixture of hydroquinone and p-benzoquinone over the electrodes suppressed bubble formation at field strengths as high as 215 Vcm^{-1}.

Fonslow *et al.* demonstrated that electrolysis bubbles could be effectively cleared by simply fabricating electrodes in channels that are deeper than the separation channel.[93] Lubrication theory predicts that linear velocity in a planar channel is proportional to the square of the channel depth.[94] An electrode channel that was 4× deeper than the separation channel generated a 16-fold increase in linear velocity, eliminating electrolysis bubbles while keeping the buffer velocity in the separation channel low enough to allow an effective separation to occur. An electric field as high as 589 Vcm^{-1} could be applied without interference from electrolysis bubbles. It was estimated that approximately 91% of the applied potential was experienced in the separation channel. Frost *et al.* found that adding a surfactant (e.g. 300 μM Triton X-100) or organic modifier (e.g. 50:50 water-methanol) to the separation buffer improved stream stability 8-fold.[95] The buffer additives lowered the surface tension of the water, resulting in smaller electrolysis bubbles, which were more eaily cleared from the μFFE device. A separation of fluorescent dyes at an electric field strength of 75 Vcm^{-1} was stable for ≥2 hours.

Over the past several decades there have been tremendous advances in μFFE fabrication and design. Fabrication is now possible in a range of chemically diverse substrates and costs are dropping dramatically. Both open and closed channel designs are available that support continuous operation over several hours at reasonable separation potentials. The choice between open and closed channel designs is largely driven by the fabrication strategies available. Open channel designs are simpler to fabricate and easier to operate. Closed channel designs are more effective at isolating electrolysis bubbles but require more complex fabrication procedures, may introduce resistive barriers that lower the effective separation potential and can introduce electrodynamic broadening.

1.3.3 μFFE Separation Theory

While μFFE appears in many ways analogous to other microfluidic separations, the relative direction of flow and field introduce a number of differences that influence separation optimization. To this end, μFFE is able to draw on established FFE separation theory.[55,96,97] The position where an analyte crosses the detection zone, or deflection distance (*d*), is determined by the analyte's overall mobility (μ_{total}), the electric field applied across the separation channel (*E*) and the time the analyte spends in the electric field (*t*)[96,98]:

$$d = \mu_{total} E t \tag{1.8}$$

The product (*Et*) is commonly referred to as the separation power of a FFE separation. A notable difference from other electrophoretic separations is that the electric field and the time an analyte spends in the electric field are independent in FFE. The time the analyte spends in the electric field can be manipulated in FFE by changing the buffer flow rate (*v*), or the separation channel length (*L*), neither of which impact, or are impacted by, the electric field. Multiple combinations of electric field and time are possible that give the same separation power and therefore an identical deflection distance. The electric field and buffer velocity can therefore be changed independently to optimize μFFE resolution.

Factors that contribute to broadening in FFE have been discussed at length in literature.[55,99] The contributing factors to overall peak variance (σ_{FFE}^2) in FFE are injection stream width (σ_{inj}^2), diffusion of the analyte (σ_D^2), electrodynamic broadening (σ_{ED}^2), hydrodynamic broadening (σ_{HD}^2), and electrohydrodynamic broadening (σ_{EHD}^2)[55]:

$$\sigma_{FFE}^2 = \sigma_{inj}^2 + \sigma_D^2 + \sigma_{ED}^2 + \sigma_{HD}^2 + \sigma_{EHD}^2 \tag{1.9}$$

The variance due to injection stream width is simply determined by the width of the sample stream as it enters the FFE separation channel. The variance caused by diffusion can be quantified according to:

$$\sigma_D^2 = 2Dt \quad (1.10)$$

where *D* is the diffusion coefficient of the analyte and *t* is the transit time through the FFE separation channel.[100] Electrodynamic broadening is a phenomenon observed in closed channel devices where the electrodes are physically segregated from the separation channel. The physical barriers prevent bulk flow generated by EOF from exiting the separation channel. Instead, EOF recirculates back through the center of the channel, introducing a crescent shaped flow profile.[101,102]

Hydrodynamic broadening is a consequence of the difference in the profiles of the pressure driven flow acting on the analyte longitudinally while the electric field moves the analyte laterally.[97] The pressure driven flow of the buffer generates a parabolic flow profile. Analytes near the wall of the separation channel move slower through the separation channel and therefore spend more time in the electric field. Increased time in the electric field increases the deflection distance. A crescent shaped profile is generated where analytes travelling through the center of the channel are deflected less than analytes nearer the separation channel walls.[101] Hydrodynamic broadening (σ_{HD}^2) is determined by:

$$\sigma_{HD}^2 = \frac{h^2 d^2 v}{105DL} \quad (1.11)$$

where *h* is height of the channel, *d* is the deflection distance, *v* is the buffer linear velocity, *D* is the diffusion constant of the analyte and *L* is the length of the separation channel.[97] Hydrodynamic broadening is more prevalent for analytes that are deflected most in the separation channel.

Electrohydrodynamic broadening is caused when the conductivity of the buffer solution is higher than that of the sample stream.[55] A difference in conductivity between the sample stream and the separation buffer generates a discontinuity in the electric field, which causes analytes to either speed up or slow down as the exit the sample stream. If the conductivity of the sample stream is higher than that of the separation buffer, the migration velocity of analytes increases as they cross the boundary, generating broader peaks through de-stacking.

Fonslow and Bowser were able to demonstrate that in an open channel μFFE device, where the sample matrix was well matched with the separation buffer, stream width was primarily determined by injection width, diffusion and hydrodynamic broadening:[97]

$$\sigma_{\mu FFE}^2 = \sigma_{inj}^2 + \sigma_D^2 + \sigma_{HD}^2 \quad (1.12)$$

The expression could be further expanded to predict the effect of various experimental parameters on broadening:

$$\sigma_{\mu FFE}^2 = \frac{w_{inj}^2}{12} + \frac{2DL}{v} + \frac{h^2 d^2 v}{105DL} \quad (1.13)$$

where w_{inj} is the baseline width of the injection stream, *D* is the diffusion coefficient of the analyte, *L* is the length of the μFFE separation channel and *v* is the linear velocity of the separation buffer.[97] Equation 6 is analogous to the Van Deemter equation that predicts the effect of mobile phase velocity on peak width in chromatography.[103] Fonslow and Bowser demonstrated that stream width could be minimized at a buffer linear velocity that balanced diffusion and hydrodynamic broadening.[97] It should also be noted that hydrodynamic broadening scales with the square of the separation channel depth, reinforcing an important performance advantage of μFFE over conventional scale FFE.

Combining equations for stream position (eq. 1.8) and width (eq. 1.13) allows the effect of experimental parameters on the resolution of a pair of streams to be predicted[97]:

$$R_s = \frac{d_1 - d_2}{(w_1 - w_2)/2} = \frac{(\mu_{total,1} - \mu_{total,2})Et}{2\left(\sqrt{\frac{w_{inj}^2}{12} + \frac{2D_1 L}{v} + \frac{h^2 d_1^2 v}{105 D_1 L}} + \sqrt{\frac{w_{inj}^2}{12} + \frac{2D_2 L}{v} + \frac{h^2 d_2^2 v}{105 D_2 L}}\right)} \quad (1.14)$$

At lower buffer velocities, where diffusion is the dominant factor for broadening, equation 7 can be approximated by[97]:

$$R_s \approx \Delta\mu E \sqrt{\frac{L}{32Dv}} \quad (1.15)$$

Under these conditions, resolution scales linearly with the electric field and inversely with the square root of the buffer linear velocity.

At higher buffer velocities and deflection distances, where hydrodynamic broadening dominates, equation 7 can be approximated by[97]:

$$R_s \approx \frac{\Delta\mu}{4h\mu} \sqrt{\frac{105L}{v}} \quad (1.16)$$

In this case, resolution is independent of the electric field and again inversely proportional to the square root of the buffer linear velocity. These equations suggest that in μFFE, high combinations of electric field and buffer linear velocity are not necessary to achieve optimal resolution. Fonslow and Bowser used equation 7 to demonstrate that in μFFE a practically achievable resolution maximum occurs at a relatively low combination of buffer linear velocity and electric field.[97] They suggested that the separation power should be maximized to spread analyte streams across the full width of the separation channel. The linear velocity of the buffer could then be adjusted to minimize stream width while also adjusting the electric field to keep the separation power, and therefore stream positions, constant. The low combination of electric field

and buffer linear velocity necessary to optimize μFFE separations is an important contrast with most microscale electrophoretic separations where high electric fields and shorter analysis times almost always improve resolution.[104,105] It is also of practical importance since it demonstrates that high pressure pumps and high voltage power supplies are not necessary to achieve optimum μFFE performance.

By analogy to capillary electrophoresis, early μFFE publications included broadening terms for wall adsorption and Joule heating.[59,89] More recently, Geiger *et al.* have demonstrated that adsorption does not broaden stream width in μFFE separations.[106] Analytes with no affinity for the wall stream directly through the separation channel. If an analyte adsorbs onto the surface it is fixed in position, moving neither in the pressure driven flow or electric field. When the analyte desorbs it returns to its original flow path determined by its mobility and the linear velocity of the separation buffer. Geiger *et al.* were even able to demonstrate effective μFFE separations of proteins that strongly adsorbed onto the glass surface of the separation channel.[106] It is important to note that while surface adsorption does not contribute to μFFE broadening in the spatial dimension, it does affect the time required for an analyte to travel through the separation channel. This temporal broadening is an important consideration for monitoring applications where μFFE is used to continuously assay a changing analyte stream over time.

Recent modeling by Okhonin *et. al.* has suggested that performing FFE separations with electric fields that are not perpendicular to the separation channel (i.e. non-orthogonal) can increase resolution at the expense of sample residence time.[107] However, fabrication challenges have prevented this approach from being confirmed experimentally at this time.

1.3.4 Detection in μFFE

Due to size and volume constraints, conventional scale FFE detection is usually performed offline via UV analysis of collected fractions.[55,57] Using a similar offline analysis strategy for μFFE is generally infeasible due to the reduced volumes and complex channels necessary to collect multiple fractions from across the separation channel. Conversely, fabrication of a separation channel with a smaller detection zone in an optically clear substrate facilitates direct online detection. A consequence of this approach is that μFFE devices are usually used in analytical separations while conventional scale FFE is more often used as a preparative separation.

Early μFFE utilized a point source detector with translational movement of the device to scan across the width of the separation channel.[59,89,108] Unfortunately, scanning limits the sampling rate of the separation and physical translation complicates reliable alignment of the optical system. μFFE systems quickly migrated to imaging detectors with a larger field of view which allowed continous imaging of the separation channel.[90-93,95,109,110] Fluorescence detection is ideal due to its high sensitivity and the wide availabilty of fluorescence microscopes. Excitation with a lamp is easily performed in an epifluorescence alignment and can illuminate a large portion of the separation channel. Limits of detection can be further improved using laser-induced flourescence (LIF).[111,112] Integration of LIF can be as simple as focusing a laser line that extends across the width of the separation channel. Emission is recorded using a standard fluorescence microscope.

Optical detection in μFFE is more analogous to imaging than a typical separation detector. In chromatography or CE separations the detector only has a short period of time to measure the intensity of a peak as it exits the column. In μFFE, continuous

injection of a sample presents a static sample stream that can be imaged over longer time periods. Turgeon *et. al.* used signal averaging over relatively long exposure times to significantly improve the detection limit of a simple μFFE LIF detector.[112] The limit of detection improved 20 to 24-fold by collecting and averaging 500 sequential images over 2 min. The observed limit of detection for fluorescein was 14 pM.

While extremely sensitive, the drawbacks of fluorescence detection are well known. Most analytes are not natively fluorescent and must be labeled with a fluorophore in order to be detected, which can dramatically affect the chemistry of those samples. Expanded strategies for label free μFFE detection are needed. Unfortunately, few examples have been reported in the literature to date. An obvious candidate for label free detection would be UV-Vis absorbance. This is challenging in microscale devices, however, due to the short optical path lengths.[113] Köler *et al.* fabricated a fused silica μFFE device that allowed deep UV fluorescence scanning for the detection of aromatics and proteins.[108] Lysozyme and chymotrypsinogen, were separated and detected using a single point scanning method and a 266 nm Nd:YAG laser. Challenges included low sensitivity due to large autofluorescence background signal from the buffer components. Wavelength versatility was was limited by the availability of deep UV laser sources. Jezierski *et al.* used cells adhered to the separation channel walls as biosensors for ATP.[114] The position of a 20 μM stream of ATP was successfully visualized using human embroyonic kidney cells doped with a calcium-sensitive fluorescent probe. The cells could be subjected to linear buffer velocities as high as 4.6 mm s^{-1} and an electric field of 100 V cm^{-1} before they would detach from the walls.

Becker *et al.* reported using surface enhanced Raman spectroscopy (SERS) as a label free detection mode for an isotachophoretic μFFE separation of myoglobin.[115]

However, the silver colloids used in SERS frequently blocked channel flow, and more experimentation is necessary to determine the feasibility of the technique.

Coupling the planar μFFE separation channel to mass spectrometry (MS) remains a significant technical challenge. Benz *et al.* recently coupled μFFE to nanospray MS by manipulating the buffer flow velocity from different inlets to sequentially shift analyte streams to an outlet channel.[116] A sample stream of 4 fluorescent dyes were visualized via fluorescence to assist directing the dye of interest into the outlet MS connection. The authors then applied this detection scheme to analyze the products of a multicomponent [3+2]-cycloannulation reaction. Only 2.5 min was necessary to fully scan the width of the separation channel.

1.4 Applications of μFFE

Design and technical improvements in μFFE devices have made continuous, stable operation over long time periods possible. The majority of μFFE applications reported to date have been static, proof of concept separations either used to assess the progress of this design development or replicate separations similar to those employed in conventional scale FFE. μFFE separations for a wide range of analytes have been reported including: fluorescent dyes,[67,78,97] peptides,[117,118] amino acids,[119] and proteins.[91,120] μFFE separation modes demonstrated to date include zone electrophoresis,[59,64,71,89,106,121,122] isoelectric focusing,[92,123-128] isotachophoresis,[90,129] and field step electrophoresis.[130] While these applications demonstrate the breadth and flexibility of μFFE separations, they generally don't perform significantly better than existing microscale separations. For μFFE to find widespread use applications that take advantage of its unique properties must be developed. The continuous nature of μFFE separations allow it to be utilized in applications not typically associated with

separations. Specifically, μFFE is particularly well suited for microscale purification and online continuous monitoring applications.

1.4.1 Microscale Purification

Sample flow rates into μFFE devices are typically 100-500 nL/min.[68,119,122,131-133] These flow rates make purifications on a low microliter scale possible in a reasonable time period. Fractionation is as simple as directing flow streams to specific outlet channels for collection. Purifications on this volume scale are challenging with limited competing technologies available.

Chartogne *et al.* used μFFE as an online bridging step between capillary isoelectric focusing (cIEF) and electrospray ionisation mass spectrometry (ESI-MS).[134] High concentrations of carrier ampholytes in cIEF cause sensitivity issues in ESI-MS due to ion suppression of proteins.[135,136] Ampholytes also cause salt buildup in the ESI interface which in turn leads to electrospray instability. μFFE was shown to effectively remove carrier ampholytes from a cIEF separation prior to ESI-MS analysis. A separation of myoglobin, carbonic anhydrase 1, and β-lactoglobulin B was demonstrated.

Jing *et al.* used μFFE to isolate aptamers for human IgE by Systematic Evolution of Ligands by EXponential enrichment (SELEX).[122] High affinity aptamers (K_d = 20 nM) were isolated within 2-4 rounds of selection. The continuous nature of the μFFE separation greatly simplified the reliability of the fraction collection. Significantly larger volumes could be enriched using μFFE selections (3 μL) than was possible in similar CE based selections (~8 nL). The increased sample volume allowed 1.8×10^{14} ssDNA ligands to be assessed in every round of selection, a 300-fold increase over CE-SELEX.

Podszun *et al.* used μFFE to concentrate viable bacteria from mL to μL volumes.[68] Charged bacteria samples were concentrated in a tris-borate-EDTA buffer at a constant current of 250 μA. Bacteria were continuously streamed into the μFFE device at 300 nL/min where they were deflected toward the electrode, which was blocked by a gel barrier. Bacteria were collected at the barrier for 30 min. The polarity of the electrode was then flipped to migrate the bacteria back into the separation channel for collection. Enrichment efficiencies of up to 80% were reported. Concentration factors of 13 and 25 were reported for 100 μL and 200 μL samples, respectively.

Kostal *et al.* used μFFE to assess the electrophoretic properties of mitochondria isolated from rat myoblasts.[131] The distribution of mitochondria mobilities were assessed in less than 30 s. The mobility distributions correlated well with CE-LIF measurements of the same sample. The benefits of the μFFE separation included less reagents, lower electric field, and shorter analysis time when compared to the CE method. The lower electric field of the μFFE separation was particularly important since it was determined that extrapolation to account for particle polarization was not necessary, eliminating the need to make measurements across a range of separation potentials.

1.4.2 Continuous Monitoring

The ability of μFFE to separate and analyze a continous analyte stream makes the technique ideally suited for online monitoring applications. The temporal response of the separation is only limited by the exposure time of the detection system, which can be 100 ms or faster.[112] μFFE analyses offer the potential to combine the selectivity of a separation with the time response typically associated with a electrochemical or optical sensor.

Fonslow and Bowser used gradient μFFE as an efficient way to optimize electrophoretic separation conditions.[137] μFFE was used to continuously monitor a separation of NBD-F labeled amino acids as the separation buffer was increased from 0 to 50 mM hydroxypropyl-β-cyclodextrin (HP-β-CD) over a 5 min period. μFFE separations were recorded every 5 s, allowing the resolution to be assessed at 60 different HP-β-CD concentrations. This nearly continuous coverage allowed the optimum HP-β-CD concentration to be unambiguously identified in 5 min. A similar optimization using CE would take several hours.

Turgeon *et al.* used gradient μFFE to measure aptamer affinities for their targets across a range of ligand concentrations.[132] A constant concentration of aptamer was mixed in an online reaction tee with an increasing concentration of ligand. μFFE was used to continuously measure the ratio of bound to free aptamer as the ligand concentration was increased over a 5 min period. μFFE separations were recorded every 1 s allowing the equilibrium to be assessed at 300 distinct ligand concentrations in 5 min. Aptamers for IgE and HIV-RT were assessed. The nearly continuous coverage of the binding isotherm allowed the affinity and stoichiometry of the equilibrium to be assessed with greater confidence.

1.4.3 2D Separations Utilizing μFFE

Under sampling has been shown to have detrimental effects on peak capacity in 2D separations.[31] The cycle time of the ^{2}D separation plays a critical role in maximizing attainable peak capacity in a 2D separation. Cycle times as fast as 12-21 seconds still have destructive effects on peak capacity when the ^{1}D separation is shorter than 30 minutes. To overcome this under sampling limitation comprehensive 2D separations

often couple a very slow first dimension separation with a faster than optimum second dimension separation.

Historically, FFE has been used in off-line 2D separations to collect fractions for later analysis on RPLC.[138,139] However these separations offered limited peak capacity in long analysis times (10 hours, 12 peaks/min). However, the continuous nature of FFE separations make it ideally suited to act as the second dimension of a comprehensive 2D separation. Since the eluent of the ^{1}D separation can be streamed directly into the μFFE separation channel, the cycle time effectively becomes the amount of time necessary to detect an analyte. The benefit of this method becomes obvious when compared to other current ^{2}D separation cycle times. Assume an analyte in a 5 minute 1D separation with a 4σ peak width of 4 seconds is sampled by LC, CE, and μFFE as ^{2}D separations. A 12 second cycle time[32,33] for LC would only sample the peak once, and results in only 18% of 1D peak capacity retained. A 1 second cycle time for CE,[35] would sample the peak 4 times and result in 90% peak capacity retained. A μFFE separation coupled with a CCD camera with an exposure time of 100 msec, would result in 40 samples and >99% peak capacity retained. Continuous μFFE separation effectively eliminates under sampling as a limitation, allowing peak capacity to be increased significantly without increasing the first dimension separation time.

Geiger *et al.* coupled nano-liquid chromatography (nLC) with μFFE to perform 2D separations of peptides and amino acids.[119,140] Coupling was achieved via a connection capillary introduced directly into the μFFE separation channel to make a zero dead volume connection. Analyte peaks were streamed directly into the μFFE separation channel as they eluted from the nLC column. No complicated modulation or valving was necessary to couple the two separations. A separation of a fluorescently labeled BSA

tryptic digest yielded an ideal 2D peak capacity of 1,320 in a 5 min separation window (264 peaks/min).[119]

Technical restrictions currently limit further improvements to 2D nLC × μFFE analysis time. The speed of the first dimension nLC separation is restricted by how fast the pumps can generate a gradient and transport eluent to the column, limiting the total analysis time of nLC × μFFE separations to ≥11 min.[117,119] Efficient mass transfer becomes increasingly problematic as nLC separation times decrease. CE is not afflicted by either of these limitations. High-speed CE separations with high efficiency can be achieved with a combination of short separation channels, high separation potential and efficient dispersion of Joule heating.[141]

1.5 Scope of Thesis

The advent of "-omics" fields have increased interest in a rising number of analytes. The tens to hundreds of thousands of analytes that can be found in a single cell have reduced 1D separation techniques effectiveness for analyzing biological samples. Even the more powerful 2D comprehensive on-line separations have been overpowered by the magnitude of analytes found. The ideal peak capacity of a 2D separation is limited by the under sampling of ^{1}D peaks, and the orthogonality between the two separation modes. Chapter 2 will detail a novel separation platform coupling CE to μFFE. A zero dead volume connection between the two separation modes will be shown, and measuring the peak widths before and after the connection will show the simple connection is effective. The high peak capacity generated with CE×μFFE will show the promising potential of the technique. Chapter 3 will detail an exploration of orthogonality of CE×μFFE by using different μFFE separation modes. The significance of separation modes in orthogonality will be examined to optimize peak capacity.

Chapter 4 will discuss a new label-free detector for use in µFFE. The use of LIF requires samples to be fluorescently labeled, which can adversely affect sample dimensionality. Figures of merit will detail the promising nature of this detection apparatus. Lastly, Chapter 5 will summarize the work done, and provide an outlook on future applications for the technology.

Chapter 2

High-Speed, Comprehensive, Two Dimensional Separations of Peptides and Small Molecule Biological Amines Using Capillary Electrophoresis Coupled with Micro Free Flow Electrophoresis

Johnson, A. C.; Bowser, M. T. *Anal. Chem.* **2017**, *89*, 1665-1673.

2.1 Summary

Two-dimensional (2D) separations are able to generate significantly higher peak capacities than their one dimensional counterparts. Unfortunately, current hyphenated 2D separations are limited by the speed of the second dimension separation and the consequent loss of peak capacity due to under sampling of peaks as they elute from the first dimension separation. Continuous micro free flow electrophoresis (μFFE) separations eliminate under sampling as a limitation when incorporated as the second dimension of a 2D separation. In the current manuscript we describe the first coupling of capillary electrophoresis (CE) with μFFE to perform 2D CE × μFFE separations. The CE separation capillary was directly inserted into the μFFE separation channel using an edge on interface. Analyte peaks were streamed directly into the μFFE separation channel as they migrated off the CE capillary. No complicated injection, valving or voltage changes were necessary to couple the two separation modes. 2D CE × μFFE generated an ideal peak capacity of 2,592 in a 9 min separation of fluorescently labeled peptides (7.6 min separation window, 342 peaks/min). Data points were recorded every 250-500 msec (>8 data points/peak), effectively eliminating under sampling as a source of band broadening. CE × μFFE generated an ideal peak capacity of 1885 in a 2.7 min separation of fluorescently labeled small molecule bioamines (1.8 min separation window, 1053 peaks/min). Peaks in the 2D CE × μFFE separation of peptides covered 30% of the available separation space, resulting in a corrected peak capacity of 778 (102 peaks/min). The fractional coverage of the 2D CE × μFFE separation of small molecule bioamines was 20%, resulting in a corrected peak capacity of 377 (209 peaks/min).

2.2 Introduction

Over the past three decades, 2D separations have been developed to provide the increased peak capacity necessary to separate complex biomedical and environmental samples. As described by Giddings, the ideal peak capacity of a 2D separation ($n_{c,2D}$) is the product of the individual first (${}^{1}n_c$)and second dimension (${}^{2}n_c$) peak capacities[28]:

$$n_{c,2D} = {}^{1}n_c \times {}^{2}n_c \quad (2.1)$$

Coupling two separations together therefore has the potential to dramatically improve peak capacity. Many combinations of separation modes have been coupled including LC × LC,[142-145] LC × GC,[146,147] LC × CE,[148-151] GC × GC,[152-157] CE × CE,[35,158-163] and IC × CE[164]. For these hyphenated 2D approaches to be effective analyte peaks must be sampled with sufficient frequency by the second dimension separation as they elute off the first dimension column. The second dimension separation must therefore cycle faster than the width of the peaks that elute from the first dimension separation. Peak capacity generated by the first dimension separation is lost if this criterion is not met. Davis *et al.* quantified the effect that under sampling can have on the 2D peak capacity[43]:

$$n_{c,2D} = {}^{1}n_c \times {}^{2}n_c \times f \times \frac{1}{\beta} \quad (2.2)$$

$$\frac{1}{\beta} = \frac{1}{\sqrt{1+3.35*\left(\frac{t_S}{{}^{1}w}\right)^2}} \quad (2.3)$$

where *f* is the fractional coverage of the available separation space, 1/β is the fraction of peak capacity retained from the first dimension, t_s is the cycle time of the second dimension separation and ${}^{1}w$ is the average baseline width of peaks in the first dimension separation. Challenges associated with cycling the second dimension

separation fast enough to avoid losses in peak capacity due to under sampling limits the speed with which the first dimension separation can be operated, resulting in relatively long analysis times.

The high-speed separations possible using capillary electrophoresis (CE) can be used to address the under sampling limitations of hyphenated 2D separations.[165] Bushey *et al.* were the first to couple HPLC with CE to perform a 2D separation.[148] CE separations were performed every 1 min, generating an ideal peak capacity of 420 in a 245 min analysis (1.7 peaks/min). Moore and Jorgenson used optical gating to perform second dimension CE separations as fast as 2.4 s, generating an ideal peak capacity of 650 in a 2.8 min HPLC separation window (232 peaks/min).[166] Michels *et al.* first described a directly coupled, online 2D CE × CE separation in 2002.[167] Second dimension CE separations were performed in 5 min. Peaks were held stationary in the first dimension CE capillary during the second dimension analysis to accommodate this relatively long separation time. The complete 2D CE × CE analysis required 8 h. Improvements in CE separation times and transfer efficiency increased the ideal peak capacity to 600 in a 50 min 2D CE × CE separation (12 peaks/min).[168] Ramsey *et al.* were the first to integrate a 2D CE × CE separation into a microfluidic device.[35] Second dimension CE separations were performed every 1.0 s, generating an ideal peak capacity of 4200 in 15 min (280 peaks/min). Through instrumental optimization Henley and Ramsey were able to increase the performance of their microfluidic 2D CE × CE separations to generate an ideal peak capacity of 1950 in 5.4 min (361 peaks/min).[162] Shadpour and Soper demonstrated relatively inexpensive fabrication of a microfluidic 2D CE × CE device using hot embossing in poly(methyl methacrylate) (PMMA).[169] They were able to generate an ideal peak capacity of 1000 in a 12 min separation (83 peaks/min).

While integration of CE as the second dimension separation has allowed liquid phase 2D separations to be performed on reasonable timescales for the first time, it is unclear how much further improvement can be made using this approach. Hyphenated 2D CE × CE with second dimension separations on a 1 s timescale require complex instrumentation to modulate injections at the interface and high sensitivity detectors to detect the miniscule analyte volumes used in high-speed CE separations. We have recently introduced an alternative approach that uses micro free flow electrophoresis (μFFE) as a second dimension separation.[117,119] In μFFE, sample is continuously streamed through a planar separation channel in which an electric field is applied perpendicularly.[78] Analytes are deflected laterally based on their electrophoretic mobilities as they travel through the electric field. The first μFFE device was fabricated in silicon by Raymond et. al., in 1994.[59] More recently, μFFE devices have been fabricated in glass,[78,170] and polydimethylsiloxane (PDMS).[91,171] μFFE has been used to separate a wide range of analytes including: mitochondria,[172] aptamers,[170,173] fluorescent dyes,[67,78,97] peptides,[117,118] amino acids,[119] and proteins.[91,120] Novel applications of μFFE include aptamer-ligand affinity measurements,[173] aptamer isolation,[170] CE buffer optimization,[174] and mitochondria isolation.[172]

Geiger *et al.* coupled nLC with μFFE to perform 2D separations of fluorescently labeled peptides and amino acids.[117] Eluent from the first dimension nLC separation was directly streamed into the μFFE device eliminating the complicated injection modulation necessary in other hyphenated 2D techniques. 2D nLC × μFFE was able to generate an ideal peak capacity of 2,352 in a 10 min separation window (235 peaks/min). The effective peak capacity was reduced to 776 (78 peaks/min) after the fractional coverage of available separation space was considered. With further optimization an ideal peak capacity of 1320 and a corrected peak capacity of 694 were

obtained in a 5 min separation window (264 and 139 peaks/min, respectively).[175] Technical restrictions currently limit further improvements to 2D nLC × μFFE analysis time. The speed of the first dimension nLC separation is restricted by how fast the pumps can generate a gradient and transport eluent to the column, limiting the total analysis time of nLC × μFFE separations to ≥11 min.[117,119] Efficient mass transfer becomes increasingly problematic as nLC separation times decrease. CE is not afflicted by either of these limitations. High-speed CE separations with high efficiency can be achieved with a combination of short separation channels, high separation potential and efficient dispersion of Joule heating.[141] In the current manuscript we present the first demonstration of 2D CE × μFFE separations. This combination of separation modes is ideally suited to achieve even faster 2D separations than previously possible while maintaining high peak capacities.

2.3 Experimental

2.3.1 Buffers and Solutions

All solutions were made using deionized water (18.3 MΩ, Milli-Q; Millipore, Bedford, MA) and filtered with a 0.22 μm nitrocellulose membrane filter (Fisher Scientific, Fairlawn, NJ). For separations of fluorescent dyes, the CE separation buffer was 25 mM N-cyclohexyl-3-aminopropanesulfonic acid (CAPS, Sigma-Aldrich, St. Louis), 35 mM α-cyclodextrin (α-CD, CTD, Inc., Alachua, FL), adjusted to pH 10.01 with 1 M NaOH (Macron Chemicals, Center Valley, PA) in water. For the BSA digest separations the CE buffer was 25 mM CAPS, 35 mM α-CD, and 1 mM tetraethylenepentamine (TEPA, Sigma-Aldrich, St. Louis) adjusted to pH 10.01 with 1 M NaOH in water. For the small molecule bioamine separations the CE buffer was 25 mM CAPS, and 35 mM α-CD adjusted to pH 10.01 with 1 M NaOH in water. For separations of fluorescent dyes the

μFFE separation buffer was 25 mM 2-(N-morpholino)-ethanesulfonic acid hydrate (MES, Sigma-Aldrich, St. Louis), and 300 μM Triton X-100 (Sigma-Aldrich, St. Louis), adjusted to pH 5.2 with 1 M HCl (Macron Chemicals, Center Valley, PA) in 95:5 H_2O:MeOH (HPLC Grade, Fischer Scientific, Waltham, MA). For BSA digest and small molecule bioamine separations the μFFE buffer was 25 mM MES, with 1 mM TEPA, 300 μM Triton X-100 (Sigma-Aldrich, St. Louis), adjusted to pH 5.2 with 1 M HCl in 95:5 H_2O:MeOH. Poly (ethylene oxide) (PEO) (Sigma-Aldrich, St. Louis) was dissolved in 0.1 M HCl to 0.2% by mass at 90 ^oC with stirring overnight.

2.3.2 BSA Digestion and Labeling

Bovine serum albumin (BSA, Sigma Aldrich) was digested with trypsin following a standard digestion procedure. 1.0 mg of BSA was dissolved in 1.00 mL of 25 mM $NaHCO_4$ with 6.0 M urea. A standard reduction was then performed using tris(2-carboxyethyl)phosphine, (TCEP, Pierce Chemical, Rockford, IL) at 37 ^oC for 1 h in the dark, followed by alkylation with iodoacetamide (IAA, Sigma Aldrich) for 1 h at 37 ^oC in the dark. Sequencing grade trypsin (Promega, Madison, WI) was then used in a 1:30 w/w ratio to digest the BSA sample overnight at 37 ^oC. The newly digested sample was lyophilized under vacuum and stored at -80 ^oC until analysis. The BSA sample was thawed and dissolved in 1.00 mL of CE separation buffer. 4-fluoro-7-nitro-2,1,3-benzoxadiazole (NBD-F) (TCI, Portland, OR) was added in a 5:1 label to peptide molar ratio and incubated at 80 ^oC for 20 min to complete the labeling reaction. The sample was filtered using a 0.45 μm cellulose acetate syringe filter (Sterlitech, Kent, WA) prior to analysis. Small molecule bioamines were labeled in a similar fashion. 100 μM solutions of each amine were labeled with NBD-F in a 3:1 ratio.

2.3.3 µFFE Device Fabrication

A µFFE device with an edge on capillary inlet was fabricated according to a previously described procedure.[117] Briefly, an initial round of photolithography was performed on two 1.1 mm borofloat wafers (Precision Glass & Optics, Santa Ana, CA) to create an 85 µm deep capillary channel. The process was repeated to etch 30 µm deep electrode channels. A third photolithography step was performed to create a 1 cm wide × 2.5 cm long × 10 µm deep separation channel. 150 nm layers of Ti and Au were deposited on one of the wafers using a Temescal electron beam evaporator. Standard photolithography was performed to remove unwanted Ti and Au, leaving patterned electrodes in the side channels. 1 mm access holes were drilled for inlet, outlet, and electrode connections and a ~90 nm thick layer of amorphous silica was deposited onto the second wafer. Both wafers were aligned under a microscope and bonded anodically (900 V, 3 h, 450 °C, 5 µbar) using a Karl Suss SB-6 wafer bonder (Munich, Germany). When the two wafers were bonded the combined final depths in the completed µFFE device for the capillary, electrode and separation channels were 125 µm (~250 µm wide), 80 µm, and 20 µm, respectively. The bonded µFFE device was diced at the University of Minnesota Electrical Engineering Machine Shop to expose the capillary inlet channel. NanoPorts (Upchurch Scientific, Oak Harbor, WA) were aligned and adhered using epoxy rings (IDEX, Lake Forest, IL) over the inlet and outlet access holes. Connecting wires were bonded to the electrodes using silver conductive epoxy (MG Chemicals, Surrey, BC, Canada). The separation chamber was rinsed with 1 M NaOH solution at 1.0 mL/h for ~14 h to remove amorphous silica. Finally, the µFFE device was placed on a hotplate set to 120 ^{o}C and vacuum was applied to the separation channel while a 30 cm long × 20 µm i.d. × 150 µm o.d. fused silica capillary (Polymicro Technologies, Phoenix, AZ) was placed into the capillary channel. The CE separation

capillary was bonded into place using Crystalbond 509 (Polymicro Technologies, Phoenix, AZ). Figure 2.1 shows the completed µFFE device with the CE capillary inserted.

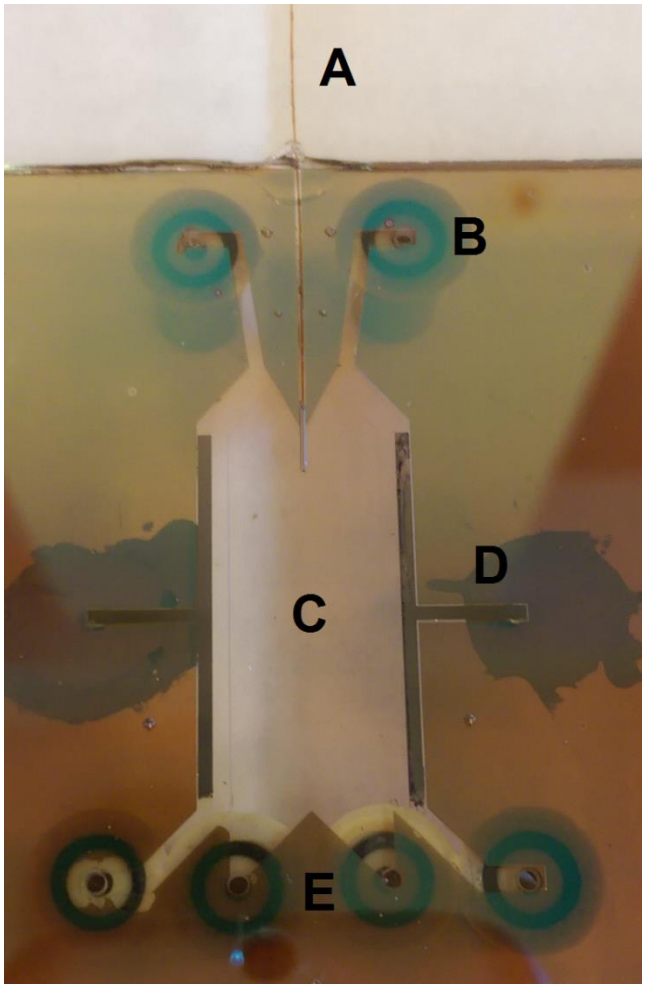

Figure 2.1 Image of a fully fabricated µFFE device. A) CE separation capillary. B) Buffer inlet channels. C) µFFE separation channel (2.5 cm long × 1 cm wide × 20 µm deep). D) Electrodes. E) Buffer outlet channels.

2.3.4 2D CE × µFFE Separations

The µFFE device channels were coated with PEO to suppress electroosmotic flow using a previously reported capillary coating method.[176] 0.1 M HCl was perfused through the device at 6 mL/min for 10 min, followed by 0.2% PEO by mass in 0.1 M HCl at 3 mL/min for 10 min. A CE instrument was assembled in house using a machined

acrylic sample holder, a Spellman CZE 1000R high voltage power supply (Spellman, Hauppauge, NY), and a platinum wire (0.25 mm diameter, Goodfellow Cambridge Ltd., Huntingdon, England) soldered to a 35 kV rated high voltage lead cable (Allied Wire & Cable Inc., Collegeville, PA). The CE separation capillary was conditioned with 1 M NaOH at 0.3 µL/min for 20 min, followed by separation buffer at 0.3 µL/min for 20 min. Samples were loaded onto the separation capillary electrokinetically at a voltage of 15 kV (0.5 kV/cm) for 15 s. After injection, the inlet of the capillary was placed in separation buffer and a separation voltage of 30 kV (1 kV/cm) was applied unless otherwise noted. The µFFE separation channel was perfused with µFFE separation buffer throughout the 2D separations using a syringe pump (Harvard Apparatus, Hollison, MA) at a flow rate of 0.5 mL/min (~0.15 cm/s). The µFFE separation potential was set to the maximum value that gave stable stream trajectories and did not migrate analytes into the side channels. For separations of BSA digests a 175 V potential was applied to the left electrode of the µFFE device while the right electrode was held at ground. For separations of small molecule bioamines a 225 V potential was applied to the left electrode of the µFFE device while the right electrode was held at ground. The CE separation capillary was rinsed after every other run using 0.1 M NaOH at 0.3 µL/min for 10 min.

2.3.5 Data Collection and Processing

A Cascade 512B CCD camera (Photonics, Tuscon, AZ) was fitted to an AZ100 Stereomicroscope (Nikon Corp., Tokyo, Japan) with a GFP bandpass emission filter cube (Nikon Corp.) containing two bandpass filters (450-490 and 500-550 nm) and a dichroic mirror (495 nm cutoff) for fluorescence imaging. A 150 mW, 488 nm emission argon-ion laser (Melles Griot, Carlsbad, CA) was expanded into a ~2.5 cm×~150 µm line and used as the excitation source for laser induced fluorescence (LIF) detection.[112]

The entire setup was enclosed in a black, light tight box. The acquisition rates for 1D CE and 2D CE × µFFE separations of BSA digests were 4 and 2 Hz, respectively. The acquisition rate for 1D CE and 2D CE × µFFE separations of small molecule bioamines was 4 Hz. The CE power supply was controlled using LabVIEW (National Instruments, Austin, TX) and set to trigger the CCD data acquisition in MetaVue (Molecular Devices, Sunnyvale, CA) once the separation voltage was applied. Data was extracted and then analyzed with in-house Matlab programs. Peak Finder (panomics.pnnl.gov/downloads/PeakFinder.zip) was used to analyze extracted CE electropherograms and µFFE linescans. Orthogonal background correction was performed on the 2D separations as outlined by Filgueira, *et. al.*[177]

2.4 Results and Discussion

Figure 2.2 illustrates the mechanism of the 2D CE × µFFE separation. Analytes are separated in the first dimension using identical conditions as traditional 1D CE. The exit of the CE capillary is inserted directly into the µFFE separation channel (see Figure 2.1). The potential at the CE inlet is determined by the CE power supply. The potential at the exit of the CE separation capillary is determined by the potential at its position in the µFFE electric field (~90-115 V). The CE and µFFE separations share a common ground (i.e. the right electrode in Figure 2.2). As analytes migrate off the CE capillary they immediately enter the µFFE separation channel. The trajectory of the peak through the µFFE separation channel is determined by the analyte's migration in the perpendicular electric field and the buffer flow rate. The time it takes for an analyte to cross the µFFE detection zone is determined by the first dimension CE separation. The position that an analyte crosses the µFFE detection zone is determined by the second dimension µFFE separation. A plot of CE separation time *vs.* µFFE deflection distance

therefore gives a 2D separation plot. The simplicity of the interface should be emphasized. No complicated timing, voltage changes or valving is necessary to couple the two separations. µFFE is a continuous separation technique, effectively eliminating under sampling as a limitation to peak capacity. The sampling rate in 2D µFFE separations is only limited by the exposure time of the CCD used to measure fluorescence across the detection zone (100-500 ms).

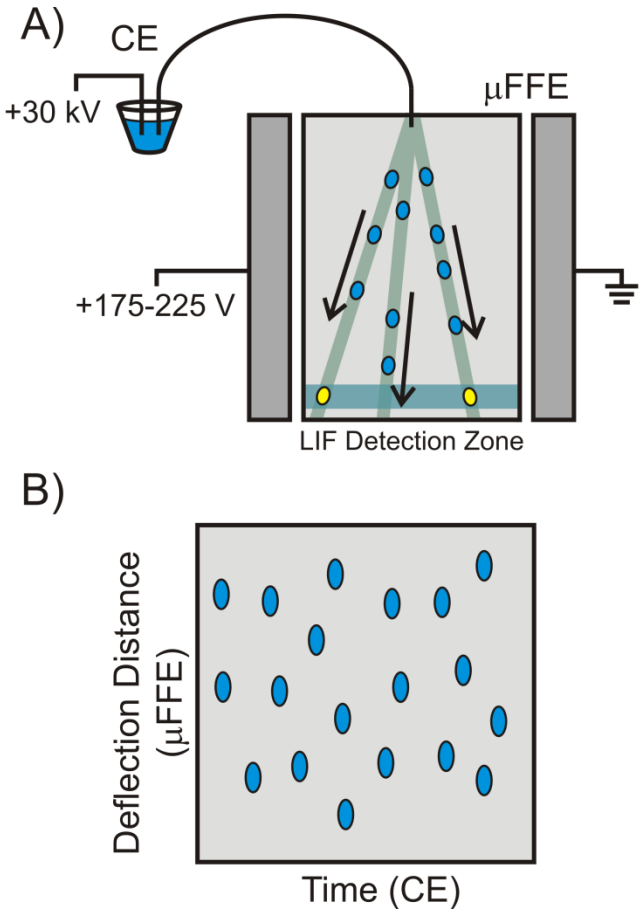

Figure 2.2 (A) Schematic demonstrating the mechanism of a 2D CE × µFFE separation. Analyte peaks migrate off the CE capillary directly into the µFFE separation channel where they are deflected laterally based on their mobility in the second dimension separation. The time required to reach the LIF detection zone is determined by the first dimension CE separation. The position that an analyte peak crosses the LIF detection zone is determined by the second dimension µFFE separation. B) A plot of CE separation time *vs.* µFFE deflection distance gives a 2D separation.

2.4.1 CE × µFFE Interface

One of the criteria to perform an effective 2D separation is that no remixing can occur at the interface between the two separations. We have previously demonstrated that the direct, edge on interface shown in Figure 1 is not a significant source of band broadening when used to couple 2D nLC × µFFE separations.[117] Interfacing CE with a second dimension separation is more challenging than LC due to the lower flow rates exiting the capillary. For example, the nLC flow rate used in our earlier 2D nLC × µFFE separations was 300 nL/min, more than sufficient to clear the ~1 nL dead volume at the interface.[117,119] The EOF exiting the 20 µm capillary used in our 2D CE × µFFE separations was only 86 nL/min. We were concerned that the lower flow rate exiting the CE capillary would not efficiently clear the dead volume at the interface. Figure 2.3 compares an electropherogram of rhodamine 123, rhodamine 110 and fluorescein measured on the CE capillary with one recorded after the interface in the µFFE separation channel.

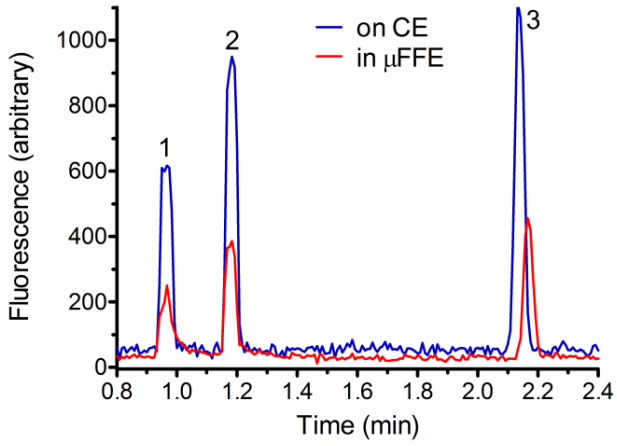

Figure 2.3 Comparison of CE electropherograms for 1) rhodamine 123, 2) rhodamine 110 and 3) fluorescein recorded before the CE-µFFE interface in the CE separation capillary (blue) and after the CE-µFFE interface in the µFFE separation channel (red). Electropherograms were aligned to facilitate direct comparison of peak width before and after the CE-µFFE interface.

Peak shapes on the CE capillary and in the μFFE separation channel were nearly identical, indicating that no significant broadening occurs at the interface. The baseline peak width for fluorescein was 7.08 s both on capillary and after the interface. The baseline widths of rhodamine 110 were 6.60 s and 7.08 s in the CE capillary and μFFE separation channel, respectively. Rhodamine 123 was the only peak that showed significant broadening in the μFFE separation channel (6.48 s on capillary *vs.* 7.80 s in the μFFE separation channel). We have previously demonstrated that interactions between positively charged analytes such as rhodamine 123 and the negatively charged silanols of the μFFE surface induce temporal broadening as analyte peaks travel through the separation channel.[106] The μFFE separation channel was coated with PEO and TEPA was added to the separation buffer for all further experiments to mediate the contribution of surface adsorption to broadening in the temporal dimension.

2.4.2 1D CE Separation of BSA Digest

Figure 2.4 shows an electropherogram from a traditional 1D CE separation of an NBD labeled, BSA tryptic digest. Clearly, the complexity of the sample overwhelms the peak capacity of the 1D CE separation. A tryptic digest of BSA is expected to produce 74 unique peptide fragments, as predicted by the ExPASy peptide cutter tool.[178] Approximately 41 peaks were observed, of which only 4 were baseline resolved. Ten peaks were chosen at random for further analysis. The average efficiency of these 10 peaks was 93,000 theoretical plates and the average peak width was 6.01 s. Considering this peak width, the 1D CE separation generated a peak capacity of 76 in a 7.6 min migration window (10 peaks/min).

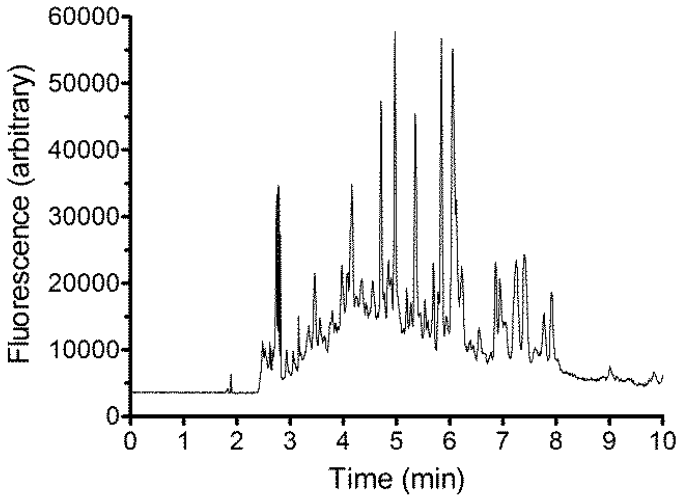

Figure 2.4 1D CE electropherogram of an NBD labeled BSA tryptic digest. CE buffer: 25 mM CAPS, 35 mM α-CD, 1 mM TEPA, pH = 10.01.

2.4.3 2D CE × μFFE Separation of BSA Digest

Figure 2.5A shows a 2D CE × μFFE analysis of the same NBD labeled BSA digest separated by 1D CE in Figure 2.4. It is important to note that no changes in the first dimension CE separation conditions were necessary to couple with μFFE. A pH difference (CE buffer pH=10.01, μFFE buffer pH=5.2) and buffer additive (35 mM α-CD in the CE buffer) were used to generate orthogonality between the two separation dimensions. Others have demonstrated that changing the mobile phase pH between two reversed phase columns is a simple way to achieve high fractional coverage in 2D LC×LC separations of peptides.[42] α-CD was also added to the first dimension CE buffer since we have previously shown that it improves the selectivity of separations of NBD labeled amino acids.[179] Analytes must cross from the first dimension CE buffer into the second dimension μFFE buffer at the interface. Little diffusion is expected during the 10-20 s transit time through the μFFE separation channel.[97] A discrete boundary between the two buffers is therefore expected to persist as the CE buffer streams through the

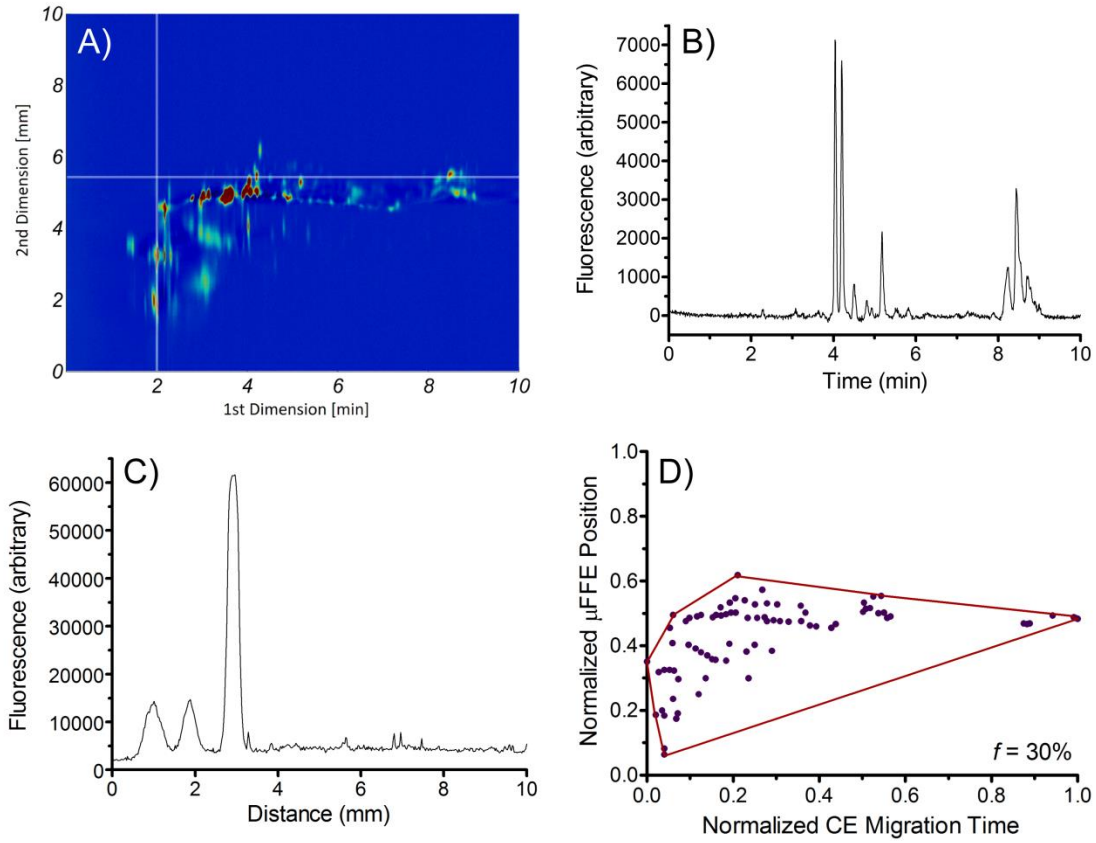

Figure 2.5 A) A 2D CE×µFFE separation of an NBD labeled BSA tryptic digest. CE buffer: 25 mM CAPS, 35 mM α-CD, 1 mM TEPA, pH = 10.01. µFFE buffer: 25 mM MES, 1 mM TEPA, 300 µM Triton X-100, pH = 5.2, 95:5 H2O:MeOH. The µFFE potential is positive at the top of the plot. B) Electropherogram extracted from the 2D CE×µFFE separation at 5.84 mm (see horizontal line in A)). C) µFFE linescan extracted from the 2D CE×µFFE separation at 2.1 min (see vertical line in A)). The µFFE potential is positive at the left of the plot. D) Contour hull plot of the 2D CE×µFFE separation shown in A) depicting the fraction of available separation space where peaks are found.

µFFE separation channel. It should be noted that stacking or de-stacking could occur in the µFFE dimension if analytes change their mobility as they cross this boundary, similar to what is observed in CE when there is a mismatch between the sample matrix and the separation buffer.81 peaks were observed in the 9 min 2D CE × µFFE separation. The number of observed peaks is greater than the 74 unique peptide fragments predicted by the ExPASy peptide cutter tool.[178] Labeling with NBD can increase the complexity of peptide samples due to the presence of multiple labeling sites.[119] The positions of peaks

in replicate analyses were reproducible in both the CE and μFFE dimensions. Figure 2.6 shows three replicate CE × μFFE separations of the same NBD-F labeled BSA digest. 36 peaks were chosen at random from across the 2D separation and were assessed for reproducibility. The relative standard deviation for peaks in the CE and μFFE dimensions were 7.9% and 0.7%, respectively. When measured on a different day the positions of peaks in the CE and μFFE dimensions only changed 9.5% and 2.2%, respectively. It should be emphasized that observed errors in peak position were highly correlated, causing a shift in the overall peak pattern rather than a redistribution of peaks or loss of resolution. Figure 2.5B shows an electropherogram extracted from the 2D CE × μFFE separation. Coupling with the second dimension μFFE separation dramatically decreases the complexity of the electropherogram when compared with the 1D CE separation shown in Figure 2.4. The narrow peaks also demonstrate that the efficiency and peak capacity generated by the CE separation is retained. Seventeen well-resolved peaks were chosen at random from several extracted electropherograms for further analysis. The average baseline width of these peaks in the first dimension CE separation was 4.2 s and the average efficiency was 94,000 theoretical plates. Considering this average peak width, the first dimension CE separation generated a peak capacity of 108 in a 7.6 min separation window.

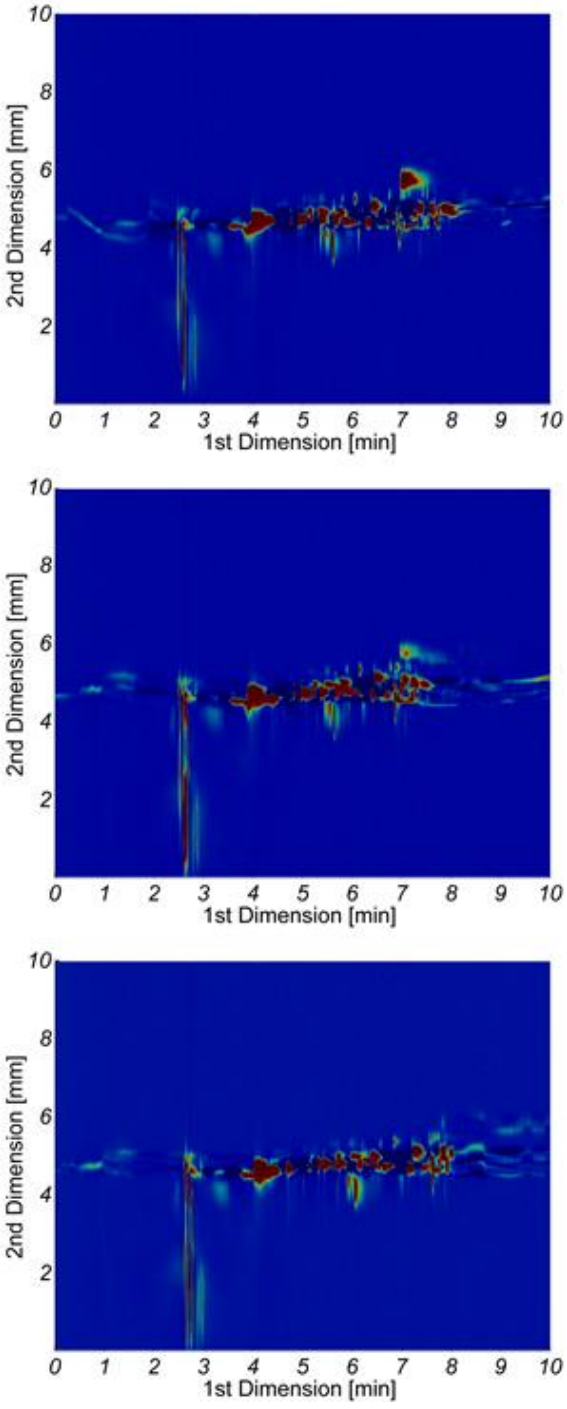

Figure 2.6 Three replicate CE×μFFE analyses of an NBD labeled BSA tryptic digest. CE buffer: 25 mM CAPS, 35 mM α-CD, 1 mM TEPA, pH = 10.01. μFFE buffer: 25 mM MES, 1 mM TEPA, 300 μM Triton X-100, pH = 5.2, 95:5 H2O:MeOH. The μFFE potential is positive at the top of the plot. The relative standard deviations for peaks in the CE and μFFE dimensions were 7.9% and 0.7%, respectively.

The CCD recorded a fluorescent image every 0.5 s. At this data acquisition rate, >8 data points were recorded across each peak giving rise to the well-defined peaks shown in Figure 2.5B. According to equation 3, at this acquisition rate <2% of the first dimension peak capacity is lost due to under sampling. The observed first dimension peak widths in the 2D CE × µFFE BSA digest separations were actually lower than those observed for the 1D CE separation. This discrepancy is likely the result of the high peak density of the 1D CE separation, which makes it difficult to make accurate peak width estimates.

Figure 2.5C shows an example of a µFFE line scan extracted from the 2D CE × µFFE separation. The same 17 peaks that were used to assess peak capacity in the first dimension CE separation were used to assess the performance of the second dimension µFFE separation. The average baseline width of peaks in the µFFE dimension was 0.42 mm. The pixel width in the CCD image was 21 µm giving rise to >19 data points across each peak in the µFFE dimension. Well shaped peaks are observed, demonstrating the potential of this technique for analysis and quantitation. Considering the 10 mm width of the µFFE separation channel, the second dimension peak capacity is 24. Combining the observed first dimension CE and second dimension µFFE peak capacities gives an ideal 2D CE × µFFE peak capacity of 2592 (i.e., 108×24) in a 7.6 min separation window (342 peaks/min).

The ideal 2D peak capacity does not account for the useable fraction of available separation space. Figure 2.5D delineates the fraction of separation space where peaks are found in our 2D CE × µFFE analysis of a NBD labeled BSA digest using a minimum convex hull plot.[47] To generate this plot, the position of each peak maximum is marked and a polygon is drawn through the outermost points using straight lines with internal

angles ≤180^0. Fractional coverage (*f*) is determined by comparing the area of the polygon to the area of the available separation space. Using this method, the fractional coverage of our 2D CE × µFFE analysis of a NBD labeled BSA digest was estimated to be 30%. Accounting for fractional coverage (see equation 2) the corrected peak capacity of our 2D CE × µFFE analysis of a NBD labeled BSA digest was 770 in a 7.6 min separation window (102 peaks/min).

2.4.4 1D CE and 2D CE × µFFE Separations of Small Molecule Bioamines

Figure 2.7 shows a 1D CE separation of a mixture of 25 NBD-labeled, small molecule, biological amines. As with the BSA digest, the complexity of this mixture overwhelms the peak capacity of the 1D CE separation.

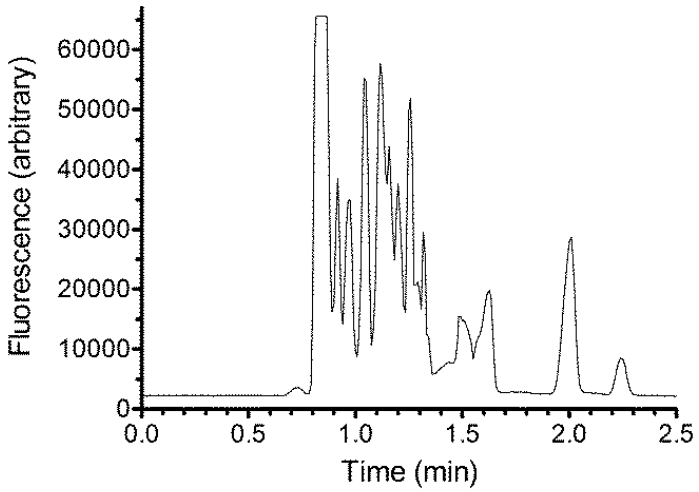

Figure 2.7 1D CE electropherogram of a mixture of 25 NBD labeled small molecule bioamines. CE buffer: 25 mM CAPS, 35 mM α-CD,, pH = 10.01.

Figure 2.8A shows a 2D CE × µFFE separation of the same mixture. Again, no modification of the first dimension CE separation conditions was necessary for coupling with the second dimension µFFE separation. Clearly, the increased peak capacity of the 2D separation improved resolution with 23 distinct peaks identified in a 3 min separation.

Peak properties in the CE and μFFE dimensions were determined. The average baseline width of peaks in the CE first dimension was 1.65 s and the average efficiency was 21,000 theoretical plates. Considering this peak width, the first dimension CE separation generated a peak capacity of 65 in a 1.8 min separation window. The CCD recorded images every 0.25 s, generating >6 data points for every peak. The average baseline width of peaks in the μFFE dimension was 0.34 mm, generating a peak capacity of 29. The ideal peak capacity of the 2D CE × μFFE separation of small molecule bioamines was therefore 1885 in a 1.8 min separation window (1053 peaks/min). Figure 2.8F shows the convex hull plot for the 2D CE × μFFE separation. Peaks only covered 20% of the available separation space giving rise to a corrected peak capacity of 369 (206 peaks/min). Sample dimensionality in the small molecule amine mixture is relatively low, especially after labeling with NBD-F. As performed, our 2D CE × μFFE used a change in pH and a cyclodextrin buffer additive to generate orthogonality in the two separation dimensions. NBD labeled small molecule bioamines do not have a remaining functional group that is expected to exhibit a significant change in ionization over the pH ranges used. As a result, peaks were narrowly distributed across the 2D separation space. Combinations of separation modes that are able to better take advantage of differences in the chemical properties of the analyte mixture would be expected to distribute peaks across a higher fraction of available separation space, giving rise to a higher useable peak capacity.

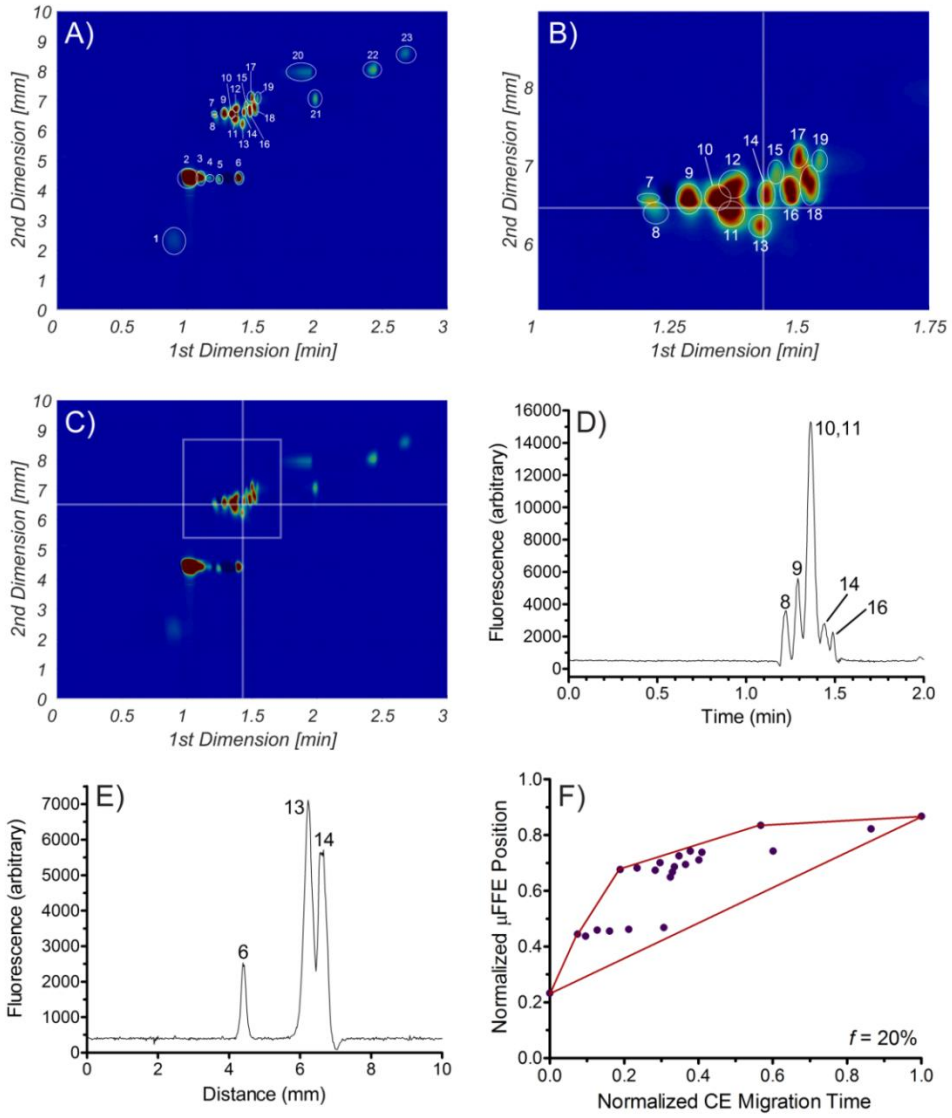

Figure 2.8 A) A 2D CE × µFFE separation of a mixture of 25 NBD labeled small molecule bioamines. CE buffer: 25 mM CAPS, 35 mM α-CD, pH = 10.01. µFFE buffer: 25 mM MES, 1 mM TEPA, 300 µM Triton X-100, pH = 5.2, 95:5 H_2O:MeOH. The µFFE potential is positive at the top of the plot. B) Expanded region of the 2D CE × µFFE separation shown in A) (see box in C)). C) 2D CE × µFFE separation of a mixture of 25 NBD labeled small molecule bioamines illustrating the area expanded in B) and where data is extracted to generate the electropherogram in D) (horizontal line) and µFFE linescan in E) (vertical line). D) Electropherogram extracted from the 2D CE × µFFE separation at 1.43 mm (see horizontal line in B) & C)). E) µFFE linescan extracted from the 2D CE × µFFE separation at 6.45 min (see vertical line in B) & C)). The µFFE potential is positive at the left of the plot. D) Contour hull plot of the 2D CE × µFFE separation shown in A) depicting the fraction of available separation space where peaks are found. Labeled peaks are: (1) arginine, (2) threonine, (3) serine, (4) lysine, (5) ornithine, (6) histidine, (7) leucine, (8) isoleucine, (9) methionine/asparagine, (10) NBD-OH, (11) phenylalanine, (12) α-ABA, (13) γ-ABA, (14) valine, (15) β-alanine, (16) glutamine/citrulline, (17) alanine/cysteine, (18) β-ABA/glycine, (19) taurine, (20) NBD-OH, (21) PEA, (22) glutamate, and (23) aspartate.

2.5 Conclusions

CE × µFFE provides a simple approach for performing high peak capacity 2D separations with relatively fast analysis times. The edge on interface allows the first dimension CE separation to be directly coupled with the second dimension µFFE separation without increasing analysis time or changing separation conditions. CE × µFFE generated an ideal peak capacity of 2,592 in a 9 min separation of peptides (7.6 min separation window, 342 peaks/min). CE × µFFE generated an ideal peak capacity of 1885 in a 2.7 min separation of small molecule bioamines (1.8 min separation window, 1053 peaks/min). These values compare well with previously reported benchmarks for 2D LC × CE (ideal peak capacity = 650; separation window = 2.8 min; 232 peaks/min)[166] and CE × CE separations (ideal peak capacity = 1950; separation window = 5.4 min; 361 peaks/min).[162] These LC × CE and CE × CE separations were able to perform second dimension CE separations every 1.0 – 2.4 s. It is unclear how much faster 2D separations can be performed using this approach without incurring losses in peak capacity due to under sampling. In contrast, the CE × µFFE separations described here are relatively simple to operate with no complicated timing, valving or voltage changes necessary at the interface. Images of the µFFE detection zone were recorded every 250-500 ms. CCD exposure times can easily be reduced to <100 ms, suggesting that even faster 2D CE × µFFE separations are possible.

The 2D CE × µFFE separations presented here also compare favorably with our previous nLC × µFFE separations. nLC × µFFE was able to generate ideal peak capacities of 2352 (10 min separation window; 235 peaks/min) and 264 (75 s separation window; 211 peaks/min) for similar BSA digest and small molecule bioamine samples, respectively.[117,119] While the peak capacities generated are comparable, CE × µFFE

performed better as separation time was reduced. Decreasing the nLC × μFFE separation window from 10 min to 5 min reduced the ideal peak capacity of the BSA digest separation from 2352 (235 peaks/min) to 1320 (264 peaks/min).[119] The efficiency of nLC separations typically drops with faster gradient times. In contrast, high-speed CE separations often retain or even improve efficiency and peak capacity if performed in short capillaries at high potentials.[141] The overall analysis time of the CE × μFFE separations was also superior to nLC × μFFE. Although gradients as short as 75 s could be generated in our nLC instrument, ~10 min was required to load the sample and move the gradient through the dead volume before and after the column.[117,119] The total analysis time of our previously reported nLC × μFFE separations therefore ranged from 11 to 23 min even though the separation windows were only 75 s – 10 min.[117,119] CE × μFFE does not suffer from similar dead volume delays. As shown in Figures 5 and 7 the 2D CE × μFFE separations made a much more effective use of separation time with total analysis times of only 2.7–9.0 min.

We have reported ideal 2D peak capacities for our CE × μFFE separations to facilitate direct comparisons with the existing literature. It is noted that the ideal peak capacity does not account for the fractional coverage of the separation space and therefore overestimates the useable peak capacity generated by the separation. Unfortunately, reporting of corrected 2D peak capacities that account for fractional coverage remains inconsistent in the field. The fractional coverage of our 2D CE × μFFE separation of a BSA digest was 30%, resulting in a corrected peak capacity of 778 (102 peaks/min). The fractional coverage of our 2D CE × μFFE separation of a mixture of small molecule bioamines was only 20%, resulting in a corrected peak capacity of 377 (209 peaks/min). For comparison, nLC × μFFE separations of similar mixtures obtained

fractional coverages of 53% and 36% resulting in corrected peak capacities of 694 (139 peaks/min) and 95 (76 peaks/min) for BSA digest and small molecule bioamine separations, respectively.[117,119] Clearly, the nLC separation is more orthogonal to the second dimension µFFE separation than CE using the separation modes described here. We performed our CE × µFFE with "zone" electrophoresis separations in both dimensions, with a pH change and cyclodextrin buffer additive as the only sources of orthogonality. Considering that NBD labeling removes the functional group (i.e. the amine) on the analytes that would be most susceptible to a pH change, it is perhaps surprising that the two separation dimensions were as orthogonal as they were. In the future additional combinations of electrophoresis modes will be explored in both the CE and µFFE dimensions to maximize the fractional coverage of 2D CE × µFFE separations. Modes that could be incorporated include micellar electrokinetic chromatography (MEKC), affinity capillary electrophoresis (ACE), isoelectric focusing (IEF) and gel electrophoresis.

Chapter 3

Effect of μFFE Buffer Additives on CE × μFFE Separation Orthogonality

3.1 Summary

CE × µFFE was previously shown as a simple way to eliminate loss in peak capacity from under sampling. The orthogonality of the two electrophoretic based separation techniques has never been explored. In the current chapter, different surfactants are added to the µFFE separation to alter the orthogonality of CE × µFFE. Negatively charged sodium dodecyl sulfate (SDS), neutral charge Triton X-100, and positively charged cetyltrimethylammonium bromide (CTAB) were used to study their effects on the fractional coverage of CE × µFFE separations of 25 small molecule bioamines and trypsin digested BSA. CE × µFFMEKC of 25 bioamines with 300 µM Triton X-100 gave the largest fractional coverage at 20.0%. Using 3 mM CTAB on the same 25 small molecule bioamines gave a fractional coverage of 13.0%. 15 mM SDS of 19 small bioamines gave a fractional coverage of 1.6%. Increasing the CTAB concentration to 15 mM increased the fractional coverage to 17.7%, but increased current in the device causing stream disruptions. Increasing the Triton X-100 concentration to 3 mM caused a decrease in fractional coverage to 4.3%. CE × µFFMEKC with trypsin digested BSA yielded similar results with 300 µM Triton X-100 yielding the highest measured fractional coverage at 30.0%. 3 mM CTAB gave a measured fractional coverage of 7.4%, however, the BSA digest sample was different from the Triton X-100 separation which can contribute to some of the differences. Overall for both samples 300 µM Triton X-100 gave the best fractional coverage, however 3 mM CTAB holds promise for utilizing the most separation space, but further optimization is required.

3.2 Introduction

Over the last several decades separation scientists have developed multi-dimensional separations, in which two or more conventional separation techniques are coupled together, to generate this increase in peak capacity. On-line comprehensive multidimensional separations have been demonstrated with various combinations of CE, LC, and GC.[22,28,180,181] Multi-dimensional separations generate a much higher ideal peak capacity when compared to their 1D counterparts.[32,33] Microfluidic CE × CE has generated ideal peak capacities of over 4000 in 15 minutes.[35] On-line comprehensive LC × LC has generated ideal peak capacities of over 1500 in 15 minutes.[182] As detailed in Section 1.2, there are a few caveats to obtaining the ideal peak capacity of a comprehensive 2D separation. First, there must be no under sampling or remixing at the interface between the two separations. Second, the separation mechanisms chosen must be orthogonal.[28,30,43] Chapter 2 reported the first ever coupling of CE × μFFE and showed that μFFE eliminated under sampling when used as the ^{2}D separation. In the current chapter, the orthogonality of CE × μFFE will be explored. Fractional coverage is used to determine the orthogonality of the ^{1}D and ^{2}D separations. There are many different methods for calculating f, but we use the convex hull method for the reasons outlined in Rutan et al.[47]

Coupling CE with μFFE provides its own unique challenges, particularly in orthogonality. Without modification (i.e. CZE × μFFZE), both techniques rely on analyte electrophoretic mobility for separation leading to ineffective use of the 2D separation space, in other words, low fractional coverage. Similarly, CE × CE suffers from the same challenge. One logical step would be to couple CE with LC based techniques, however this is not as straightforward as it seems. Offline hyphenated techniques like LC-CE or CE-LC are very time consuming and include tedious amounts of sample collection.[183-187]

Online comprehensive LC × CE on the other hand requires complicated injection interfacing, large dead volumes, and challenges with sample volume in LC versus CE.[165,188] However, CE can easily operate in many different separation modes, to alter the separation mechanism from electrophoretic mobility alone. A few examples of separation modes in CE are, MEKC, CIEF, CGE, and capillary isotachophoresis.[189] In order to increase the fractional coverage in 2D CE, different operation modes of CE such as CZE,[167] MEKC,[190] CGE/CSE,[191,192] CIEF,[193] and CEC[194] have been reported. The Dovichi Group took an interesting approach by doing CZE × CZE coupled by a microreactor to chemically modify the analytes as they transition from one capillary to the second.[195-197] However, there are no reported fractional coverage values for these examples. Since µFFE is an electrophoretic based technique, it can also operate in other separation modes similar to CE. µFFZE, µFFIEF, and µFFMEKC have all been demonstrated.[198] We will take advantage of the flexibility and ease for µFFE to switch separation modes in an effort to maximize the orthogonality of CE × µFFE.

While 2D CE techniques operating under different separation modes do provide an increase in fractional coverage, it is not a metric that is commonly reported. There are few examples in literature of reported fractional coverage values, nor is there a comparison of coupling different CE × CE electrophoretic separation modes while analyzing the same complex sample. CE × µFFE was previously shown to have great success in separating small biological amines and peptides, with only a cyclodextrin buffer additive and a pH change as the only sources of orthogonality between the two separations. CE was performed at pH 10.01 with α-cyclodextrin, and µFFE at 5.2. Fractional coverage values for the small biological amines and the peptides were 20% and 30% respectively (Chapter 2). It is important to understand how other separation

modes affect the potential fractional coverage of the separation particularly in CE × μFFE to see if further improvements can be made to this exciting separation platform.

3.3 Experimental

3.3.1 Buffers and Solutions

All solutions were prepared using deionized water (18.3 MΩ, Milli-Q, Millipore, Bedford, MA). All solutions were then filtered with a 0.22 μm nitrocellulose membrane filter (Fisher Scientific, Fairlawn, NJ) unless otherwise noted. One buffer for ^{1}D CE separations was prepared as follows; 25 mM N-cyclohexyl-3-aminopropanesulfonic acid (CAPS, Sigma-Aldrich, St. Louis), 35 mM α-cyclodextrin (α-CD, CTD, Inc., Alachua, FL), adjusted to pH 10.01 with 1 M NaOH (Macron Chemicals, Center Valley, PA) in water. Six different buffer solutions for the ^{2}D μFFE separations were prepared as follows; one, 25 mM 2-(N-morpholino)-ethanesulfonic acid hydrate (MES, Sigma-Aldrich, St. Louis), 300 μM Triton X-100 (Sigma-Aldrich, St. Louis), and 1 mM tetraethylenepentamine (TEPA, Sigma-Aldrich, St. Louis) adjusted to pH 5.2 with 1 M HCl (Macron Chemicals, Center Valley, PA) in 95:5 H_2O:MeOH (HPLC Grade, Fischer Scientific, Waltham, MA). Two, 25 mM MES, 15 mM Triton X-100, and 1 mM TEPA, adjusted to pH 5.2 with 1 M HCl (Macron Chemicals, Center Valley, PA) in 95:5 H_2O:MeOH (HPLC grade, Fischer Scientific, Waltham, MA). Three, 25 mM MES, 15 mM SDS, and 1 mM TEPA, adjusted to pH 5.2 with 1 M HCl in 95:5 H_2O:MeOH. Four, 25 mM MES, 75 mM SDS, and 1 mM TEPA, adjusted to pH 5.2 with 1 M HCl in 95:5 H_2O:MeOH. Five, 25 mM MES, 3 mM cetyltrimethylammonium bromide (cTAB, Sigma Aldrich, St. Louis), and 1 mM TEPA, adjusted to pH 5.2 with 1 M HCl in 95:5 H_2O:MeOH. Six, 25 mM MES, 15 mM cTAB, and 1 mM TEPA, adjusted to pH 5.2 with 1 M HCl in 95:5 H_2O:MeOH. Poly (ethylene oxide)

(PEO) (Sigma-Aldrich, St. Louis), for reduction of the electroosmotic flow in the µFFE device, was dissolved in 0.1 M HCl to 0.2% by mass at 90 ^{o}C with stirring overnight.

3.3.2 BSA Digestion and Labeling

Bovine serum albumin (BSA, Sigma Aldrich) was digested with trypsin following a standard digestion procedure. 1.0 mg of BSA was dissolved in 1.00 mL of 25 mM $NaHCO_4$ with 6.0 M urea. A standard reduction was then performed using tris(2-carboxyethyl)phosphine, (TCEP, Pierce Chemical, Rockford, IL) at 37 ^{o}C for 1 h in the dark, followed by alkylation with iodoacetamide (IAA, Sigma Aldrich) for 1 h at 37 ^{o}C in the dark. Sequencing grade trypsin (Promega, Madison, WI) was then used in a 1:30 w/w ratio to digest the BSA sample overnight at 37 ^{o}C. The newly digested sample was lyophilized under vacuum and stored at -80 ^{o}C until analysis. The BSA sample was thawed and dissolved in 1.00 mL of CE separation buffer. 4-fluoro-7-nitro-2,1,3-benzoxadiazole (NBD-F) (TCI, Portland, OR) was added in a 5:1 label to peptide molar ratio and incubated at 80 ^{o}C for 20 min to complete the labeling reaction. The sample was filtered using a 0.45 µm cellulose acetate syringe filter (Sterlitech, Kent, WA) prior to analysis. Small molecule bioamines were labeled in a similar fashion. 100 µM solutions of each amine were labeled with NBD-F in a 3:1 ratio.

3.3.3 µFFE Device Fabrication

A µFFE device with an edge on capillary inlet was fabricated according to a previously described procedure.[78] Briefly, an initial round of photolithography was performed on two 1.1 mm borofloat wafers (Precision Glass & Optics, Santa Ana, CA) to create an 85 µm deep capillary channel. The process was repeated to etch 30 µm deep electrode channels. A third photolithography step was performed to create a 1 cm wide × 2.5 cm long × 10 µm deep separation channel. 150 nm layers of Ti and Au were

deposited on one of the wafers using a Temescal electron beam evaporator. Standard photolithography was performed to remove unwanted Ti and Au, leaving patterned electrodes in the deeper side channels. 1 mm access holes were drilled for inlet, outlet, and electrode connections and a ~90 nm thick layer of amorphous silica was deposited onto the second wafer. Both wafers were aligned under a microscope and bonded anodically (900 V, 3 h, 450 °C, 5 µbar) using a Karl Suss SB-6 wafer bonder (Munich, Germany). When the two wafers were bonded the combined final depths in the completed µFFE device for the capillary, electrode and separation channels were 125 µm (~250 µm wide), 80 µm, and 20 µm, respectively. The bonded µFFE device was diced at the University of Minnesota Electrical Engineering Machine Shop to expose the capillary inlet channel. NanoPorts (Upchurch Scientific, Oak Harbor, WA) were aligned and adhered using epoxy rings (IDEX, Lake Forest, IL) over the inlet and outlet access holes. Connecting wires were bonded to the electrodes using silver conductive epoxy (MG Chemicals, Surrey, BC, Canada). The separation chamber was rinsed with 1 M NaOH solution at 1.0 mL/h for ~14 h to remove amorphous silica. Finally, the µFFE device was placed on a hotplate set to 120 ^{o}C and vacuum was applied to the separation channel while a 30 cm long × 20 µm i.d. × 150 µm o.d. fused silica capillary (Polymicro Technologies, Phoenix, AZ) was placed into the capillary channel. The CE separation capillary was bonded into place using Crystalbond 509 (Polymicro Technologies, Phoenix, AZ).

3.3.4 CE × µFFE Separations

The µFFE device channels were coated with PEO to suppress electroosmotic flow using a previously reported capillary coating method.[176] 0.1 M HCl was perfused through the device at 6 mL/min for 10 min, followed by 0.2% PEO by mass in 0.1 M HCl

at 3 mL/min for 10 min. A CE instrument was assembled in house using a machined acrylic sample holder, a Spellman CZE 1000R high voltage power supply (Spellman, Hauppauge, NY), and a platinum wire (0.25 mm diameter, Goodfellow Cambridge Ltd., Huntingdon, England) soldered to a 35 kV rated high voltage lead cable (Allied Wire & Cable Inc., Collegeville, PA). The CE separation capillary was conditioned with 1 M NaOH at 0.3 µL/min for 20 min, followed by separation buffer at 0.3 µL/min for 20 min. Samples were loaded onto the separation capillary electrokinetically at a voltage of +15 kV (0.5 kV/cm) for 15 s. After injection, the inlet of the capillary was placed in separation buffer and a separation voltage of +30 kV (1 kV/cm) was applied unless otherwise noted. The µFFE separation channel was perfused with µFFE separation buffer throughout the 2D separations using a syringe pump (Harvard Apparatus, Hollison, MA) at a flow rate of 0.5 mL/min (~0.15 cm/s). The µFFE separation potential was set to the maximum value that gave stable stream trajectories and did not migrate analytes into the side channels. For separations of BSA digests a +175 V potential was applied to the left electrode of the µFFE device while the right electrode was held at ground. For separations of small molecule bioamines a +225 V potential was applied to the left electrode of the µFFE device while the right electrode was held at ground. The CE separation capillary was rinsed after every other run using 0.1 M NaOH at 0.3 µL/min for 10 min.

3.3.5 Data Collection and Processing

A Cascade 512B CCD camera (Photonics, Tuscon, AZ) was fitted to an AZ100 Stereomicroscope (Nikon Corp., Tokyo, Japan) with a GFP bandpass emission filter cube (Nikon Corp.) containing two bandpass filters (450-490 and 500-550 nm) and a dichroic mirror (495 nm cutoff) for fluorescence imaging. For the 15 mM SDS 19 small bioamine separation only, a Quantem 512SC CCD camera (Photometrics, Tucson, AZ)

was used. A 150 mW, 488 nm emission argon-ion laser (Melles Griot, Carlsbad, CA) was expanded into a ~2.5 cm×~150 μm line and used as the excitation source for laser induced fluorescence (LIF) detection.[173] The entire setup was enclosed in a black, light tight box. The acquisition rates for 1D CE and 2D CE×μFFE separations of BSA digests were 4 and 2 Hz, respectively. The acquisition rate for 1D CE and 2D CE×μFFE separations of small molecule bioamines was 4 Hz. The CE power supply was controlled using LabVIEW (National Instruments, Austin, TX) and set to trigger the CCD data acquisition in MetaVue (Molecular Devices, Sunnyvale, CA) once the separation voltage was applied. Data was extracted and then analyzed with in-house Matlab programs. Peak Finder (panomics.pnnl.gov/downloads/PeakFinder.zip) was used to analyze extracted CE electropherograms and μFFE linescans. Orthogonal background correction was performed on the 2D separations using in house MATLAB programs as outlined by Filgueira, *et. al.*[177]

3.4 Results and Discussion

As stated previously, initial CE × μFFE separations were both performed as zone electrophoresis with only pH changes and a cyclodextrin buffer additive as the primary sources of orthogonality in the separation. Since the peptides and small molecule bioamines in those separations were labeled with NBD-F, which removes the functional group (i.e. the amine) on the analytes that would be most susceptible to a pH change, it was surprising to see much spread at all in the 2D separation space. However, as shown in Chapter 2, most of the observed spread was from the CE separation, while little of the μFFE separation space was utilized. In order to see the versatility of CE × μFFE, different buffer additives were used in the μFFE separation buffer to see if better separation orthogonality could be achieved therefore covering more separation space.

We hypothesized since the majority of analytes in the μFFE separation were still negatively charged at pH 5.1, adding a positively charged buffer additive could induce greater coverage of the 2D separation space, especially in the μFFE separation.

3.4.1 Micro Free Flow Micellar Electrokinetic Chromatography (μFFMEKC)

In this case, using charged surfactants via MEKC was a good candidate to achieve the increase in orthogonality. MEKC has been commonly used in CE separations to alter the selectivity of the separation and gain resolution primarily in the separation of neutral analytes, but has been used for a broad spectrum of analytes.[189] The first reported use of micelles in a capillary electrophoresis separation was by Terabe et. al. in 1984.[199] In MEKC, a surfactant with a hydrophobic tail and a functional group end cap is added in a concentration above the critical micelle concentration (CMC) so that it forms micelles in solution, with the hydrophobic tail facing inward and the hydrophilic functional group facing outward (Figure 3.1D). In solution, the micelles act as a pseudostationary phase as analytes partition in and out of the micelle. MEKC is particularly useful for the separation of neutral analytes in CE, but it has been used in many different applications.[200-203]

Separation selectivity can be easily modified by changing the added surfactants in the buffer solution. Three common surfactants used in CE based MEKC separations were chosen for these experiments (Figure 3.1). They include negatively charged sodium dodecyl sulfate (SDS), neutral charge Triton X-100, and positively charged cetyltrimethylammonium bromide (CTAB). Two concentrations were chosen for each surfactant, one at about two times the CMC, and one at about ten times the CMC. The CMC is the minimum concentration required for surfactants to form micelles. CMCs for SDS, Triton X-100, and CTAB were reported as 7.2 mM, 0.20 mM, and 0.99 mM

respectively.[204] The CE × µFFMEKC separation conditions would be the same as the CE × µFFE separations in Chapter 2, with the exception of the Triton X100 being substituted in the µFFE buffer for the other surfactants. Of these surfactants, we hypothesized that since the amino acids are largely negatively charged at pH 5.01, CTAB would have the largest effect on fractional coverage, while negatively charged SDS would show detrimental effects on the fractional coverage.

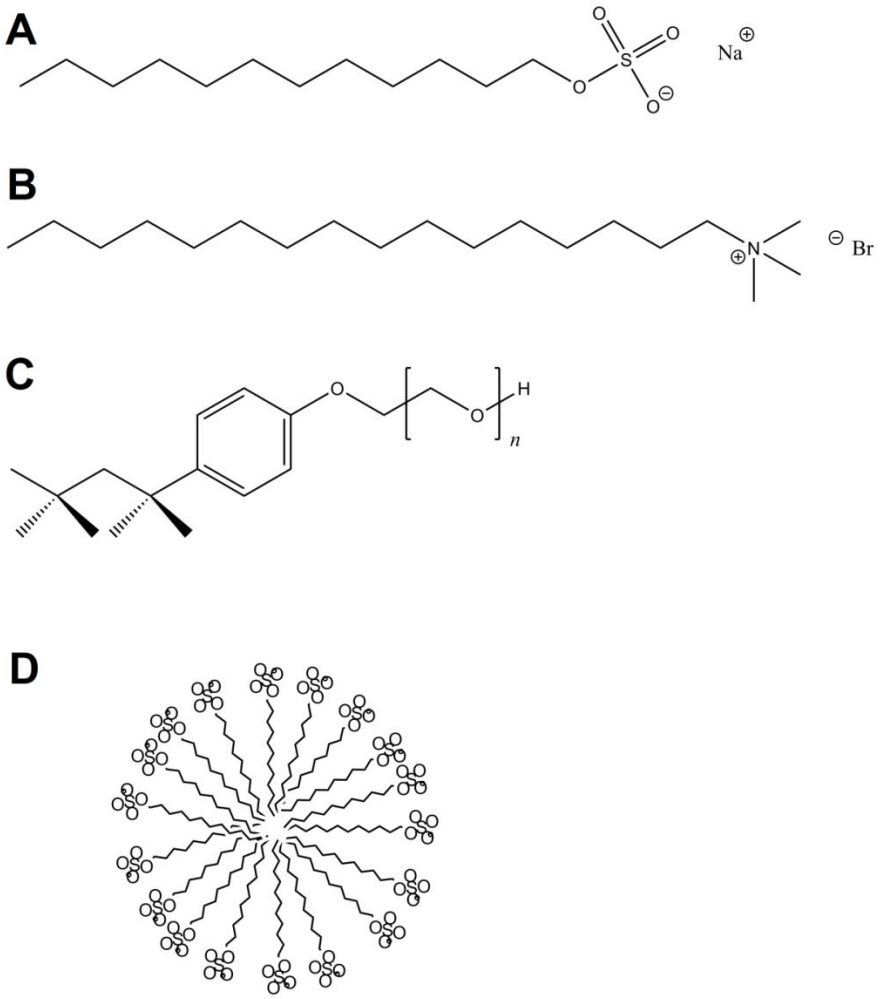

Figure 3.1 Chemical structures for three surfactants commonly used in MEKC, sodium dodecyl sulfate (A), cetrimonium bromide (B), and triton X-100 (C). The triton X-100 $–OCH_2CH_2$ chain repeats approximately 9-10 times. They are all characterized by a large hydrophobic alkyl chain, along with a hydrophobic functional group which provides the surface that interacts with analytes in MEKC separations. The surfactant interacts with itself to form micelles (D), with the hydrophobic chain in the center, and the hydrophilic functional group facing outward.

3.4.2 CE × µFFMEKC Separation of Small Molecule Bioamines

In order to only observe the effects of the different surfactants in µFFMEKC, the CZE buffer was held constant (i.e.25 mM CAPS, 35 mM α-cyclodextrin, pH 10.01) for all the separations. The resulting separation orthogonalities were analyzed via the convex hull method. Separations will be compared to the proof of concept separations shown in Chapter 2. CE × µFFMEKC with 300 µM Triton X-100 gave a fractional coverage value of 20.0% at an applied voltage of 225 V (Figure 3.2).

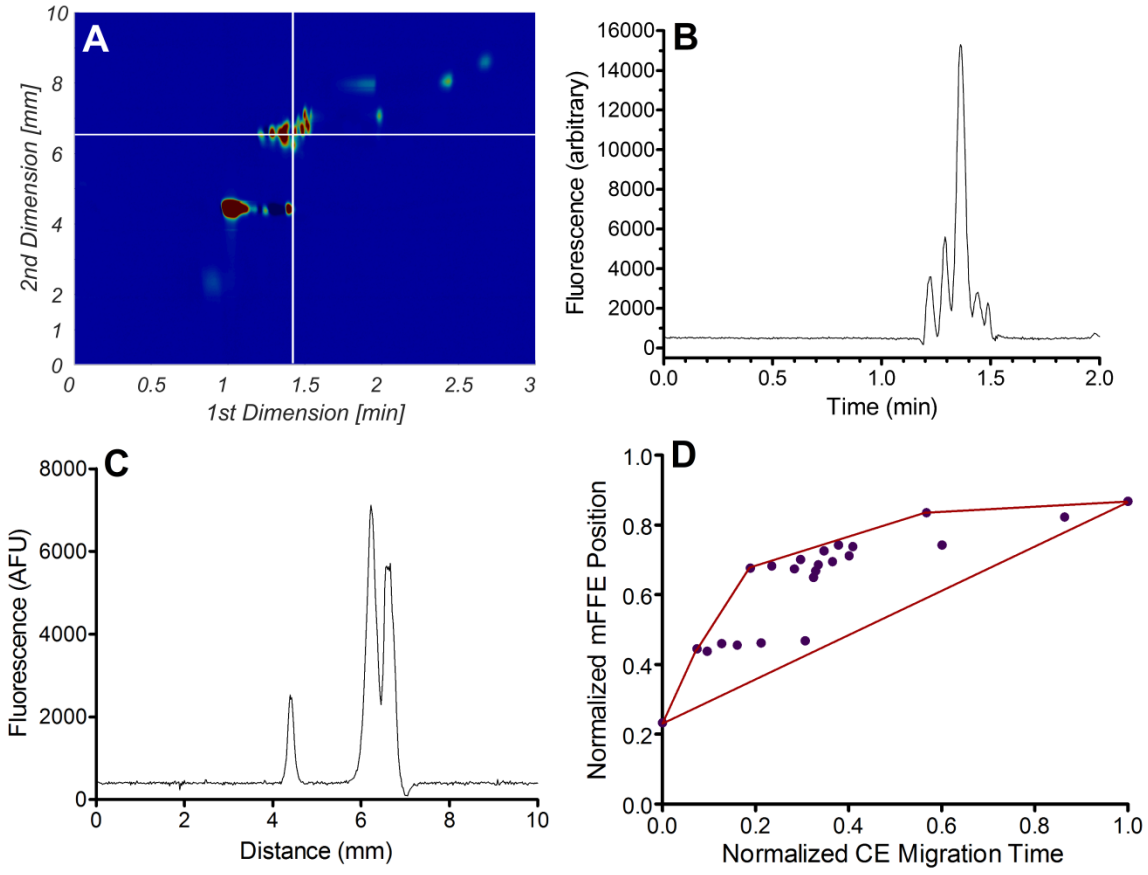

Figure 3.2 A) A 2D CE × µFFE separation of a mixture of 25 NBD labeled small molecule bioamines. CE buffer: 25 mM CAPS, 35 mM α-CD, pH = 10.01. µFFE buffer: 25 mM MES, 1 mM TEPA, 300 µM Triton X-100, pH = 5.2, 95:5 H2O:MeOH, with an applied voltage of 225 V. The µFFE potential is positive at the top of the plot. B) Electropherogram extracted from the 2D CE × µFFE separation at 6.45 mm. C) Linescan extracted from the 2D CE × µFFE separation at 1.43 min. D) Contour hull plot of the 2D CE × µFFE separation shown in A) depicting the fraction of available separation space where peaks are found. The observed fractional coverage was 20%.

These are the same conditions as performed in the proof-of-concept separations shown in Chapter 2. It provided the highest fractional coverage however, there is unclear how much further the separation can be improved. The separation occurs at the center of the separation channel, and a higher applied voltage would result in analytes deflected into the electrode channels. Peak widths for peaks in both dimensions were analyzed in a similar fashion to Chapter 2. ^{1}D separation average width was observed as 1.65 s, and ^{2}D separation average width was observed as 0.34 mm.

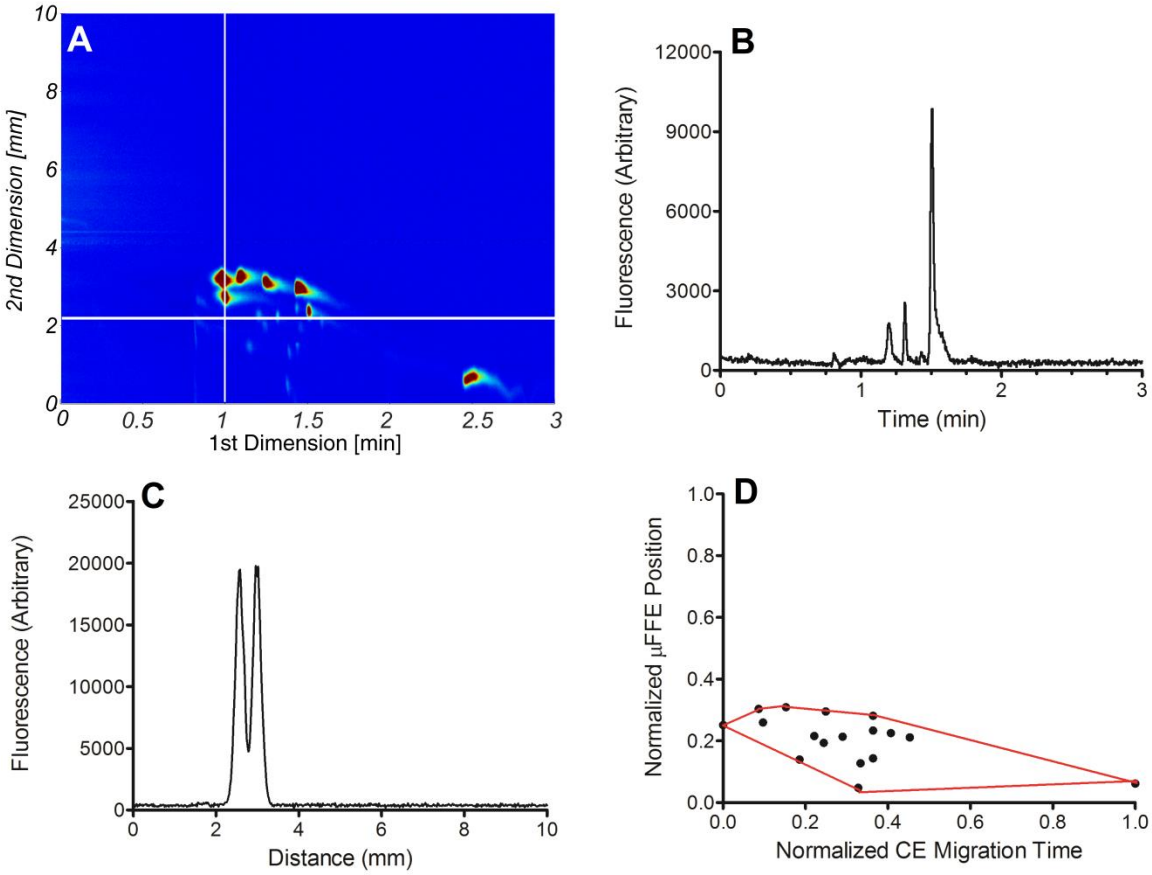

Figure 3.3 A) A 2D CE × µFFMEKC separation of 25 small bioamines. CE buffer: 25 mM CAPS, 35 mM α-CD, pH = 10.01. µFFE buffer: 25 mM MES, 1 mM TEPA, 3 mM CTAB, pH = 5.1, 95:5 H2O:MeOH, with an applied µFFE voltage of 200V. The µFFE potential is positive at the top of the plot. B) Electropherogram extracted from the plot at 2.2 mm. C) Linescan extracted from the plot at 1.0 min. D) Resulting convex hull plot with 17 observed peaks, and an observed fractional coverage of 13.0%.

Figure 3.3 shows the resulting CE × µFFMEKC separation utilizing 3 mM CTAB. CE × µFFMEKC with 3 mM CTAB gave a fractional coverage value of 13.0% at an applied voltage of 200 V. As expected, it was the most intriguing of the three separations. It appeared to have the most random distribution of peaks in the separation. Baseline peak widths were calculated from fully resolved peaks in both dimensions. More tailing was observed in the ^{1}D separation with and average width of 3.9 s. This large increase from the 300 µM Triton X-100 separation is due to the significant interaction with the CTAB micelles. We believe the CTAB is interacting with the PEO coating on the separation channel walls causing temporal broadening to be observed. The average calculated peak width for the ^{2}D separation was 0.34 mm. Even though there is strong interaction with the CTAB, there is no observed broadening in the µFFMEKC separation, which agrees with previously reported nLC × µFFE wall adsorption studies.[106] The positively charged CTAB micelles clearly interacted with the analytes strongly, altering selectivity. However, the separation only covered the bottom half of the separation space, from 0-4 mm. Replicate separations also occupied only this part of the separation space. An increase in voltage only resulted in more analytes deflected into the electrode channels. The negatively charged bioamines interacted strongly with the positively charged CTAB micelles causing them to have an observed deflection toward the cathode. If the separation could be performed in the center of the device, with a higher applied voltage, it would likely achieve the highest fractional coverage out of all three of the surfactants.

CE × µFFMEKC with 15 mM SDS gave a fractional coverage value of 1.6% (Figure 3.4). It is important to note that this data was obtained from a 19 small bioamines sample on a less sensitive instrument. This accounts for the large noise in the extracted linescan and electropherogram. α-ABA, β-ABA, β-Alanine, ornithine, PEA, and citrulline

were not included in this sample. While this makes a direct comparison challenging, the main source of spread from the 2D separation comes from the µFFE separation, which

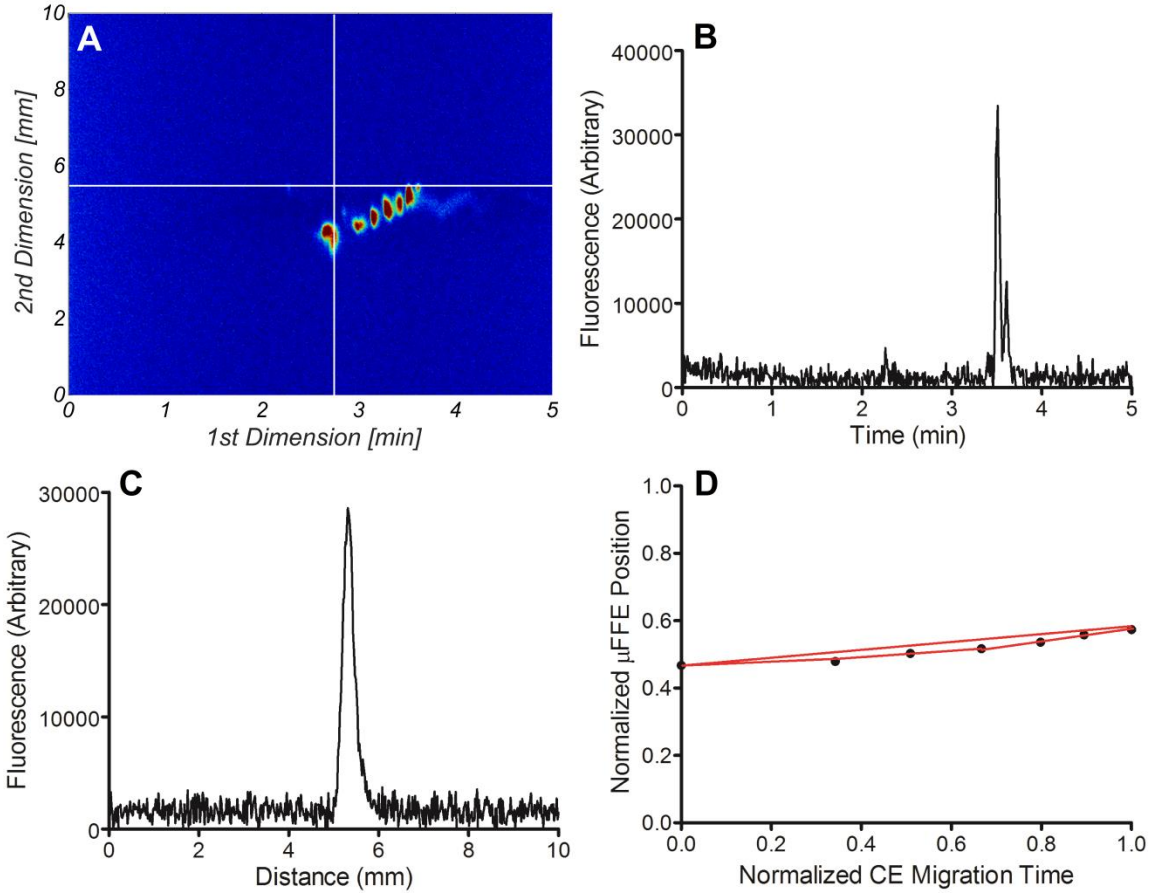

Figure 3.4 A) A 2D CE × µFFMEKC separation of 19 small bioamines. CE buffer: 25 mM CAPS, 35 mM α-CD, pH = 10.01. µFFE buffer: 25 mM MES, 1 mM TEPA, 15 mM SDS, pH = 5.1, 95:5 H2O:MeOH, with an applied µFFE voltage of 125 V. The µFFE potential is positive at the top of the plot. B) Electropherogram extracted from the plot at 4.1 mm. C) Linescan extracted from the plot at 2.65 min. D) Resulting convex hull plot with 7 observed peaks, and an observed fractional coverage of 1.6%.

should not greatly affect the fractional coverage due to their negative charge at a pH of 5.1. Additionally, the fractional coverage is normalized to the first and last eluting peak in CE separation, which uses the same buffers as the previous separations. Since none of the missing bioamines are the first or last eluting peak, they shouldn't affect observed fractional coverage in the CE separation. The observed fractional coverage of 1.6% was by far the lowest of the three separations. The shape of the separation followed a linear

diagonal path indicating a highly correlated separation mechanism. Logically, since the majority of the bioamines are negatively charged with the NBD-F label, there would be little to no interaction with the negatively charged SDS. This agrees with little tailing observed in the ^{1}D separation and average peak widths of 6.14 s. The peaks are broader because there are multiple bioamines in each peak. This is also true for the observed average peak width from the ^{2}D separation which was 0.54 mm. The few positive and neutral bioamines would interact strongly with the SDS and exhibit an observed mobility as if they were negatively charged or neutral. The negative charge of the SDS actively inhibits separation between the largely negatively charged bioamines.

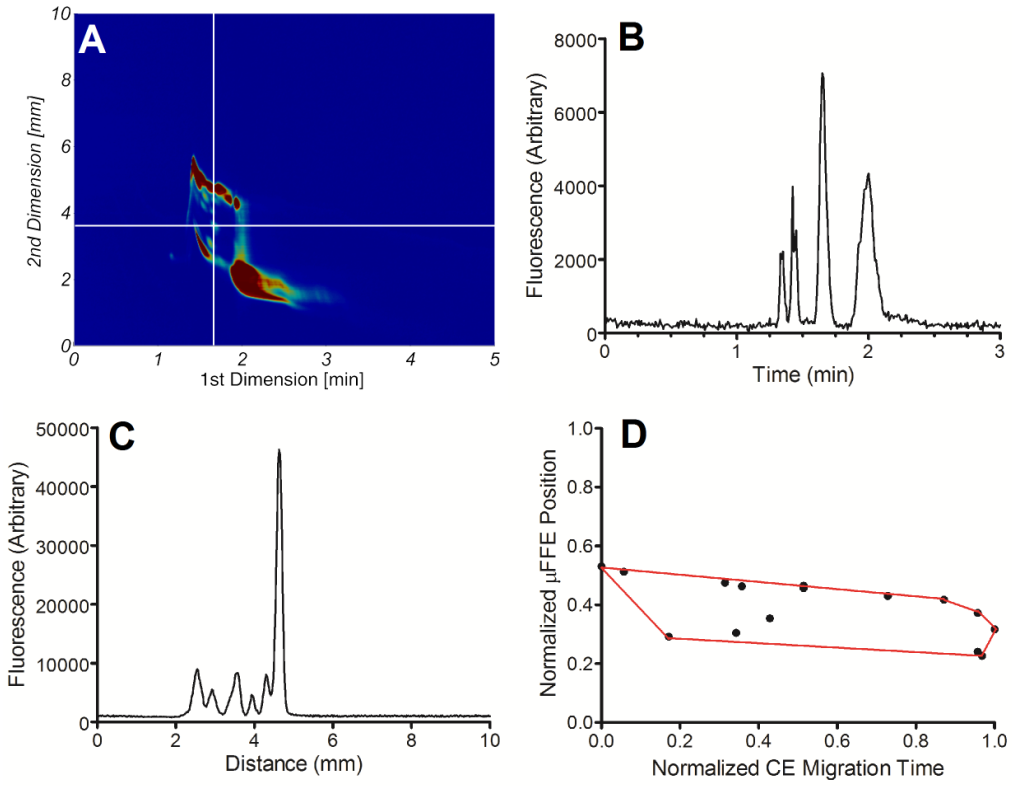

Figure 3.5 A) A 2D CE × µFFMEKC separation of 25 small bioamines. CE buffer: 25 mM CAPS, 35 mM α-CD, pH = 10.01. µFFE buffer: 25 mM MES, 1 mM TEPA, 15 mM CTAB, pH = 5.1, 95:5 H2O:MeOH, with an applied µFFE voltage of 150V. The µFFE potential is positive at the top of the plot. B) Electropherogram extracted from the plot at 3.6 mm. C) Linescan extracted from the plot at 1.64 min. D) Resulting convex hull plot with 14 observed peaks, and an observed fractional coverage of 17.7%.

CE × µFFMEKC was also performed with 15 mM CTAB at a voltage of 150V (Figure 3.5).The increase in concentration of CTAB in this separation also resulted in an increase of fractional coverage to 17.7%. While fractional coverage was raised, the larger concentration of CTAB resulted in a more unstable separation stream. The curved tailing, otherwise known as smearing, of peaks in the µFFE dimension in the 2D plot represents an unstable stream. This was caused by a higher current in the µFFE device resulting in more electrolysis bubbles, which interfered with the stream. The same was observed for 75 mM SDS. The current was too high, and caused so much of a stream disruption that no usable data could be collected with 75 mM SDS as the surfactant.

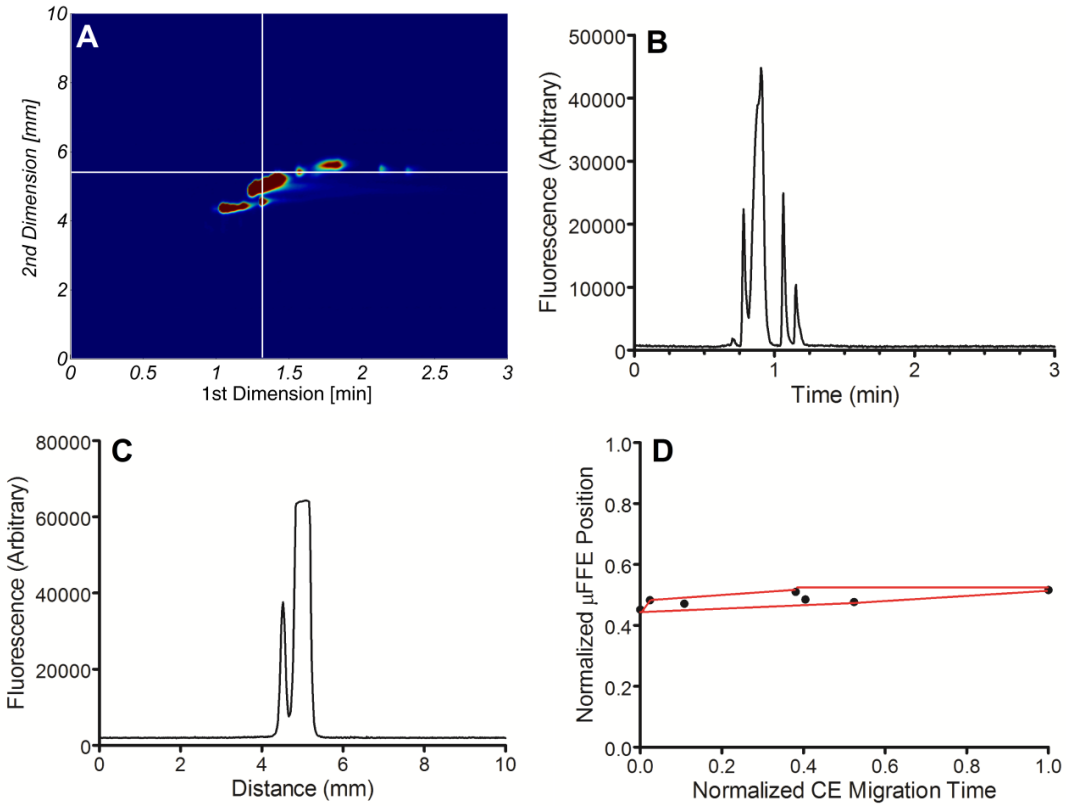

Figure 3.6 A) A 2D CE × µFFMEKC separation of 25 small bioamines. CE buffer: 25 mM CAPS, 35 mM α-CD, pH = 10.01. µFFE buffer: 25 mM MES, 1 mM TEPA, 3 mM Triton X-100, pH = 5.1, 95:5 H2O:MeOH, with an applied µFFE voltage of 150 V. The µFFE potential is positive at the top of the plot. B) Electropherogram extracted from the plot at 5.5 mm. C) Linescan extracted from the plot at 1.35 min. D) Resulting convex hull plot with 7 observed peaks, and an observed fractional coverage of 4.3%.

Finally, CE × µFFMEKC was performed with 3 mM Triton X-100 (Figure 3.6). The increase in surfactant concentration pulled the amino acids toward neutral, which lowered the fractional coverage to 4.3% compared to the 20% from its 300 µM counterpart. Average baseline peak widths were obtained for each dimension and calculated as 4.67 s and 0.41mm. Overall there is less spread, and there is less over all resolution between the peaks. The interaction with the much more massive Triton X-100 (m.w.~ 647 g/mol) has decreased the observed mobility of the small bioamines. This has caused the peaks to lose resolution maxing out the CCD detector, and results in fewer peaks observed in the convex hull plot.

3.4.3 CE × µFFMEKC Separation of BSA Digest

The effects of different µFFMEKC surfactants on a sample of trypsin digested BSA was also assessed. Two surfactants were chosen to run a sample of BSA digest, which were 3 mM CTAB, and 300 µM Triton X-100, while the ^{1}D CE separation was the same buffer as used previously in the small molecule bioamine separations. These were directly compared to the 2D separation of BSA utilizing 300 µM Triton X-100 obtained in Chapter 2 (Figure 3.7). The separation using 300 µM Triton X-100 generated much more spread in the µFFMEKC dimension with deflection distances ranging from 0-6 mm utilized in the free flow dimension alone. Fractional coverage was measured as 30% (Figure 3.7D). Baseline peak widths for the CE separation were calculated as an average of 4.2 s, and average baseline width of the µFFE separation was 0.39 mm.

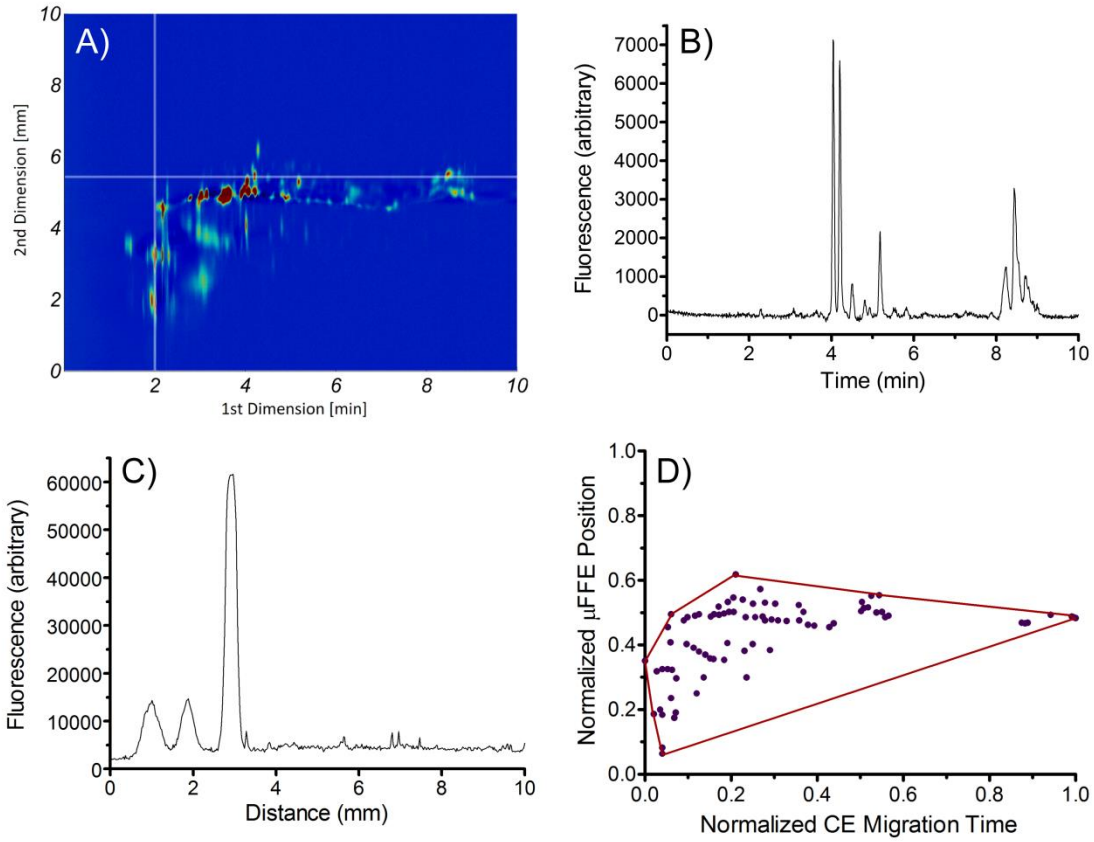

Figure 3.7 A) A 2D CE × µFFMEKC separation of trypsin digested BSA labeled with NBD-F. CE buffer: 25 mM CAPS, 35 mM α-CD, 1mM TEPA pH = 10.01. µFFE buffer: 25 mM MES, 1 mM TEPA, 300 µM Triton X-100, pH = 5.1, 95:5 H2O:MeOH, with an applied µFFE voltage of 175 V. The µFFE potential is positive at the top of the plot. B) Electropherogram extracted from the plot at 5.8 mm. C) Linescan extracted from the plot at 2.1 min. D) Resulting convex hull plot with 81 observed peaks, and an observed fractional coverage of 30%.

Figure 3.8 shows the resulting CE × µFFMEKC separation of the BSA digest with 3mM CTAB. It is important to note that the 3mM CTAB, and 3mM Triton X-100 separations utilized a different BSA digest sample than the 300 µM Triton X-100 sample. This makes direct comparison challenging. The significant differences in fractional coverage are mostly attributed to the difference in sample, however broad observations can still be made regarding the separations. When compared to the 300 µM Triton X-100 separation, the 3 mM CTAB produced a similar box shape that was observed as in the small bioamine separation, and only the lower half of the separation space was utilized. In fact, only deflection distances ranging from 1-3 mm were observed.

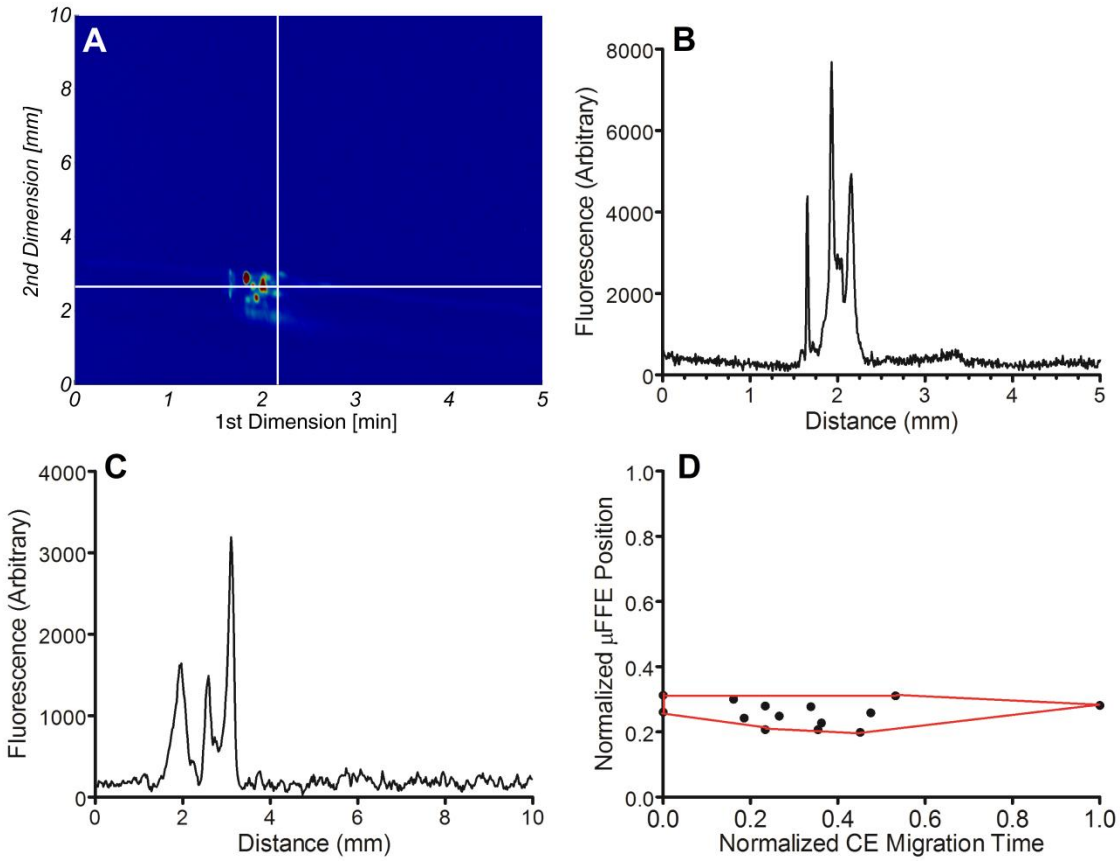

Figure 3.8 A) A 2D CE × µFFMEKC separation of trypsin digested BSA labeled with NBD-F. CE buffer: 25 mM CAPS, 35 mM α-CD, 1mM TEPA pH = 10.01. µFFE buffer: 25 mM MES, 1 mM TEPA, 3 mM CTAB, pH = 5.1, 95:5 H2O:MeOH, with an applied µFFE voltage of 150 V. The µFFE potential is positive at the top of the plot. B) Electropherogram extracted from the plot at 2.6 mm. C) Linescan extracted from the plot at 2.21 min. D) Resulting convex hull plot with 14 observed peaks, and an observed fractional coverage of 7.4%.

Interestingly, when the BSA digest sample was run with an increased surfactant concentration of 3 mM Triton X-100, the spread in the free flow dimension suffered (Figure 3.9). The increased concentration of Triton X-100 from 300 µM to 3 mM greatly lowered the fractional coverage to 2.7%. In fact, there is hardly any spread in the free flow dimension at all. I hypothesize that the increase in the concentration of Triton X-100 from 300 µM to 3 mM causes the more micellar interaction with the peptides and by doing so, reduces the observed mobility of the peptides in the free flow separation. The micelles could interact with the peptides and effectively add mass to the peptides

causing the peptides to be observed neutral and reducing migration in the free flow separation.

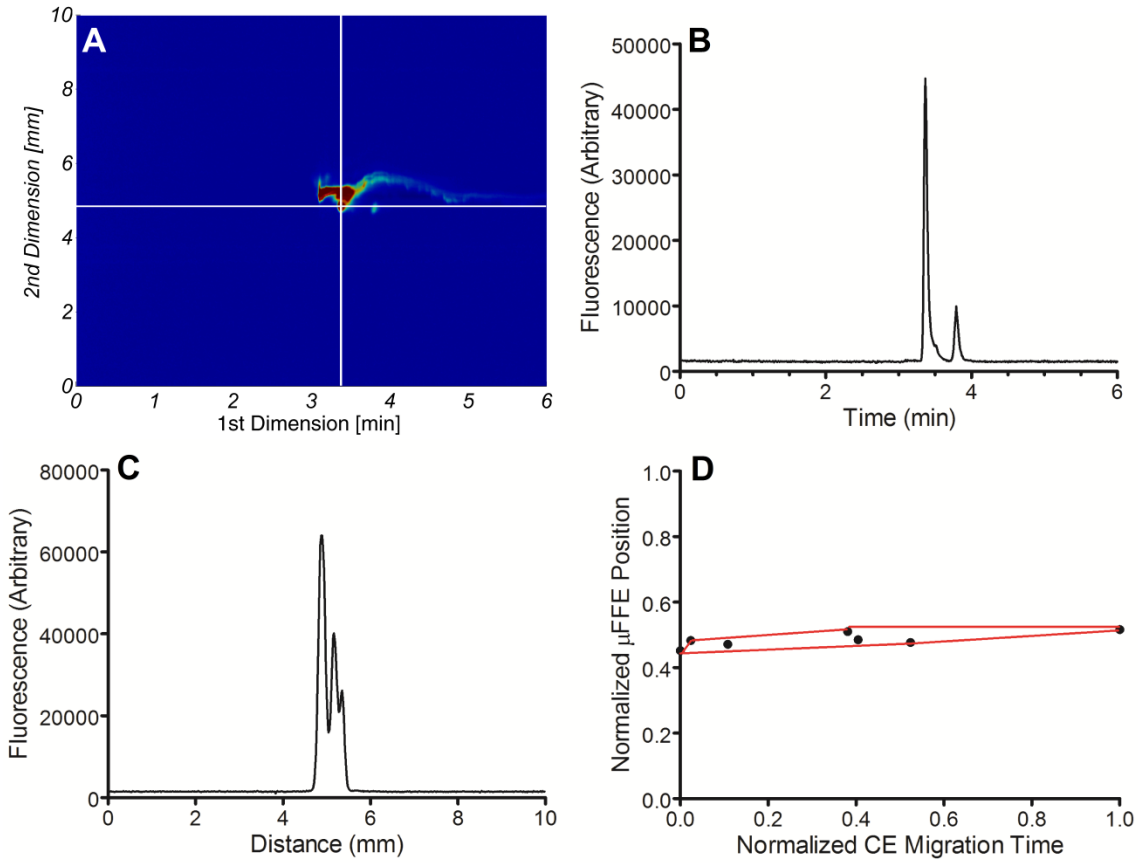

Figure 3.9 A) A 2D CE × µFFMEKC separation of trypsin digested BSA labeled with NBD-F. CE buffer: 25 mM CAPS, 35 mM α-CD, 1mM TEPA pH = 10.01. µFFE buffer: 25 mM MES, 1 mM TEPA, 3 mM Triton X-100, pH = 5.1, 95:5 H2O:MeOH, with an applied µFFE voltage of 150 V. The µFFE potential is positive at the top of the plot. B) Electropherogram extracted from the plot at 4.8 mm. C) Linescan extracted from the plot at 3.37 min. D) Resulting convex hull plot with 81 observed peaks, and an observed fractional coverage of 2.7%.

The only direct comparison that can be made is between the 3 mM CTAB and 3 mM Triton X-100 separation. 3 mM CTAB provided a larger fractional coverage and better coverage of the separation space. However, further experimentation is necessary to conclude which µFFMEKC surfactant provides the best separation for trypsin digested

BSA. Experiments that utilize the same exact samples for separation must be performed on the same day to provide conclusive results for this study.

3.5 Conclusions

The orthogonality of CE × µFFE separations was explored. Since both techniques rely on electrophoretic mobility as their separation mechanism, surfactants were added to the µFFE running buffer to observe their effects on the orthogonality of the two separations. CE × µFFMEKC provides an easy alternative to alter the orthogonality of CE × µFFE by only adding different surfactants to the µFFE separation buffer. In previous 2D separations involving µFFE, 300 µM Triton X-100 was used as a buffer additive, however, its effects on the separation were unclear, and have not been studied in a 2D separation capacity. In order to isolate the effects of chosen surfactants, three different surfactants were chosen and run at two different concentrations to observe their effects on separations of 25 small molecule bioamines, and trypsin digested BSA. Negatively charged SDS, neutral Triton X-100, and positively charged CTAB, were added to the µFFE running buffer at varying concentrations.

2D CE × µFFMEKC of 25 small molecule bioamines using 3 mM CTAB, 300 µM Triton X-100, and 15 mM SDS gave observed fractional coverages of 13.0%, 20.0%, and 1.6% respectively (Table 1).

Table 3.1 Comparison of fractional coverage values, average baseline peak widths for each separation dimension, and the peak capacity for small bioamine separations using different µFFE buffer surfactants.

µFFMEKC Surfactant	f	^{1}D $w_{avg,4\sigma}$ (s)	^{2}D $w_{avg,4\sigma}$ (mm)	$n_{c,\mu FFE}$
3 mM CTAB	0.130	3.90	0.34	29
15 mM CTAB	0.177	6.14	0.38	26
300 µM Triton X-100	0.200	1.65	0.34	29
3 mM Triton X-100	0.043	4.67	0.41	24
15 mM SDS	0.016	4.38	0.54	18

While 300 µM Triton X-100 gave the largest fractional coverage, there is not much more room for improvement. A higher applied voltage would result in analytes moving off the separation channel and into the electrode channel. 3 mM CTAB provided the most promising shape of the three separations. It was a box-like shape, however, the separation only occupied the bottom half of the separation space from deflection distances of 0-4 mm. The separation was run multiple times and the analytes always occupied this space. We hypothesize this is caused by the strong interaction of the negatively charged bioamines with the CTAB. The CTAB effectively carries the bioamines toward the cathode. If the separation could occupy the center of the separation channel, and a higher voltage applied in the µFFE device, a higher fractional coverage would be observed. Further experimentation would be required to achieve this optimized separation. 15 mM SDS performed the worst of the three separations. Since this separation was only performed with 19 bioamines we cannot make a direct comparison. α-ABA, β-ABA, β-Alanine, ornithine, PEA, and citrulline were not included in this sample. The main source of spread from the 2D separation comes from the µFFE separation, which should not greatly affect the fractional coverage due to their negative charge at a pH of 5.1. Additionally, the fractional coverage is normalized to the first and last eluting peak in CE separation, which uses the same buffers as the previous separations. Since none of the missing bioamines are the first or last eluting peak, they shouldn't affect observed fractional coverage in the CE separation. The separation gave a highly linear arrangement of peaks in the separation space. This suggests a highly correlated separation mechanism between the two dimensions. This can be explained by looking at the charges of the NBD-F labeled amines. Most are negatively charged, which would interact little with the SDS, the few neutral amines would interact with SDS to give an observed mobility as if the amine was negatively charged. The positively

amines would interact the most with the negatively charged SDS and cause it to appear more neutral or negative according to its deflection distance.

Increasing the surfactant concentrations to those around 10 times the CMC generally reduced separation quality. 3 mM Triton X-100 gave a fractional coverage of 4.3%. The separation failed to spread over much of the separation space, instead occupying deflection distances between 4-6 mm. This is roughly a five times reduction in fractional coverage. We hypothesize that this is caused by more micelles forming and effectively masking the charged functional groups of the bioamines. This reduces the spread of the separation in the free flow separation. In a separation utilizing 15 mM CTAB the fractional coverage increased to 17.7%. The analytes again occupied the lower half of the separation space from deflection distances of 1-6 mm. However, due to the increase concentrations of charged surfactants, current in the device increased. The current increase caused more bubble formation from electrolysis of the water and disrupted the separation stream. This also caused the 75 mM SDS run to be incredibly unstable and generated no usable data.

Table 3.2 Comparison of fractional coverage values, average baseline peak widths for each separation dimension, and the peak capacity for trypsin digested BSA separations using different μFFE buffer surfactants.

μFFMEKC Surfactant	f	^{1}D $w_{avg,4\sigma}$ (s)	^{2}D $w_{avg,4\sigma}$ (mm)	$n_{c,\mu FFE}$
3 mM CTAB	0.074	4.1	0.36	28
300 μM Triton X-100	0.300	4.2	0.39	25
3 mM Triton X-100	0.027	4.5	0.42	24

2D CE × μFFMEKC of trypsin digested BSA using 3 mM CTAB and 300 μM Triton X-100 yielded fractional coverages of 7.4% and 30% respectively (Table 2). Similar to the bioamines, 300 μM Triton X-100 yielded the best spread of separation space, but 3 mM CTAB gave an observed box shape that has greater potential to make

better use of the 2D separation space. The 3 mM CTAB occupied deflection distances from 2-4 mm. If the analytes could occupy the center of the separation channel and a greater potential applied, CTAB could provide greater orthogonality between the two separation techniques. Again, similar to the bioamines, increasing the concentration of Triton X-100 to 3 mM reduced the fractional coverage by roughly ten times to 2.7%. The separations for 3 mM CTAB and Triton X-100 used a different BSA digest sample from the 300 µM Triton X-100 separation. This accounts for the large difference in fractional coverage from each separation, and makes direct comparisons challenging. In the future, to eliminate any discrepancies between separations, each separation should utilize the same sample, the same instrumental setup, and be run on the same day.

Overall, 300 µM Triton X-100 afforded the best fractional coverages for both peptides and small molecule bioamines, but there is no room for improvement. When using CTAB, the analytes occupied a box shape, with a random distribution of peaks within that box. This indicates good orthogonality between separations. However, the analytes only occupied the lower regions of separation space. Further optimization is required to perform the separation in the center of the separation channel with a higher applied voltage to achieve higher fractional coverages.

Chapter 4

Novel Two Dimensional Absorbance Detection for Micro Free Flow Electrophoresis

4.1 Summary

Micro free flow electrophoresis (μFFE) is developing into a powerful analytical tool for continuous analysis of biological and chemical processes. Unlike time based separation techniques, μFFE separates analytes in space across the width of a separation channel, which raises interesting online detection challenges. The most commonly used detection technique for μFFE is laser induced fluorescence (LIF). Unfortunately, this limits the analytes to those that are natively fluorescent, or those that can be fluorescently tagged. In the current chapter we report the first coupling of μFFE to an absorbance detector capable of imaging the entire separation channel. Separations of rhodamine 123, rhodamine 110 and fluorescein were performed and calibration plots were constructed for each. Detection limits for fluorescein, rhodamine 110 and rhodamine 123 were calculated as 119 μM, 66.0 μM, and 64.4 μM respectively. The reported limits of detection are promising considering the path length for absorbance is only the depth of the separation channel, which in this case, is 20 μm. The design of the μFFE device can be easily modified to allow for a deeper separation channel which could greatly decrease these preliminary limits of detection.

4.2 Introduction

Micro free flow electrophoresis is a versatile analytical technique that is emerging as a powerful micro separation tool for online monitoring of biological and chemical processes.[130,205] In μFFE, analyte is streamed continuously into a planar separation channel while an electric field is applied perpendicularly. Analytes are then deflected laterally based on their electrophoretic mobilities as they travel through the electric field. Raymond et al. were the first to fabricate a fully functional μFFE device in a silicon wafer in 1994.[59] To date, μFFE devices have been fabricated in a wide variety of materials

including glass,[64-66,93,106] polydimethylsiloxane (PDMS),[60,62,63,206] and rigid polymers.[69,70,108,207,208] μFFE has been used as an analytical separation technique on a diverse number of analytes including fluorescent dyes,[64,75,209] amino acids,[119,133,210] peptides,[118,119,133,140] aptamers,[122,132] proteins,[91,208,211,212] mitochondria,[131] and bacteria.[68] Novel applications of μFFE include, capillary electrophoresis buffer optimization,[137] online chemical reaction monitoring,[116,213] viable bacteria preconcentration,[68] aptamer selection and binding measurements,[122,132] mitochondria isolation,[131] and a buffer purification step coupling capillary isoelectric focusing to electrospray ionization mass spectrometry.[214]

Online fluorescence detection is the most common detection method for analysis on μFFE.[205] Excitation for fluorescence detection is split between two types, lamp illumination through a microscope (epifluorescence) and laser induced fluorescence (LIF). LIF is prized in μFFE for its selectivity, low limits of detection, and high sensitivity.[112] However, analytes must be inherently fluorescent or tagged with a fluorophore to be analyzed. Since not all analytes can be fluorescently tagged, there is a pressing need for label free detection modes in μFFE to make this analytical technique universal. Unfortunately, few label free detection schemes in μFFE have been reported in literature. Köhler et al. used intrinsic UV fluorescence scanning to detect tryptophan, serotonin, propranolol, lysozyme, and chymotrypsinogen.[108] The technique used point raster scanning across the width of the separation channel and suffered from low sensitivity due to significant background noise from buffers and tubing connected to the device. Concentrations for detection of the proteins were as high as 170 μM. This technique was also limited by the speed at which the laser could scan, and the number of measured points across the separation channel. Surface enhanced raman spectroscopy (SERS) has also been reported for label free detection in μFFE.

Preliminary work by Becker *et al.* mixed 5 to 8 µm diameter silver colloids with running buffer and a 568 nm krypton ion laser to perform SERS on a µFFIEF separation of proteins.[115] However, the separation stream was unstable due to blockages in the channel by the aggregation of the silver colloids into clusters. Limits of detection were not measured. Jezierski *et al.* took a unique approach to label-free detection by immobilizing human embryonic kidney (HEK) cells in the separation channel of a µFFE device for the biosensing of adenosine triphosphate (ATP).[114] The method was able to detect the fluorescent response of the HEK cells to ATP concentrations as low as 20 µM in complex solutions. While novel and label free for the target molecule, this method is by no means universal or easy to perform. Mass spectrometry would be a logical choice for unmodified detection, but coupling MS with µFFE separations occurring in space is a unique challenge. Benz *et al.* reported the first and only on-line coupling of µFFE with nanospray MS.[116] A µFFE device with one outlet was coupled with nanospray MS. The flow in the separation channel of the device was then manipulated to sweep the stream from one electrode to the other such that the separated analyte streams are steered to the MS outlet. The amount of time required to scan through the entire width of the separation channel (11.7 mm) was 180 seconds. While this method was successfully used to monitor a multicomponent [3+2]-cycloannulation reaction to completion, reactions that occur on a timescale less than 180 seconds would be challenging to study. It would also be incompatible with a 2D separation as under sampling would have detrimental effects on the peak capacity. For example, using data from chapter 2 on the CE×µFFE biological amine separation (${}^{1}w = 1.65\ seconds$) and Equation 1.5, a cycle time of 180 seconds would equate to a $\frac{1}{\beta} = 0.005$. In other words, greater than 99% of the first dimension peak capacity would be lost from under sampling.

In the current chapter, we present the first demonstration of a commercially available UV-VIS absorbance detector coupled to µFFE capable of imaging the entire separation channel via LED source absorbance measurements. This detector is particularly suitable to µFFE measurements since it can map the deflected position of streams in space, unlike other point-source UV-VIS detectors commercially available for CE or HPLC.

4.3 Experimental

4.3.1 Buffers and Solutions

All solutions were made using deionized water (18.3 MΩ, Milli-Q; Millipore, Bedford, MA) and filtered with a 0.22 µm nitrocellulose membrane filter (Fisher Scientific, Fairlawn, NJ). For separations of fluorescent dyes, the µFFE separation buffer was 25 mM 4-(2-hydroxyethyl)-1-piperazineethanesulfonic acid (HEPES) with 300 µM Triton X-100 adjusted to pH 7.01 by 1 M NaOH (Macron Chemicals, Center Valley, PA) in 95:5 H_2O:MeOH. Rhodamine 110, rhodamine 123, and fluorescein, were prepared in stock solutions of 20mM in ethanol (200 proof ACS grade, Pharmco-Aaper, Brookfield, CT). They were then combined and diluted accordingly to various concentrations.

4.3.2 Amino Acid Labeling

Five amino acids (serine, lysine, histidine, phenylalanine, and glutamate) were prepped for labeling at 10 mM concentrations in a 90:10 water to methanol mixture. 4-fluoro-7-nitro-2,1,3-benzoxadiazole (NBD-F) (TCI, Portland, OR) was added to the solution in a 5:1 label to amino acid molar ratio and incubated at 80 ^{o}C for 20 min to complete the labeling reaction. The sample was filtered using a 0.45 µm cellulose acetate syringe filter (Sterlitech, Kent, WA) prior to analysis.

4.3.3 µFFE Device Fabrication

A µFFE device with an edge on capillary inlet was fabricated according to a previously described procedure.[140] Briefly, an initial round of photolithography was performed on two 1.1 mm borofloat wafers (Precision Glass & Optics, Santa Ana, CA) to create an 85 µm deep capillary channel. The process was repeated to etch 30 µm deep electrode channels. A third photolithography step was performed to create a 1 cm wide × 2.5 cm long × 10 µm deep separation channel. 150 nm layers of Ti and Au were deposited on one of the wafers using a Temescal electron beam evaporator. Standard photolithography was performed to remove unwanted Ti and Au, leaving patterned electrodes in the side channels. 1 mm access holes were drilled for inlet, outlet, and electrode connections and a ~90 nm thick layer of amorphous silica was deposited onto the second wafer. Both wafers were aligned under a microscope and bonded anodically (900 V, 3 h, 450 °C, 5 µbar) using a Karl Suss SB-6 wafer bonder (Munich, Germany). When the two wafers were bonded the combined final depths in the completed µFFE device for the capillary, electrode and separation channels were 125 µm (~250 µm wide), 80 µm, and 20 µm, respectively. The bonded µFFE device was diced at the University of Minnesota Electrical Engineering Machine Shop to expose the capillary inlet channel. NanoPorts (Upchurch Scientific, Oak Harbor, WA) were aligned and adhered using epoxy rings (IDEX, Lake Forest, IL) over the inlet and outlet access holes. Connecting wires were bonded to the electrodes using silver conductive epoxy (MG Chemicals, Surrey, BC, Canada). The separation chamber was rinsed with 1 M NaOH solution at 1.0 mL/h for ~14 h to remove excess amorphous silica. Finally, the µFFE device was placed on a hotplate set to 120 ^{o}C and vacuum was applied to the separation channel while a 30 cm long × 20 µm i.d. × 150 µm o.d. fused silica capillary (Polymicro Technologies, Phoenix, AZ) was placed into the capillary channel. The sample

introduction capillary was bonded into place using Crystalbond 509 (Polymicro Technologies, Phoenix, AZ).

4.3.4 µFFE Separation Conditions

The µFFE device channels were coated with PEO to suppress electroosmotic flow using a previously reported capillary coating method.[176] 0.1 M HCl was perfused through the device at 6 mL/min for 10 min, followed by 0.2% PEO by mass in 0.1 M HCl at 3 mL/min for 10 min. Sample was introduced into the µFFE separation channel via the inlet capillary at a rate of 300 nL/min using a µL syringe pump (Harvard Apparatus, Hollison, MA). The µFFE separation channel was perfused with µFFE separation buffer throughout the 2D separations using a syringe pump (Harvard Apparatus, Hollison, MA) at a flow rate of 0.5 mL/min (~0.15 cm/s). The µFFE separation potential was set to the maximum value that gave stable stream trajectories and did not migrate analytes into the side channels. For separations of rhodamine 110, rhodamine 123, and fluorescein, voltages ranging from 50 V – 150 V were applied. For the separation of 5 amino acids, voltages of 100 V – 200 V were applied.

4.3.5 Data Collection and Processing

Absorbance detection images were recorded using a prototype version of the ActiPix^{TM} D200 UV/VIS Imaging Platform (Paraytec, York, United Kingdom) outfitted with a 470 nm LED source. The source was located approximately one inch from the µFFE device. The absorbance of the 470 nm LED source was then measured with a spatial CMOS detector located directly below the µFFE device. The instrument was placed in a dark box to minimize stray light exposure. The detector was then used to collect a blank data set, while buffer was flowing through the µFFE device, but no analyte stream was present. Then analyte flow was started down the separation channel. Data was collected

with an exposure time of 100 msec, and data points were collected at a rate of 10 Hz. Data was then processed from the ActiPix™ D200 and was analyzed via the provided Actipix™ software.

4.4 Results and Discussion

Figure 4.1 details the ActiPix™ D200 UV/VIS detector used in conjunction with a µFFE device. As the analyte stream is flowed through the center of the separation channel, they are illuminated with a LED source. The LED wavelength is chosen as the one that aligns most closely to the maximum absorbance wavelength (λ_{max}) for the analytes of interest in the sample. The absorbance of the source light is then measured via the CMOS detector located directly underneath the µFFE device. The entire setup was enclosed in a dark box to minimize the stray light exposure to the instrument.

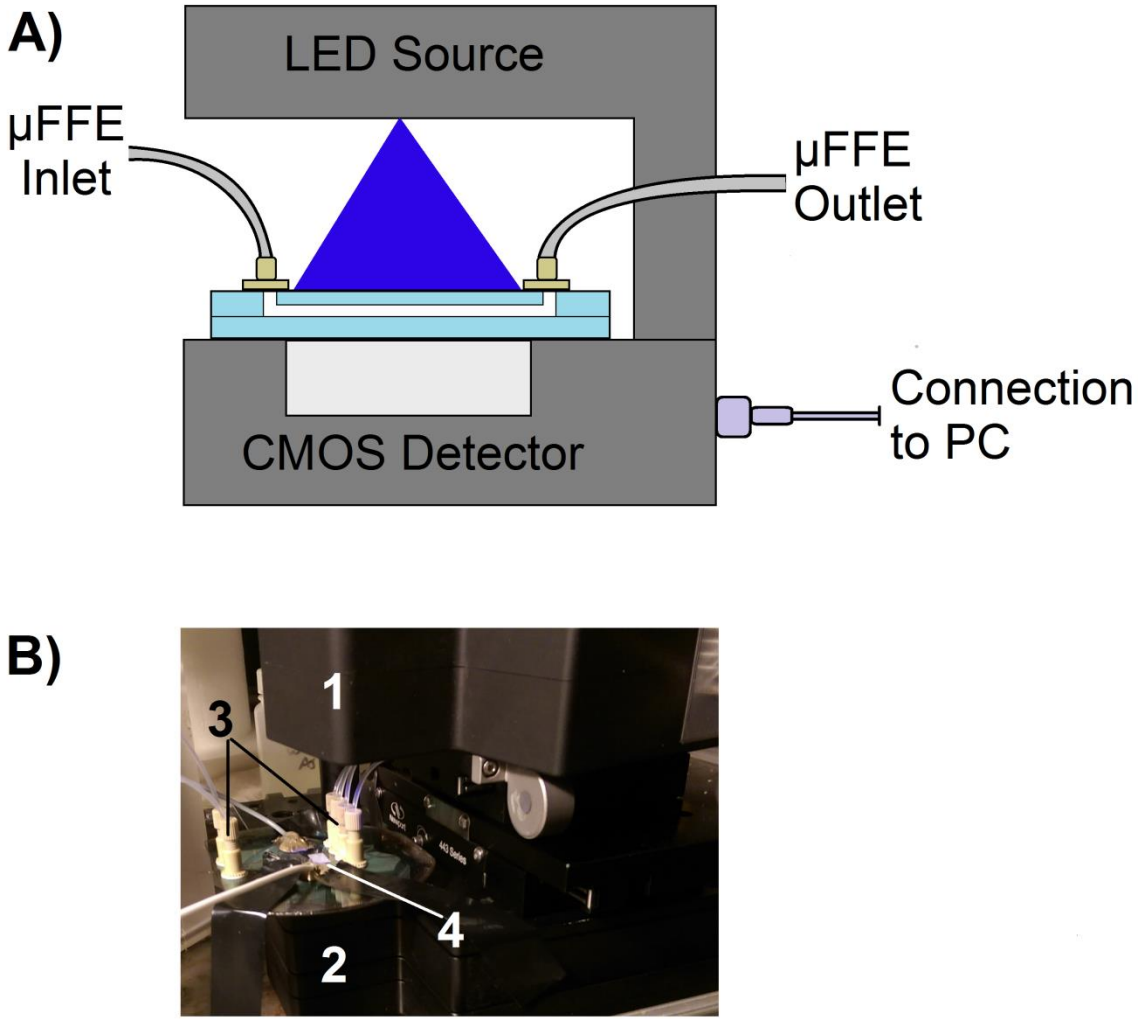

Figure 4.1 A) Cutaway schematic of the ActiPix™ D200 prototype system. The LED source, in this case 470 nm, shines on the µFFE device. The light is then absorbed by the analytes in the separation channel, and the CMOS detector below the µFFE device records the light transmission through the device. B) Actual setup of the ActiPix D200™ prototype system with the µFFE device: 1. The LED source housing. 2. The CMOS detection and processing base. 3. The inlets and outlets of the µFFE device. 4. The µFFE separation channel and the CMOS detection area.

4.4.1 Visible Dye Separations

Separations of visible dyes were used to determine the detection limits of the ActiPix D200 system. Fluorescein, Rhodamine 110, and Rhodamine 123 were chosen as model analytes because they cover a variety of charges at pH 7, and they compare well to previous µFFE separations using LIF detection.[67,78,95,97] Fluorescein is negatively charged, Rhodamine 110 is neutral, and Rhodamine 123 is positively charged. The λ_{max} of Fluorescein, Rhodamine 110, and Rhodamine 123 are 500 nm, 497 nm, and 511 nm respectively.[215,216] The 470 nm LED source was closest available source to these values and was chosen to provide the best signal possible. The fluorescein, rhodamine 110, and rhodamine 123 were prepared and combined so that each had a concentration of 10 mM. Hepes buffer was flowed through the separation channel, and an initial blank of the system was recorded. After, the three dye solution was streamed down the center of the separation channel. Figure 4.2 shows the 3 dye solution flowing down the separation channel before voltage was applied.

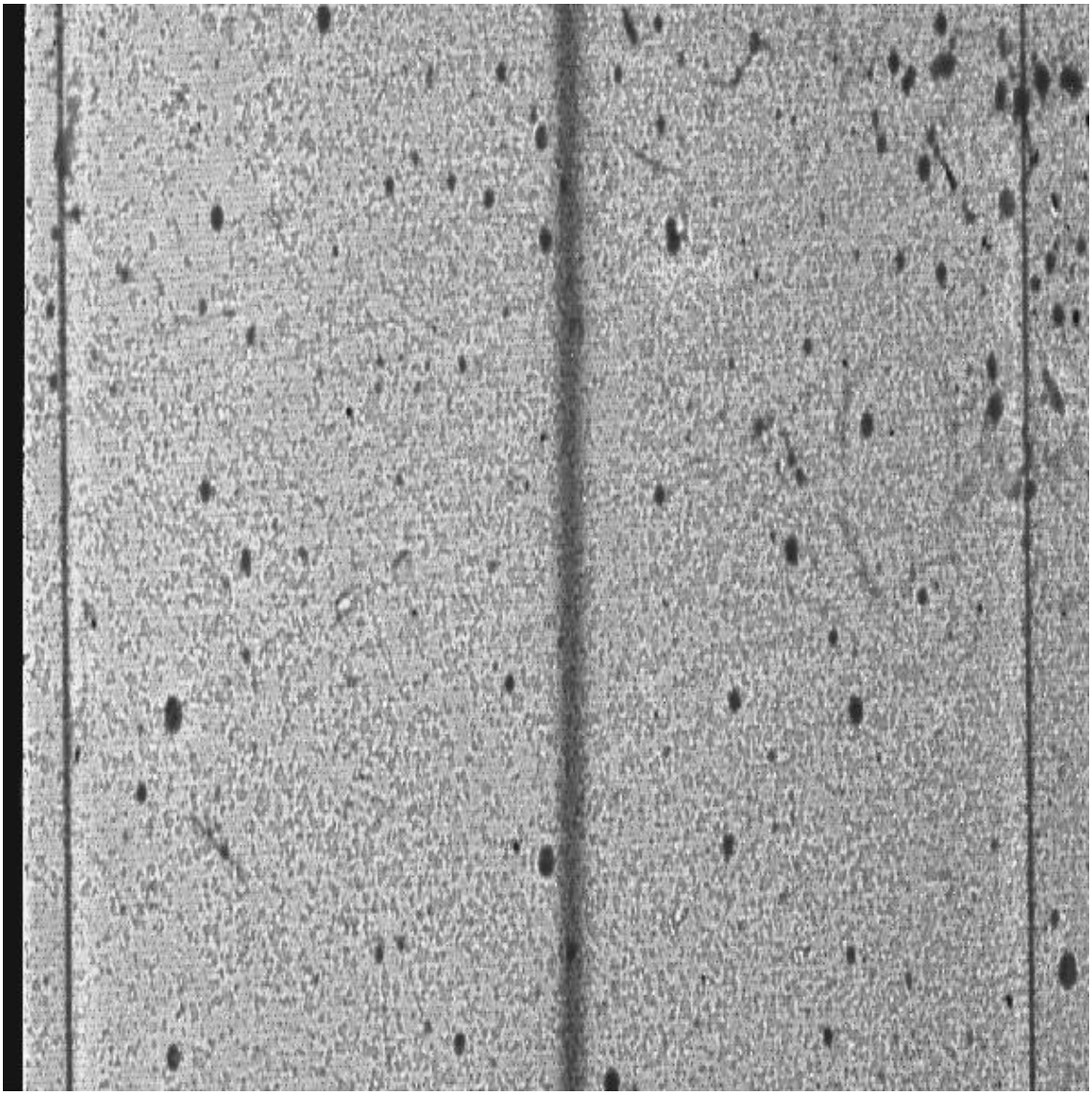

Figure 4.2 Image of the 1 mM fluorescein, rhodamine 110, and rhodamine 123 solution as it flows down the center of the µFFE solution before voltage was applied. This is from the non-background corrected feed of the ActiPix D200 instrument. The direction of flow is from the bottom of the image to the top.

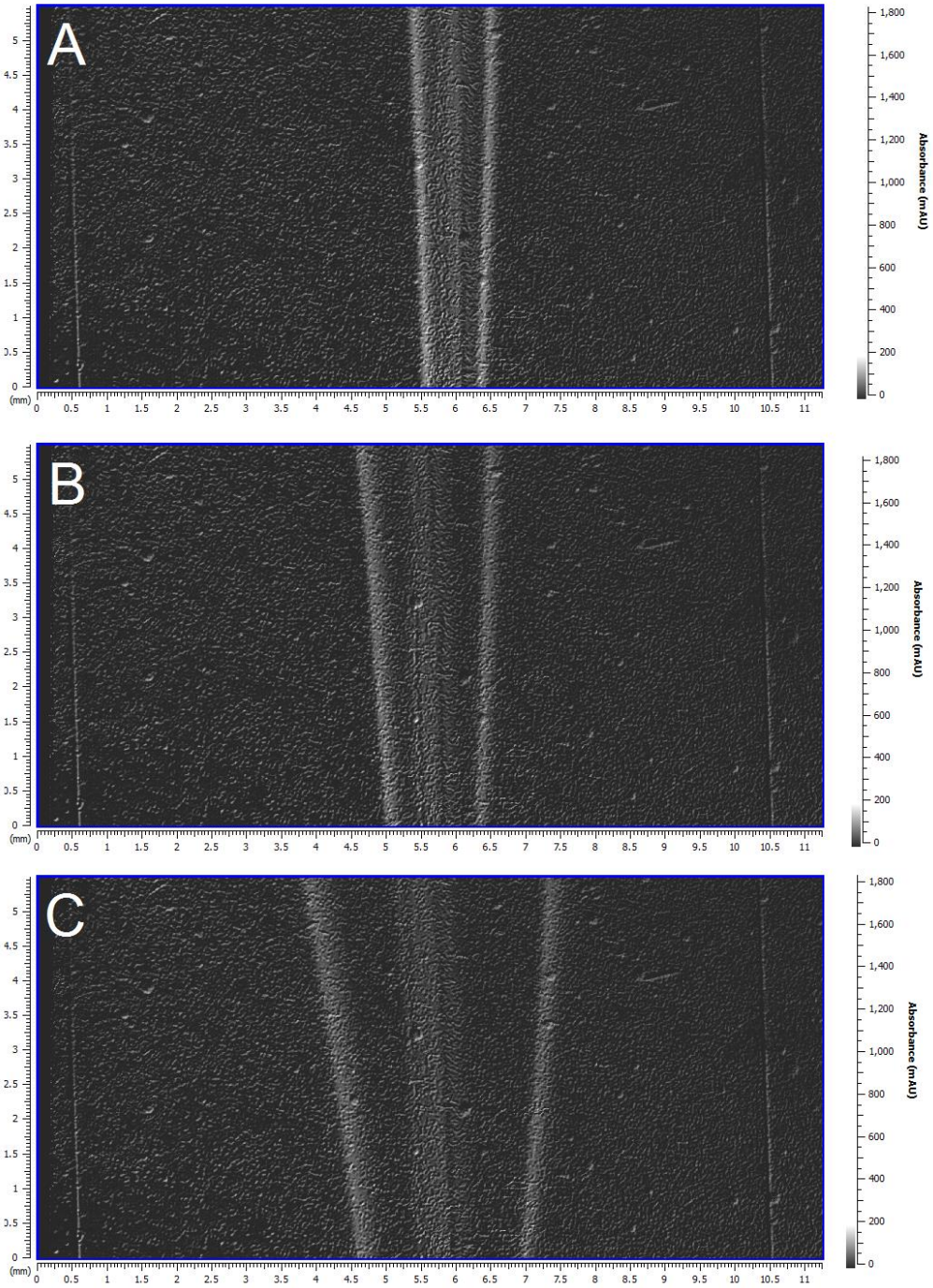

Figure 4.3 Recorded images of the three dye separation at voltages of 50 V (A), 100 V (B), and 150 V (C) on the ActiPix D200 detector. As the voltage increases the streams become further separated. The left-most stream is rhodamine 123, the center is rhodamine 110, and the right-most is fluorescein. The rhodamine 110 stream is distorted from the refractive index change between the sample stream and the µFFE buffer. The direction of flow is from the bottom of the images to the top. The left side of the images contains the negative electrode, and the right side is grounded.

After flow was established, voltages of 50 V, 100 V, and 150 V were applied to the stream and measured for their intensities (Figure 4.3). Figure 4.4 shows a sample linescan from the 150 V three dye separation. The raw absorbance data contained 1780 points spanning from 0-10 mm on the separation channel. The raw data was then smoothed with a 30 point moving average.

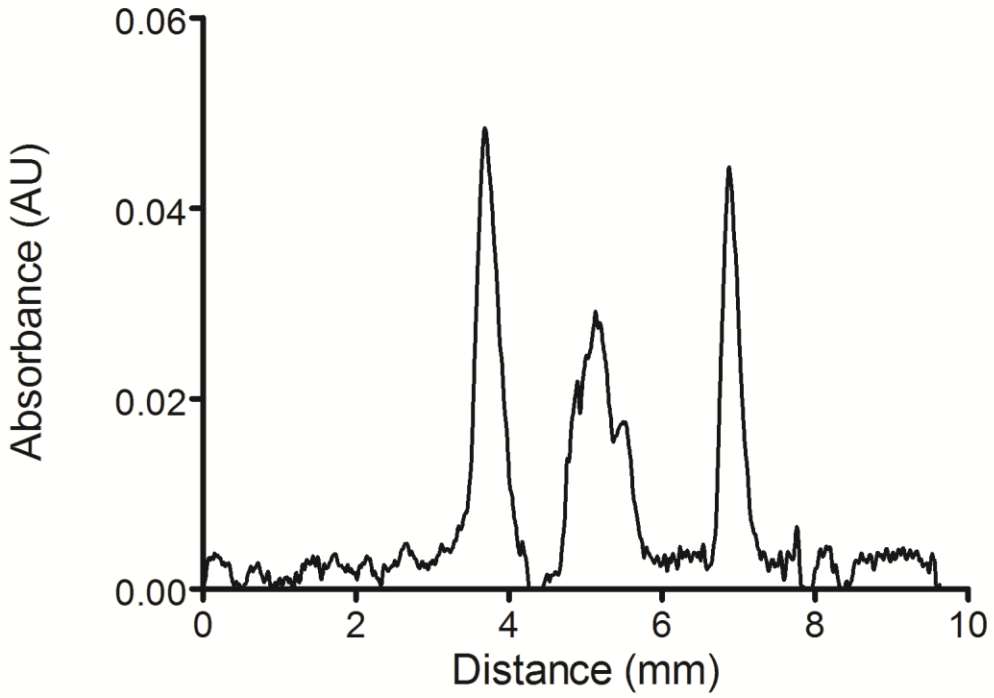

Figure 4.4 Smoothed data from the 150 V three dye separation. Identification of the peaks from left to right are rhodamine 123, rhodamine 110, and fluorescein. Rhodamine 110 exhibits two side peaks due to a refractive index change in the buffers from the analyte stream to the µFFE separation buffer. The scan was taken at 1.5 cm down the channel from the capillary inlet.

As the voltage applied increased the separation of the streams become greater. The left side of the images houses the electrode where negative voltage was applied, and the right side houses the grounded electrode. The three streams were identified from left to right as rhodamine 123, rhodamine 110, and fluorescein respectively. Rhodamine 110 exhibits two side peaks due to a refractive index change from the analyte buffer, ethanol, to the µFFE separation buffer, 95:5 H_2O: MeOH.

4.4.2 Detection Limit Study

After the feasibility of the three dye separation was established, a series of solutions containing various concentrations of fluorescein, rhodamine 110, and rhodamine 123 were streamed through the device and their absorbances were measured to construct calibration plots for each respective dye (Figure 4.5). Fluorescein absorbances were measured at concentrations of 2.86 mM, 5.73 mM, 6.91 mM, and 11.4 mM. Rhodamine 110 absorbances were measured at concentrations of 2.89 mM, 3.00 mM, 5.79 mM, and 11.6 mM. Rhodamine 123 absorbances were measured at concentrations of 1.72 mM, 3.45 mM, 6.89 mM, 13.8 mM, and 27.6 mM. The standard deviation of noise in the blank was measured as 6.34×10^{-4}, giving limits of detection for fluorescein, rhodamine 110, and rhodamine 123 as 120 µM, 66 µM, and 64 µM respectively. The limits of detection are promising considering the path length for absorbance is only the depth of the separation channel, which in this case, is 20 µm. These values compare favorably to UV-VIS absorbance detection on CE, which typically gives limits of detection on the scale of 10^{-5}-10^{-6} M for capillary i.d. of 100 µm.[217] The design of the µFFE device can be easily modified to allow for a deeper separation channel which could greatly decrease these preliminary limits of detection.

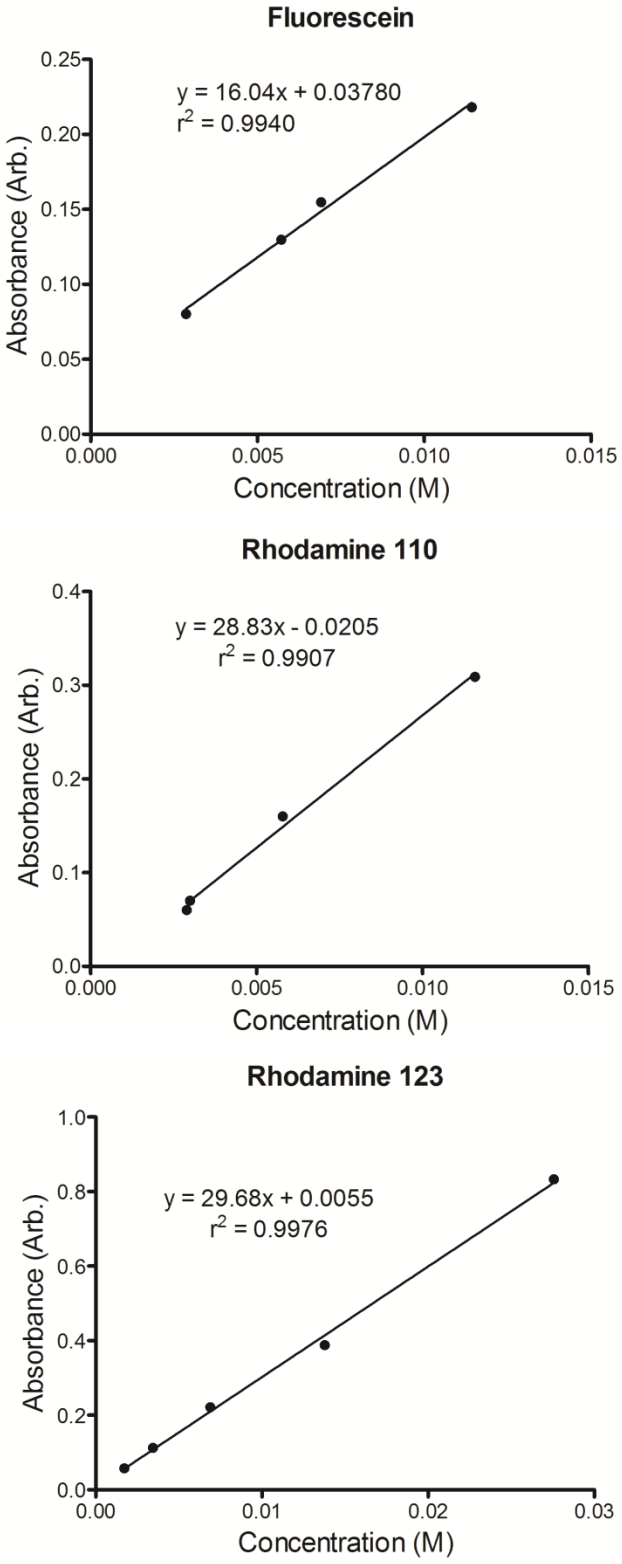

Figure 4.5 Calibration plots for fluorescein, rhodamine 110, and rhodamine 123.

4.4.3 Labeled Amino Acid Separation

One limitation of a µFFE device fabricated in boron doped glass, is that it is not fully UV transparent. In fact, Borofloat^{TM} wafers have a measured transmittance of 3% at 250 nm and a transmittance of 40% at 280 nm. With this µFFE device design having a small path length of 20 µm, we opted to perform analysis of NBD-F labeled amino acids and measure the absorbance at 470 nm, the same as the three dye solution. NBD-F labeled amino acids have a λ_{max} of 471 nm.[218,219] Figure 4.7 shows the raw images recorded on the ActiPix D200 instrument of a µFFE separation of serine, lysine, histidine, phenylalanine, and glutamate each at a concentration of 1 mM. The combined five amino acid stream was clearly visible to the detector, however, as voltage was increased it became clear that there were only two peaks present. Figure 4.6 shows the linescan data extracted from the 0 V and 200 V separations, and clearly shows the two peaks. There is tailing present in the right-most peak in Figure 4.6B, indicating that more than one amino acid is present. NBD-F labeled serine, histidine, phenylalanine, and glutamate are negatively charged at pH 7, while lysine is not, which would explain the two observed peaks.[119]

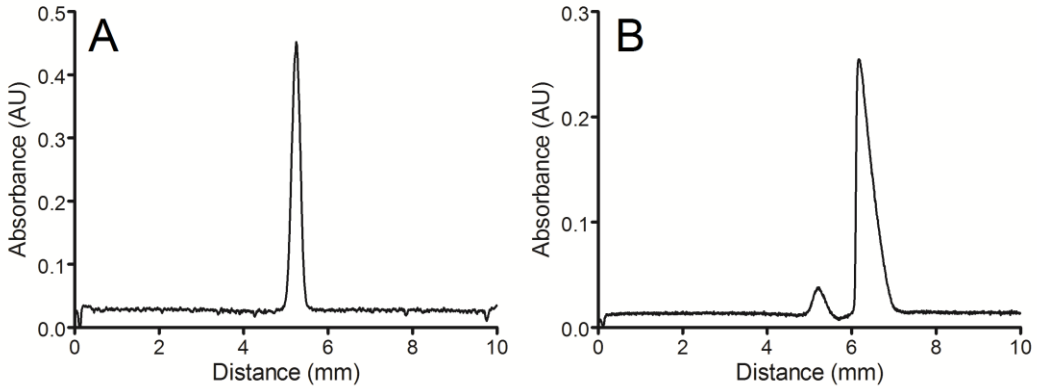

Figure 4.6 Recorded absorbance linescans of the five NBD-F amino acid separation at 0 V (A) and 200 V (B). Only two peaks are visible, with the right most peak showing signs of tailing indicating multiple amino acids are contained within that peak. Scans were taken at 1.5 cm from the capillary inlet.

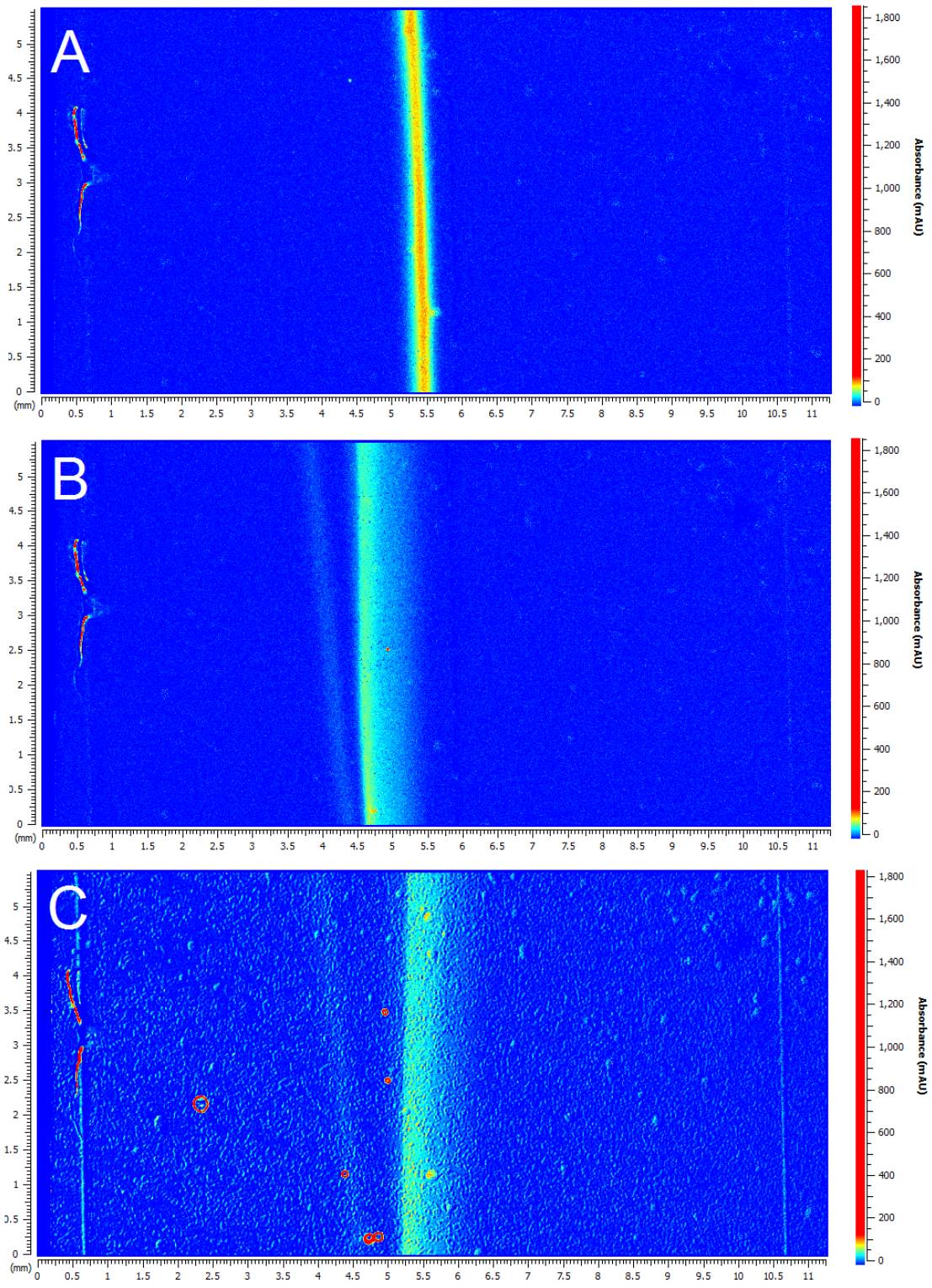

Figure 4.7 Images of the five NBD-F labeled amino acid µFFE separation at 0 V (A), 100 V (B), and 200 V (C). The left side of the image is negative electrode, while the right side is grounded.

While the separation is not ideal, we would still expect the LOD for the NBD-F labeled amino acids to be around 10^{-4}-10^{-5} M. These values are similar to the LODs for rhodamine 110, rhodamine 123, and fluorescein reported earlier. This is roughly 1000 times higher than reported LODs using µFFE-LIF for fluorescein, rhodamine 110, and rhodamine 123, which were 0.6 nM, 0.3 nM, and 3 nM respectively.[207] This was expected. LIF is a more sensitive technique than absorbance in LC and CE based applications.[220,221] However, absorbance detection has many advantages such as detection for analytes that are not natively fluorescent, or those that cannot be tagged. In 2D separations fluorescent labeling can affect the sample dimensionality greatly reducing fractional coverage. The type of fluorescent tag on samples of amino acids and BSA digest was previously shown to greatly affect separations with nLC × µFFE.[119] This limitation can be completely eliminated by using the absorbance detection provided by the ActiPix D200. While the substrate would need to be changed to quartz to perform UV absorbance detection, the preliminary results show that absorbance detection on µFFE is possible.

4.5 Conclusion

We present the first coupling of µFFE to an absorbance detector capable of imaging the whole channel at once. The ActiPix D200 2D absorbance detector provides a simple approach to using absorbance detection in µFFE based separations. A prototype of the device was successfully used to monitor separations of fluorescent dyes and NBD-F labeled amino acids. It required little to no preparation to use and the ease of setup to use with µFFE was a major strength of this technique. The detector offers light sources as LEDs in a wide range of wavelengths. Calibration plots were constructed, and detection limits for fluorescein, rhodamine 110 and rhodamine 123 were calculated

as 120 µM, 66 µM, and 64 µM respectively. The limits of detection are promising considering the path length for absorbance is only the depth of the separation channel, which in this case, is 20 µm. The design of the µFFE device can be easily modified to allow for a deeper separation channel which could greatly decrease these preliminary limits of detection. By imaging the entire separation channel, stream trajectory measurements could provide more information on µFFE separations that traditional point source detectors cannot. Currently, devices are fabricated in boron doped glass, which has a low UV light transmittance, but this could be easily changed to accommodate absorbance detection in the UV region. Fused silica and quartz would be good candidates for UV transparent fabrication media, however, the cost associated with these materials makes them unattractive. LIF detection limits the analytes to those that are natively fluorescent, or those that can be labeled. The ActiPix D200 absorbance detector, removes that limitation opening the door to other non-fluorescent analytes. In the future, different fabrication media will be explored to unlock the full potential of absorbance based µFFE detection, as well as explore its impact on 2D separations using µFFE.

Chapter 5

Summary and Outlook

5.1 Summary

Micro free flow electrophoresis is a powerful analytical separation technique with the unique ability to continuously inject and separate samples. Separations using µFFE occur in space instead of time, so discrete injections are not necessary. This capability has made it particularly suitable as the second dimensional separation for comprehensive on-line two dimensional separations. Our work focused on demonstrating the versatility of µFFE as a second dimension separation technique by showing it is capable of high speed, high peak capacity separations when coupled with capillary electrophoresis. CE × µFFE was shown to be a powerful separation platform capable of high speed, high peak capacity separations. The following chapters explored other factors that focused on taking steps toward achieving the maximum potential of CE × µFFE. Specifically we demonstrated versatility of µFFE by changing its separation mode to study its effect on CE × µFFE orthogonality. We also coupled µFFE with a two dimensional absorbance detector for label free detection of samples, opening the door to many analytes that were otherwise unable to be analyzed via µFFE.

In Chapter 2, CE was coupled to µFFE for the first time with an adapted zero dead volume coupling used in previous µFFE separations. A narrow channel large enough to fit a 150 µm o.d. capillary was fabricated in a glass µFFE device. The zero dead volume interface was tested with discrete injections of three fluorescent dyes (fluorescein, rhodamine 110, and rhodamine 123) and no significant broadening was observed. Next, the separation power of the platform was tested with separations of NBD-F labeled samples of 25 small molecule bioamines, and a tryptic BSA digest. 2D CE × µFFE generated an ideal peak capacity of 2,592 in a 9 min separation of fluorescently labeled peptides (7.6 min separation window, 342 peaks/min). An ideal peak capacity of 1885 in a 2.7 min separation of fluorescently labeled small molecule

bioamines (1.8 min separation window, 1053 peaks/min). Peaks in the 2D CE × μFFE separation of peptides covered 30% of the available separation space, resulting in a corrected peak capacity of 778 (102 peaks/min). The fractional coverage of the 2D CE × μFFE separation of small molecule bioamines was 20%, resulting in a corrected peak capacity of 377 (209 peaks/min). This was double the peak production rate reported in previous nLC × μFFE separations,[119,140] and nearly quadruple the peak production rate of the fastest comprehensive LC × LC separations.[32,33]

Chapter 3 explored the orthogonality of two electrophoretic based separation methods. In order to achieve the maximum potential of CE × μFFE as a separation platform, fractional coverage should be maximized. While various modes of μFFE have been shown in literature, a study of their effects in 2D separations has never been studied. An easy way to change the separation mechanism in electrophoretic based separation techniques is changing the mode to MEKC with buffer additives. CE × μFFMEKC was performed on bioamines and peptides with SDS, Triton X-100, and CTAB at concentrations near their CMC and concentrations almost ten times their respective CMCs. The CE separation buffer was held constant to gauge the effects of different surfactants in μFFMEKC alone. CE × μFFMEKC of 25 bioamines with 300 μM Triton X-100 gave the largest fractional coverage at 20.0%. Using 3 mM CTAB gave a fractional coverage of 13.0%. 15 mM SDS gave a fractional coverage of 1.6%. Increasing the CTAB concentration to 15 mM increased the fractional coverage to 17.7%, but increased current in the device causing stream disruptions. Increasing the Triton X-100 concentration to 3 mM caused a decrease in fractional coverage to 4.3%. CE × μFFMEKC with trypsin digested BSA yielded similar results with 300 μM Triton X-100 yielding the highest measured fractional coverage at 30.0%. 3 mM CTAB gave a measured fractional coverage of 7.4%, however, the BSA digest sample was different

from the Triton X-100 separation which can attribute to some of the differences. Overall for both samples 300 µM Triton X-100 gave the best fractional coverage, however 3 mM CTAB holds promise for utilizing the most separation space, if the separations could be optimized further.

The ability to detect biological analytes without any modifications to their structure remains extremely important to understanding the biological function of these analytes. Tagging with fluorophores can also reduce the sample dimensionality of the target species reducing the orthogonality of the separations and can result in a poor separation.[119] Chapter 4 demonstrated the first reported use of absorbance detection capable of imaging the entire width of the separation channel in the µFFE device. Separations of rhodamine 123, rhodamine 110 and fluorescein were performed and calibration plots were constructed for each. Detection limits for fluorescein, rhodamine 110 and rhodamine 123 were calculated as 119 µM, 66.0 µM, and 64.4 µM respectively. The reported limits of detection are promising considering the path length for absorbance is only the depth of the separation channel, which in this case, is 20 µm. The design of the µFFE device can be easily modified to allow for a deeper separation channel which could greatly decrease these preliminary limits of detection.

5.2 Future Applications

The work demonstrated in this thesis detailed µFFE as a second dimension separation platform capable of coupling with capillary electrophoresis for fast high peak capacity separations, as well as expanding the types of analytes available for separation via µFFE. There are still areas which need improvement to make this separation platform more powerful and universal. Peak capacity in µFFE is limited by hydrodynamic broadening of the peaks as they migrate further in the device. Reduction in this

broadening would increase peak capacity even further. Another challenge in µFFE is the cost of fabrication in glass wafers. Adoption of this technique by other disciplines is limited by the cost of the devices, as well as the specialized equipment and clean room environment required for fabrication. 3D printing could be a way to make µFFE accessible to a larger audience and encourage development of this microfluidic platform.

5.2.1 Addressing Hydrodynamic Broadening in µFFE

The three main contributions of peak broadening in µFFE are the sample injection width, diffusion, and hydrodynamic broadening (Equations 1.11 and 1.12).[97] Hydrodynamic broadening increases with the deflection distance of the analyte, and at its maximum can account for 65% of broadening in an analyte peak width. If this could be reduced or eliminated, higher peak capacity separations could be possible.

The induction of slip flow at the walls of the device would be one method to reduce the effects of hydrodynamic broadening. Slip flow has been observed extensively in nanofluidics through hydrophobic nanochannels such as carbon nanotubes,[222-225] nanoscale carbon sheets,[226,227] and nanopipes.[228,229] Slip flow occurs when weak intermolecular interactions between a fluid and the surrounding walls causes a non-zero velocity for the fluid at the wall. Zheng et. al. were the first to introduce using colloidal crystals as a packing material for ultra-efficient chromatography.[230] They found that the colloidal crystals induced slip flow and greatly increased the efficiency of their chromatographic separations. Slip flow in a column is achieved when the slip length of the fluid used is on the same order of magnitude as the minimum pore radii of the packing material.[231] If the separation channel in µFFE could be packed with colloidal crystals, a 2.5 fold increase in peak capacity could be realized.

As a first attempt of packing the separation channel with silica colloidal crystals, I fabricated an unbonded device and assembled with a 1 cm thick layer of PDMS used as a gasket between the two glass layers. Next, silica colloidal crystals were placed in the separation channel as adapted from a procedure developed by Wirth et. al.[230-232] First, silica particles of 500 nm in diameter (Discovery Scientific, Vancouver, BC, Canada) were heated at 600 ^{o}C for 6 hours in a box furnace. After cooling for 24 hours, the particles were boiled in 50% nitric acid for 2 hours to rehydroxylate them. A 30% (w/w) slurry was made by suspending the particles in HPLC grade methanol. The slurry was then transferred into the separation channel drop-wise via Pasteur pipet. After filling the channel with the slurry, it was left to dry overnight. Next, the newly deposited particles were reacted with a 50 mL mixture of 6% n-butyltrichlorosilane and 2% (v/v) methytrichlorosilane (Sigma Aldrich, St. Louis, MO) in dry toluene under dry nitrogen atmosphere. A small amount of this mixture (1 mL) was removed at a time and added to the particles so that it would wick through the channel covering all the particles. Waiting 10 minutes between depositions, this process was repeated over the course of 8 hours using all of the solution. It is important to note that both 6% n-butyltrichlorosilane and 2% methytrichlorosilane react violently with water so dry conditions are necessary for safety. This reaction achieved horizontal polymerization and served to hold the particles in place in the channel. Figure 5.1 shows Scanning electron microscopy (SEM) imaging of the particles after deposition was completed. The particles are distributed in a random fashion, and not at all in an orderly way (Figure 5.1A). So, the procedure was amended to include sonication after deposition of the particles to achieve the uniformity necessary for slip-flow. Imaging was performed again, and a much more ordered formation of silica particles was observed (Figure 5.1B). After the deposition was optimized the newly packed μFFE device was assembled and tested by pumping fluid through the device.

The device leaked however as a proper seal between the PDMS and glass was not achieved. It was just too cumbersome to work with a glass-PDMS-glass sandwich style device. Not enough pressure could be applied to the device to maintain the seal without shattering the glass devices. Another proposed packing method would be by packing the particles in an anodic bonded glass device. A frit that could be polymerized by a photochemical reaction *in situ* across the bottom of the µFFE separation channel would make the packing uniform in the device.[233-235]

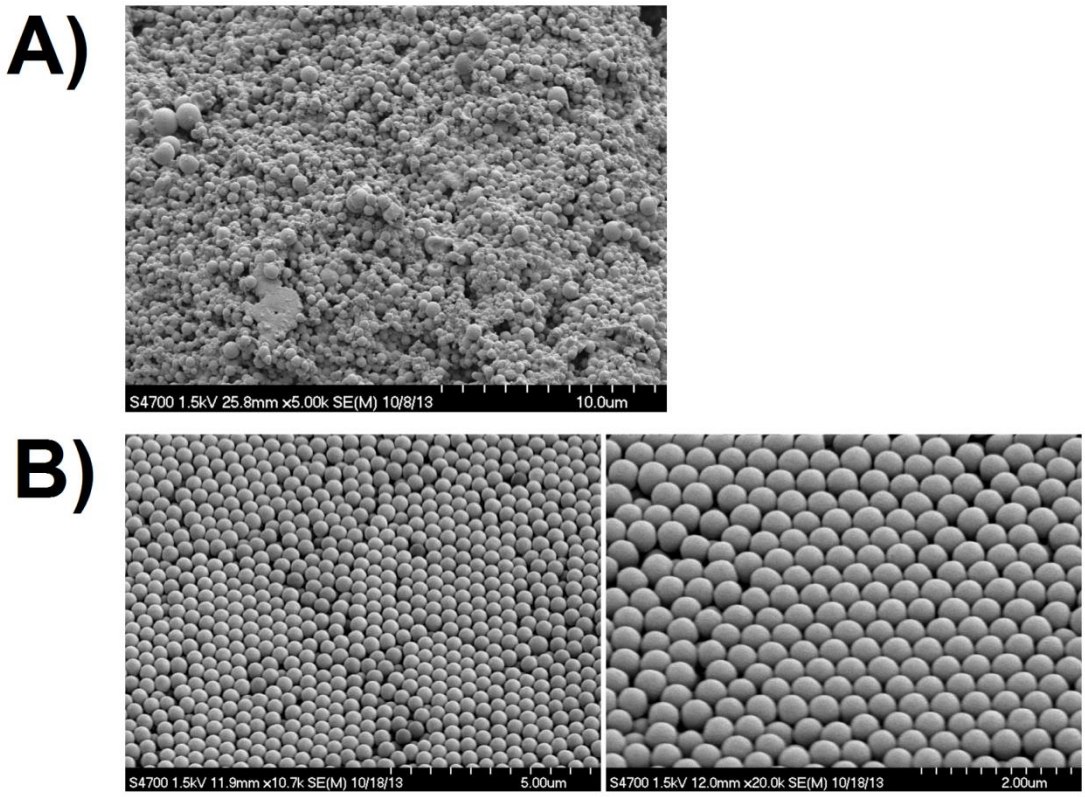

Figure 5.1 SEM images of the silica particles after deposition and crosslinking with tricholorosilane before (A) and after sonication (B). The sonicated particles showed a much more ordered structure, which is necessary for slip flow. The images were taken with a Hitachi S4700 SEM with a 1.5 kV accelerating voltage. Particles were coated with a thin film (5 nm) of Pt to assist in imaging.

If hydrodynamic broadening could be eliminated, a 2.5 fold increase of peak capacity in µFFE could be achieved. Taking the amino acid separation in Chapter 2 as

an example, the peak capacity of µFFE could be increased to 72 making the ideal 2D peak capacity 4,680 in 1.8 minutes (2600 peaks/min)! Another benefit to packing the µFFE separation channel would be functionalization of the colloidal crystals to perform chromatography and electrophoresis in the separation channel. We envision the possibility of performing three-dimensional separations where discrete samples would be injected and separated via CE on capillary, then chromatography as the sample plugs flow through the colloidal crystals while simultaneously deflected via µFFE.

5.2.2 µFFE Separation Modes and Universal Detection

Fabrication of µFFE in glass wafers is an arduous and time consuming process. Devices take a couple weeks to fabricate, and after fabrication is complete only one or two analytically viable devices are completed. Prototyping devices in glass is very expensive and time consuming, adding up to months and years of work to make new device designs. 3D printing however, can provide a faster and more cost effective way to produce prototype devices. Our group has used an Ultimaker 2 (Geldermalsen, Netherlands) extrusion printer to produce devices in as little as a day for less than 10 cents a device.[207] Figure 5.2 shows a fully functional 2D separation ready µFFE device printed in acrylonitrile butadiene styrene (ABS) plastic. With this technology, µFFE devices can be changed to suit their need.

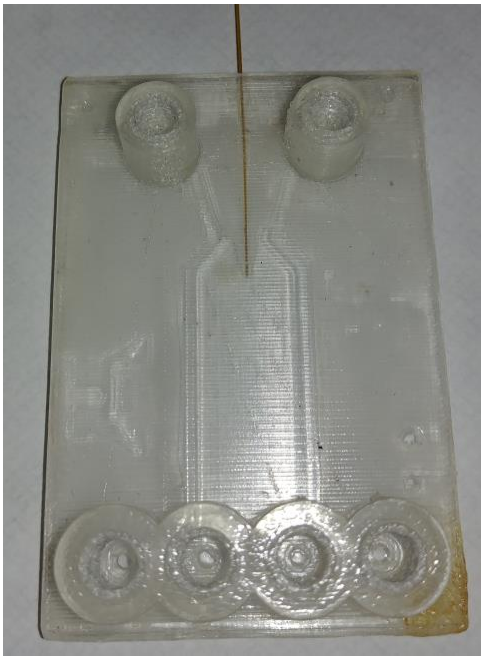

Figure 5.2 3D printed µFFE device in ABS plastic. The device is fabricated as a top and bottom piece. Both halves are then exposed to acetone vapor and pressed together to form a bond between the two pieces. Holes are drilled in the device and platinum wires inserted as the electrodes in the side channels. The capillary is sealed in place in the bonding step by placing it between the two layers. This particular device was printed and assembled in two days.

A multi-inlet device could be easily prototyped for µFFIEF, a new interface between LC and µFFE could be created, or a different design could incorporate mass spectrometry detection to universal analyte detection and identification.

In order to fully realize the potential of CE × µFFE, different separation modes must be combined such as IEF, CGE, MEKC, ITP, and affinity capillary electrophoresis. If ^{1}D could be operated as cIEF and ^{2}D operated as gel electrophoresis, it could function as a replacement for 2D PAGE in a fraction of the time required normally for these types of separations (a few days). One particular challenge would be with detection and identification. As shown in chapter 4, LIF is the most commonly used µFFE detection technique. While the novel absorption detection method fulfils the need to detect analytes that cannot be fluorescently labeled, spiking would still be the only reliable way to identify the peaks in 2D CE × µFFE analyses. Mass spectrometry coupling with µFFE

is still a great need to progress the technique further. Some progress has been made by ABS μFFE devices with an open channel at the bottom to deposit the separation on a membrane which is then taken for later analysis by MALDI-TOF/TOF mass spectrometry. However, much more work is needed to make this detection method viable.

μFFE is still a relatively young separation technique. There have been nearly 60 publications on μFFE devices since it was first reported by Raymond et. al. in 1994.[59] With the recent advances in fabrication methods, detection modes, and applications μFFE will become more widely used. The 2D CE × μFFE separation technique I developed brings unparalleled speed and high peak capacity potential to many different applications. The advances in 3D printing will make this device more accessible to researchers who do not have specialized clean rooms or access to large amounts of funding. The groundwork I have laid for label free detection on μFFE will help progress the technique to the next level of analytical separations. I hope my work will inspire the next generation of separation scientists to take advantage of the unique separation ability of μFFE.

References

(1) Human Genome Sequencing, C. *Nature* **2004**, *431*, 931-945.
(2) Görg, A.; Weiss, W.; Dunn, M. J. *PROTEOMICS* **2004**, *4*, 3665-3685.
(3) Fournier, M. L.; Gilmore, J. M.; Martin-Brown, S. A.; Washburn, M. P. *Chem Rev* **2007**, *107*, 3654-3686.
(4) Ghaemmaghami, S.; Huh, W.-K.; Bower, K.; Howson, R. W.; Belle, A.; Dephoure, N.; O'Shea, E. K.; Weissman, J. S. *Nature* **2003**, *425*, 737-741.
(5) Wolters, D. A.; Washburn, M. P.; Yates, J. R. *Anal. Chem.* **2001**, *73*, 5683-5690.
(6) Liu, H.; Sadygov, R. G.; Yates, J. R. *Anal. Chem.* **2004**, *76*, 4193-4201.
(7) Michalski, A.; Cox, J.; Mann, M. *Journal of Proteome Research* **2011**, *10*, 1785-1793.
(8) Lawson, T. N.; Weber, R. J. M.; Jones, M. R.; Chetwynd, A. J.; Rodríguez-Blanco, G.; Di Guida, R.; Viant, M. R.; Dunn, W. B. *Anal. Chem.* **2017**, *89*, 2432-2439.
(9) Zhang, Y.; Fonslow, B. R.; Shan, B.; Baek, M.-C.; Yates, J. R. *Chem Rev* **2013**, *113*, 2343-2394.
(10) Bouatra, S.; Aziat, F.; Mandal, R.; Guo, A. C.; Wilson, M. R.; Knox, C.; Bjorndahl, T. C.; Krishnamurthy, R.; Saleem, F.; Liu, P.; Dame, Z. T.; Poelzer, J.; Huynh, J.; Yallou, F. S.; Psychogios, N.; Dong, E.; Bogumil, R.; Roehring, C.; Wishart, D. S. *PLOS ONE* **2013**, *8*, e73076.
(11) Psychogios, N.; Hau, D. D.; Peng, J.; Guo, A. C.; Mandal, R.; Bouatra, S.; Sinelnikov, I.; Krishnamurthy, R.; Eisner, R.; Gautam, B.; Young, N.; Xia, J.; Knox, C.; Dong, E.; Huang, P.; Hollander, Z.; Pedersen, T. L.; Smith, S. R.; Bamforth, F.; Greiner, R.; McManus, B.; Newman, J. W.; Goodfriend, T.; Wishart, D. S. *PLOS ONE* **2011**, *6*, e16957.
(12) Horvath, C. G.; Lipsky, S. R. *Anal. Chem.* **1967**, *39*, 1893-1893.
(13) Giddings, J. C. *Anal. Chem.* **1967**, *39*, 1027-1028.
(14) Neue, U. D. *J. Chromatogr. A.* **2005**, *1079*, 153-161.
(15) Martin, M.; Herman, D. P.; Guiochon, G. *Anal. Chem.* **1986**, *58*, 2200-2207.
(16) Shen, Y.; Zhang, R.; Moore, R. J.; Kim, J.; Metz, T. O.; Hixson, K. K.; Zhao, R.; Livesay, E. A.; Udseth, H. R.; Smith, R. D. *Anal. Chem.* **2005**, *77*, 3090-3100.
(17) Han, J.; Ye, L.; Xu, L.; Zhou, Z.; Gao, F.; Xiao, Z.; Wang, Q.; Zhang, B. *Anal. Chim. Acta.* **2014**, *852*, 267-273.
(18) Busnel, J.-M.; Schoenmaker, B.; Ramautar, R.; Carrasco-Pancorbo, A.; Ratnayake, C.; Feitelson, J. S.; Chapman, J. D.; Deelder, A. M.; Mayboroda, O. A. *Anal. Chem.* **2010**, *82*, 9476-9483.
(19) Chen, D.; Shen, X.; Sun, L. *Analyst* **2017**.
(20) Karger, B. L.; Snyder, L. R.; Horvath, C. **1973**.
(21) Macgillivray, A. J.; Wood, D. R. *European Journal of Biochemistry* **1974**, *41*, 181-190.
(22) O'Farrell, P. H. *Journal of Biological Chemistry* **1975**, *250*, 4007-4021.
(23) López, J. L. *J. Chromatogr. B.* **2007**, *849*, 190-202.
(24) Rabilloud, T.; Chevallet, M.; Luche, S.; Lelong, C. *Journal of Proteomics* **2010**, *73*, 2064-2077.
(25) Deans, D. R. *J. Chromatogr. A.* **1981**, *203*, 19-28.
(26) Pursch, M.; Buckenmaier, S. *Anal. Chem.* **2015**, *87*, 5310-5317.
(27) Guiochon, G.; Gonnord, M. F.; Zakaria, M.; Beaver, L. A.; Siouffi, A. M. *Chromatographia* **1983**, *17*, 121-124.
(28) Giddings, J. C. *Anal. Chem.* **1984**, *56*, 1258A-1270A.

(29) Murphy, R. E.; Schure, M. R.; Foley, J. P. *Anal. Chem.* **1998**, *70*, 1585-1594.
(30) Davis, J. M.; Stoll, D. R.; Carr, P. W. *Anal. Chem.* **2008**, *80*, 461-473.
(31) Potts, L. W.; Stoll, D. R.; Li, X.; Carr, P. W. *J. Chromatogr. A.* **2010**, *1217*, 5700-5709.
(32) Stoll, D. R.; Cohen, J. D.; Carr, P. W. *J. Chromatogr. A.* **2006**, *1122*, 123-137.
(33) Stoll, D. R.; Carr, P. W. *J Am Chem Soc* **2005**, *127*, 5034-5035.
(34) Gu, H.; Huang, Y.; Carr, P. W. *J. Chromatogr. A.* **2011**, *1218*, 64-73.
(35) Ramsey, J. D.; Jacobson, S. C.; Culbertson, C. T.; Ramsey, J. M. *Anal. Chem.* **2003**, *75*, 3758-3764.
(36) Giddings, J. C. *J. Chromatogr. A.* **1995**, *703*, 3-15.
(37) Al Bakain, R.; Rivals, I.; Sassiat, P.; Thiébaut, D.; Hennion, M.-C.; Euvrard, G.; Vial, J. *J. Chromatogr. A.* **2011**, *1218*, 2963-2975.
(38) Dumarey, M.; Put, R.; Van Gyseghem, E.; Vander Heyden, Y. *Anal. Chim. Acta.* **2008**, *609*, 223-234.
(39) Liu, Z.; Patterson, D. G.; Lee, M. L. *Anal. Chem.* **1995**, *67*, 3840-3845.
(40) Dumarey, M.; Vander Heyden, Y.; Rutan, S. C. *Anal. Chem.* **2010**, *82*, 6056-6065.
(41) Schure, M. R. *J. Chromatogr. A.* **2011**, *1218*, 293-302.
(42) Gilar, M.; Olivova, P.; Daly, A. E.; Gebler, J. C. *Anal. Chem.* **2005**, *77*, 6426-6434.
(43) Davis, J. M.; Stoll, D. R.; Carr, P. W. *Anal. Chem.* **2008**, *80*, 8122-8134.
(44) Camenzuli, M.; Schoenmakers, P. J. *Anal. Chim. Acta.* **2014**, *838*, 93-101.
(45) Nowik, W.; Bonose, M.; Héron, S.; Nowik, M.; Tchapla, A. *Anal. Chem.* **2013**, *85*, 9459-9468.
(46) Nowik, W.; Héron, S.; Bonose, M.; Nowik, M.; Tchapla, A. *Anal. Chem.* **2013**, *85*, 9449-9458.
(47) Rutan, S. C.; Davis, J. M.; Carr, P. W. *J. Chromatogr. A.* **2012**, *1255*, 267-276.
(48) Burgman, M. A.; Fox, J. C. *Animal Conservation* **2003**, *6*, 19-28.
(49) Semard, G.; Peulon-Agasse, V.; Bruchet, A.; Bouillon, J.-P.; Cardinaël, P. *J. Chromatogr. A.* **2010**, *1217*, 5449-5454.
(50) Barrollier, J.; Watzke, E.; Gibian, H. *Z. Naturforsch. B* **1958**, *13*, 754-756.
(51) Hannig, K. *Fresen. Z. Anal. Chem.* **1961**, *181*, 244-254.
(52) Hannig, K. *J. Chromatogr.* **1978**, *159*, 183-191.
(53) Křivánková, L.; Boček, P. *Electrophoresis* **1998**, *19*, 1064-1074.
(54) Islinger, M.; Eckerskorn, C.; Völkl, A. *Electrophoresis* **2010**, *31*, 1754-1763.
(55) Roman, M. C.; Brown, P. R. *Anal. Chem.* **1994**, *66*, 86A-94A.
(56) Eckerskorn, C.; Wildgruber, R.; Nissum, M.; Weber, G. *Tec. Lab.* **2005**, *27*, 1020-1023.
(57) Wagner, H. *Nature* **1989**, *341*, 669-670.
(58) Arora, A.; Simone, G.; Salieb-Beugelaar, G. B.; Kim, J. T.; Manz, A. *Anal. Chem.* **2010**, *82*, 4830-4847.
(59) Raymond, D. E.; Manz, A.; Widmer, H. M. *Anal. Chem.* **1994**, *66*, 2858-2865.
(60) Koehler, S.; Weilbeer, C.; Howitz, S.; Becker, H.; Beushausen, V.; Belder, D. *Lab Chip* **2011**, *11*, 309-314.
(61) Song, Y.-A.; Chan, M.; Celio, C.; Tannenbaum, S. R.; Wishnok, J. S.; Han, J. *Anal. Chem.* **2010**, *82*, 2317-2325.
(62) Song, Y.-A.; Wu, L.; Tannenbaum, S. R.; Wishnok, J. S.; Han, J. *Anal. Chem.* **2013**, *85*, 11695-11699.
(63) Zhang, C.-X.; Manz, A. *Anal. Chem.* **2003**, *75*, 5759-5766.
(64) Fonslow, B. R.; Bowser, M. T. *Anal. Chem.* **2005**, *77*, 5706-5710.
(65) Becker, M.; Marggraf, U.; Janasek, D. *J. Chromatogr. A* **2009**, *1216*, 8265-8269.

(66) Jezierski, S.; Belder, D.; Nagl, S. *Chem. Commun.* **2013**, *49*, 904-906.
(67) Fonslow, B. R.; Barocas, V. H.; Bowser, M. T. *Anal. Chem.* **2006**, *78*, 5369-5374.
(68) Podszun, S.; Vulto, P.; Heinz, H.; Hakenberg, S.; Hermann, C.; Hankemeier, T.; Urban, G. A. *Lab Chip* **2012**, *12*, 451-457.
(69) Prest, J. E.; Baldock, S. J.; Fielden, P. R.; Goddard, N. J.; Goodacre, R.; O'Connor, R.; Treves Brown, B. J. *J. Chromatogr. B.* **2012**, *903*, 53-59.
(70) Akagi, T.; Kubota, R.; Kobayashi, M.; Ichiki, T. *Jpn. J. Appl. Phys.* **2015**, *54*, 1-5.
(71) Anciaux, S. K.; Geiger, M.; Bowser, M. T. *Anal. Chem.* **2016**, *88*, 7675-7682.
(72) Köhler, S.; Benz, C.; Becker, H.; Beckert, E.; Beushausen, V.; Belder, D. *RSC Adv.* **2012**, *2*, 520-525.
(73) Whitesides, G. M.; Ostuni, E.; Takayama, S.; Jiang, X.; Ingber, D. E. *Annu. Rev. Biomed. Eng.* **2001**, *3*, 335-373.
(74) Bansal, N. P.; Doremus, R. H. *Handbook of Glass Properties*; Elsevier: Cambridge, 1986.
(75) Fonslow, B. R.; Barocas, V. H.; Bowser, M. T. *Anal. Chem.* **2006**, *78*, 5369-5374.
(76) Becker, M.; Marggraf, U.; Janasek, D. *J. Chromatogr. A.* **2009**, *1216*, 8265-8269.
(77) Kohlheyer, D.; Eijkel, J. C.; Schlautmann, S.; van den Berg, A.; Schasfoort, R. B. *Anal. Chem.* **2008**, *80*, 4111-4118.
(78) Fonslow, B. R.; Bowser, M. T. *Anal. Chem.* **2005**, *77*, 5706-5710.
(79) Esashi, M.; Ura, N.; Matsumoto, Y. In *[1992] Proceedings IEEE Micro Electro Mechanical Systems*, 1992, pp 43-48.
(80) Jezierski, S.; Gitlin, L.; Nagl, S.; Belder, D. *Anal. Bioanal. Chem.* **2011**, *401*, 2651-2656.
(81) Ding, H.; Li, X.; Lv, X.; Xu, J.; Sun, X.; Zhang, Z.; Wang, H.; Deng, Y. *Analyst* **2012**, *137*, 4482-4489.
(82) Xia, Y.; Whitesides, G. M. *Annu. Rev. Mater. Sci.* **1998**, *28*, 153-184.
(83) Kane, R. S.; Takayama, S.; Ostuni, E.; Ingber, D. E.; Whitesides, G. M. *Biomaterials* **1999**, *20*, 2363-2376.
(84) Qin, D.; Xia, Y.; Whitesides, G. M. *Nat. Protocols* **2010**, *5*, 491-502.
(85) McDonald, J. C.; Whitesides, G. M. *Accounts Chem. Res.* **2002**, *35*, 491-499.
(86) Walowski, B.; Hüttner, W.; Wackerbarth, H. *Anal. Bioanal. Chem.* **2011**, *401*, 2465-2471.
(87) Köhler, S.; Benz, C.; Becker, H.; Beckert, E.; Beushausen, V.; Belder, D. *RSC Adv.* **2012**, *2*, 520-525.
(88) de Jesus, D. P.; Blanes, L.; do Lago, C. L. *Electrophoresis* **2006**, *27*, 4935-4942.
(89) Raymond, D. E.; Manz, A.; Widmer, H. M. *Anal. Chem.* **1996**, *68*, 2515-2522.
(90) Janasek, D.; Schilling, M.; Manz, A.; Franzke, J. *Lab Chip* **2006**, *6*, 710-713.
(91) Song, Y.-A.; Chan, M.; Celio, C.; Tannenbaum, S. R.; Wishnok, J. S.; Han, J. *Anal. Chem.* **2010**, *82*, 2317-2325.
(92) Lu, H.; Gaudet, S.; Schmidt, M. A.; Jensen, K. F. *Anal. Chem.* **2004**, *76*, 5705-5712.
(93) Fonslow, B. R.; Barocas, V. H.; Bowser, M. T. *Anal Chem* **2006**, *78*, 5369-5374.
(94) Reynolds, O. *Philos. Trans. R. Soc. Lond.* **1886**, *177*, 157-234.
(95) Frost, N. W.; Bowser, M. T. *Lab Chip* **2010**, *10*, 1231-1236.
(96) Kašička, V.; Prusík, Z.; Sázelová, P.; Jiráček, J.; Barth, T. *J. Chromatogr. A.* **1998**, *796*, 211-220.
(97) Fonslow, B. R.; Bowser, M. T. *Anal. Chem.* **2006**, *78*, 8236-8244.
(98) Kašička, V.; Prusik, Z.; Pospíšek, J. *J. Chromatogr. A.* **1992**, *608*, 13-22.
(99) Rhodes, P. H.; Snyder, R. S. *Electrophoresis* **1986**, *7*, 113-120.
(100) Giddings, J. C. *Unified Separation Science*; Wiley: New York, 1991.

(101) Hannig, K.; Wirth, H.; Meyer, B.-H.; Zeiller, K. *Hoppe-Seyler´ s Zeitschrift für physiologische Chemie* **1975**, *356*, 1209-1224.
(102) Dutta, D. *J. Chromatogr. A.* **2015**, *1404*, 124-130.
(103) Van Deemter, J.; Zuiderweg, F.; Klinkenberg, A. v. *Chem. Eng. Sci.* **1956**, *5*, 271-289.
(104) Moore, A. W.; Jorgenson, J. W. *Anal. Chem.* **1993**, *65*, 3550-3560.
(105) Kennedy, R. T. *Anal. Chim. Acta.* **1999**, *400*, 163-180.
(106) Geiger, M.; Harstad, R. K.; Bowser, M. T. *Anal. Chem.* **2015**, *87*, 11682-11690.
(107) Okhonin, V.; Evenhuis, C. J.; Krylov, S. N. *Anal. Chem.* **2010**, *82*, 1183-1185.
(108) Köhler, S.; Nagl, S.; Fritzsche, S.; Belder, D. *Lab Chip* **2012**, *12*, 458-463.
(109) Koehler, S.; Benz, C.; Becker, H.; Beckert, E.; Beushausen, V.; Belder, D. *RSC Adv.* **2012**, *2*, 520-525.
(110) Walowski, B.; Huttner, W.; Wackerbarth, H. *Anal. Bioanal. Chem.* **2011**, *401*, 2465-2471.
(111) Kostal, V.; Fonslow, B. R.; Arriaga, E. A.; Bowser, M. T. *Anal Chem* **2009**, *81*, 9267-9273.
(112) Turgeon, R. T.; Bowser, M. T. *Electrophoresis* **2009**, *30*, 1342-1348.
(113) Mogensen, K. B.; Kutter, J. P. *Electrophoresis* **2009**, *30*, S92-S100.
(114) Jezierski, S.; Klein, A. S.; Benz, C.; Schaefer, M.; Nagl, S.; Belder, D. *Anal. Bioanal. Chem.* **2013**, *405*, 5381-5386.
(115) Becker, M.; Budich, C.; Deckert, V.; Janasek, D. *Analyst* **2009**, *134*, 38-40.
(116) Benz, C.; Boomhoff, M.; Appun, J.; Schneider, C.; Belder, D. *Angew. Chem., Int. Ed.* **2015**, *54*, 2766-2770.
(117) Geiger, M.; Frost, N. W.; Bowser, M. T. *Anal. Chem.* **2014**, *86*, 5136-5142.
(118) Herzog, C.; Poehler, E.; Peretzki, A. J.; Borisov, S. M.; Aigner, D.; Mayr, T.; Nagl, S. *Lab Chip* **2016**, *16*, 1565-1572.
(119) Geiger, M.; Bowser, M. T. *Anal. Chem.* **2016**, *88*, 2177-2187.
(120) Shen, Q.-Y.; Guo, C.-G.; Yan, J.; Zhang, Q.; Xie, H.-Y.; Jahan, S.; Fan, L.-Y.; Xiao, H.; Cao, C.-X. *J. Chromatogr. A.* **2015**, *1397*, 73-80.
(121) Kobayashi, H.; Shimamura, K.; Akaida, T.; Sakano, K.; Tajima, N.; Funazaki, J.; Suzuki, H.; Shinohara, E. *J. Chromatogr. A.* **2003**, *990*, 169-178.
(122) Jing, M.; Bowser, M. T. *Lab Chip* **2011**, *11*, 3703-3709.
(123) Albrecht, J. W.; El-Ali, J.; Jensen, K. F. *Anal. Chem.* **2007**, *79*, 9364-9371.
(124) Kohlheyer, D.; Besselink, G. A.; Schlautmann, S.; Schasfoort, R. B. *Lab Chip* **2006**, *6*, 374-380.
(125) Kohlheyer, D.; Eijkel, J. C.; Schlautmann, S.; Van Den Berg, A.; Schasfoort, R. B. *Anal. Chem.* **2007**, *79*, 8190-8198.
(126) Song, Y.-A.; Hsu, S.; Stevens, A. L.; Han, J. *Anal. Chem.* **2006**, *78*, 3528-3536.
(127) Xu, Y.; Zhang, C.-X.; Janasek, D.; Manz, A. *Lab Chip* **2003**, *3*, 224-227.
(128) Walowski, B.; Huettner, W.; Wackerbarth, H. *Anal. Bioanal. Chem.* **2011**, *401*, 2465-2471.
(129) Janasek, D.; Schilling, M.; Franzke, J.; Manz, A. *Anal. Chem.* **2006**, *78*, 3815-3819.
(130) Kohlheyer, D.; Eijkel, J. C.; van den Berg, A.; Schasfoort, R. *Electrophoresis* **2008**, *29*, 977-993.
(131) Kostal, V.; Fonslow, B. R.; Arriaga, E. A.; Bowser, M. T. *Anal. Chem.* **2009**, *81*, 9267-9273.
(132) Turgeon, R. T.; Fonslow, B. R.; Jing, M.; Bowser, M. T. *Anal. Chem.* **2010**, *82*, 3636-3641.

(133) Johnson, A. C.; Bowser, M. T. *Anal. Chem.* **2017**, *89*, 1665-1673.
(134) Chartogne, A.; Tjaden, U. R.; Van der Greef, J. *Rapid Commun. Mass Spectrom.* **2000**, *14*, 1269-1274.
(135) Tang, Q.; Harrata, A. K.; Lee, C. S. *Anal. Chem.* **1995**, *67*, 3515-3519.
(136) Tang, Q.; Harrata, A. K.; Lee, C. S. *Anal. Chem.* **1997**, *69*, 3177-3182.
(137) Fonslow, B. R.; Bowser, M. T. *Anal. Chem.* **2008**, *80*, 3182-3189.
(138) Moritz, R. L.; Ji, H.; Schütz, F.; Connolly, L. M.; Kapp, E. A.; Speed, T. P.; Simpson, R. J. *Anal. Chem.* **2004**, *76*, 4811-4824.
(139) Xie, H.; Onsongo, G.; Popko, J.; de Jong, E. P.; Cao, J.; Carlis, J. V.; Griffin, R. J.; Rhodus, N. L.; Griffin, T. J. *Molecular & Cellular Proteomics* **2008**, *7*, 486-498.
(140) Geiger, M.; Frost, N. W.; Bowser, M. T. *Anal. Chem.* **2014**, *86*, 5136-5142.
(141) Kennedy, R. T.; German, I.; Thompson, J. E.; Witowski, S. R. *Chem Rev* **1999**, *99*, 3081-3132.
(142) Alexander, A. J.; Ma, L. *J. Chromatogr. A.* **2009**, *1216*, 1338-1345.
(143) Bushey, M. M.; Jorgenson, J. W. *Anal. Chem.* **1990**, *62*, 161-167.
(144) Filgueira, M. R.; Huang, Y.; Witt, K.; Castells, C.; Carr, P. W. *Anal. Chem.* **2011**, *83*, 9531-9539.
(145) Willmann, L.; Schlimpert, M.; Pan, D.; Bauer, C.; Trafkowski, J.; Krieger, S.; Rodamer, M.; Erbes, T.; Neubauer, H.; Kammerer, B. *J. Chromatogr. Sep. Tech.* **2015**, *6*, 1-5.
(146) de Koning, S.; Janssen, H.-G.; Udo, A. T. *J. Chromatogr. A.* **2004**, *1058*, 217-221.
(147) de Koning, S.; Janssen, H. G.; van Deursen, M.; Brinkman, U. A. T. *J Sep Sci* **2004**, *27*, 397-409.
(148) Bushey, M. M.; Jorgenson, J. W. *Anal. Chem.* **1990**, *62*, 978-984.
(149) Evans, C. R.; Jorgenson, J. W. *Anal. Bioanal. Chem.* **2004**, *378*, 1952-1961.
(150) Hooker, T. F.; Jorgenson, J. W. *Anal. Chem.* **1997**, *69*, 4134-4142.
(151) Lemmo, A. V.; Jorgenson, J. W. *Anal. Chem.* **1993**, *65*, 1576-1581.
(152) Almstetter, M. F.; Oefner, P. J.; Dettmer, K. *Anal. Bioanal. Chem.* **2012**, *402*, 1993-2013.
(153) Fitz, B. D.; Wilson, R. B.; Parsons, B. A.; Hoggard, J. C.; Synovec, R. E. *J. Chromatogr. A* **2012**, *1266*, 116-123.
(154) Klee, M. S.; Cochran, J.; Merrick, M.; Blumberg, L. M. *J. Chromatogr. A* **2015**, *1383*, 151-159.
(155) Mostafa, A.; Gorecki, T. *LC-GC Eur.* **2013**, *26*, 672, 674, 676-679.
(156) Seeley, J. V.; Seeley, S. K.; Libby, E. K.; McCurry, J. D. *Journal of chromatographic science* **2007**, *45*, 650-656.
(157) Liu, Z.; Phillips, J. B. *Journal of Chromatographic Science* **1991**, *29*, 227-231.
(158) Anouti, S.; Vandenabeele-Trambouze, O.; Koval, D.; Cottet, H. *Electrophoresis* **2009**, *30*, 2-10.
(159) Cong, Y.; Zhang, L.; Tao, D.; Liang, Y.; Zhang, W.; Zhang, Y. *J. Sep. Sci.* **2008**, *31*, 588-594.
(160) Dickerson, J. A.; Ramsay, L. M.; Dada, O. O.; Cermak, N.; Dovichi, N. J. *Electrophoresis* **2010**, *31*, 2650-2654.
(161) Flaherty, R. J.; Huge, B. J.; Bruce, S. M.; Dada, O. O.; Dovichi, N. J. *Analyst (Cambridge, U. K.)* **2013**, *138*, 3621-3625.
(162) Henley, W. H.; Ramsey, J. M. *Electrophoresis* **2012**, *33*, 2718-2724.
(163) Wang, T.; Ma, J.; Wu, S.; Sun, L.; Yuan, H.; Zhang, L.; Liang, Z.; Zhang, Y. *J. Chromatogr. B: Anal. Technol. Biomed. Life Sci.* **2011**, *879*, 804-810.

(164) Ranjbar, L.; Gaudry, A. J.; Breadmore, M. C.; Shellie, R. A. *Anal. Chem. (Washington, DC, U. S.)* **2015**, *87*, 8673-8678.
(165) Grochocki, W.; Markuszewski, M. J.; Quirino, J. P. *Electrophoresis* **2015**, *36*, 135-143.
(166) Moore, A. W.; Jorgenson, J. W. *Anal. Chem.* **1995**, *67*, 3448-3455.
(167) Michels, D. A.; Hu, S.; Schoenherr, R. M.; Eggertson, M. J.; Dovichi, N. J. *Molecular & Cellular Proteomics* **2002**, *1*, 69-74.
(168) Kraly, J. R.; Jones, M. R.; Gomez, D. G.; Dickerson, J. A.; Harwood, M. M.; Eggertson, M.; Paulson, T. G.; Sanchez, C. A.; Odze, R.; Feng, Z.; Reid, B. J.; Dovichi, N. J. *Anal. Chem.* **2006**, *78*, 5977-5986.
(169) Shadpour, H.; Soper, S. A. *Anal. Chem.* **2006**, *78*, 3519-3527.
(170) Jing, M.; Bowser, M. T. *Lab Chip* **2011**, *11*, 3703-3709.
(171) Köhler, S.; Weilbeer, C.; Howitz, S.; Becker, H.; Beushausen, V.; Belder, D. *Lab Chip* **2011**, *11*, 309-314.
(172) Kostal, V.; Fonslow, B. R.; Arriaga, E. A.; Bowser, M. T. *Anal. Chem.* **2009**, *81*, 9267-9273.
(173) Turgeon, R. T.; Fonslow, B. R.; Jing, M.; Bowser, M. T. *Anal. Chem.* **2010**, *82*, 3636-3641.
(174) Fonslow, B. R.; Bowser, M. T. *Anal. Chem.* **2008**, *80*, 3182-3189.
(175) Geiger, M.; Bowser, M. T. *Anal. Chem. (Washington, DC, U. S.)* **2016**, *88*, 2177-2187.
(176) Iki, N.; Yeung, E. S. *J. Chromatogr. A.* **1996**, *731*, 273-282.
(177) Filgueira, M. R.; Castells, C. B.; Carr, P. W. *Anal. Chem.* **2012**, *84*, 6747-6752.
(178) Gasteiger, E.; Hoogland, C.; Gattiker, A.; Dauvaud, S.; Wilkins, M. R.; Appel, R. D.; Bairoch, A. *The Proteomics Protocols Handbook*; Humana Press, 2005.
(179) Harstad, R. K.; Bowser, M. T. *Anal. Chem.* **2016**, *88*, 8115-8122.
(180) Cortes, H. J.; Winniford, B.; Luong, J.; Pursch, M. *J Sep Sci* **2009**, *32*, 883-904.
(181) François, I.; Sandra, K.; Sandra, P. *Anal. Chim. Acta.* **2009**, *641*, 14-31.
(182) Filgueira, M. R.; Huang, Y.; Witt, K.; Castells, C.; Carr, P. W. *Anal. Chem.* **2011**, *83*, 9531-9539.
(183) Jia, L.; Liu, B.-F.; Terabe, S.; Nishioka, T. *Anal. Chem.* **2004**, *76*, 1419-1428.
(184) Fang, X.; Yang, L.; Wang, W.; Song, T.; Lee, C. S.; DeVoe, D. L.; Balgley, B. M. *Anal. Chem.* **2007**, *79*, 5785-5792.
(185) Yu, W.; Li, Y.; Deng, C.; Zhang, X. *Electrophoresis* **2006**, *27*, 2100-2110.
(186) Mao, Y.; Zhang, X. *Electrophoresis* **2003**, *24*, 3289-3295.
(187) Jia, L.; Tanaka, N.; Terabe, S. *Electrophoresis* **2005**, *26*, 3468-3478.
(188) Kohl, F. J.; Sánchez-Hernández, L.; Neusüß, C. *Electrophoresis* **2015**, *36*, 144-158.
(189) Harstad, R. K.; Johnson, A. C.; Weisenberger, M. M.; Bowser, M. T. *Anal. Chem.* **2016**, *88*, 299-319.
(190) Sheng, L.; Pawliszyn, J. *Analyst* **2002**, *127*, 1159-1163.
(191) Yang, C.; Zhang, L.; Liu, H.; Zhang, W.; Zhang, Y. *J. Chromatogr. A.* **2003**, *1018*, 97-103.
(192) Yang, C.; Liu, H.; Yang, Q.; Zhang, L.; Zhang, W.; Zhang, Y. *Anal. Chem.* **2003**, *75*, 215-218.
(193) Wang, T.; Ma, J.; Wu, S.; Sun, L.; Yuan, H.; Zhang, L.; Liang, Z.; Zhang, Y. *J. Chromatogr. B.* **2011**, *879*, 804-810.
(194) Gottschlich, N.; Jacobson, S. C.; Culbertson, C. T.; Ramsey, J. M. *Anal. Chem.* **2001**, *73*, 2669-2674.

(195) Li, Y.; Wojcik, R.; Dovichi, N. J. *J. Chromatogr. A.* **2011**, *1218*, 2007-2011.
(196) Schoenherr, R. M.; Ye, M.; Vannatta, M.; Dovichi, N. J. *Anal. Chem.* **2007**, *79*, 2230-2238.
(197) Mou, S.; Sun, L.; Dovichi, N. J. *Anal. Chem.* **2013**, *85*, 10692-10696.
(198) Johnson, A. C.; Bowser, M. T. *Lab Chip* **2017**.
(199) Terabe, S.; Otsuka, K.; Ichikawa, K.; Tsuchiya, A.; Ando, T. *Anal. Chem.* **1984**, *56*, 111-113.
(200) Nishi, H.; Terabe, S. *Journal of Pharmaceutical and Biomedical Analysis* **1993**, *11*, 1277-1287.
(201) Maichel, B.; Kenndler, E. *Electrophoresis* **2000**, *21*, 3160-3173.
(202) Terabe, S. *Annual Review of Analytical Chemistry* **2009**, *2*, 99-120.
(203) Hancu, G.; Simon, B.; Rusu, A.; Mircia, E.; Gyéresi, Á. *Advanced Pharmaceutical Bulletin* **2013**, *3*, 1-8.
(204) Kile, D. E.; Chiou, C. T. *Environmental Science & Technology* **1989**, *23*, 832-838.
(205) Turgeon, R. T.; Bowser, M. T. *Anal. Bioanal. Chem.* **2009**, *394*, 187-198.
(206) Song, Y.-A.; Chan, M.; Celio, C.; Tannenbaum, S. R.; Wishnok, J. S.; Han, J. *Anal Chem* **2010**, *82*, 2317-2325.
(207) Anciaux, S. K.; Geiger, M.; Bowser, M. T. *Anal Chem* **2016**, *88*, 7675-7682.
(208) Shadpour, H.; Soper, S. A. *Anal. Chem.* **2006**, *78*, 3519-3527.
(209) Fonslow, B. R.; Bowser, M. T. *Anal. Chem.* **2006**, *78*, 8236-8244.
(210) Gan, J.; Xu, Y.; Cao, M.; Ni, Y.; Peng, J.; Ma, L.; Chuan, N. *Key Eng. Mater.* **2011**, *483*, 276-280.
(211) Herzog, C.; Beckert, E.; Nagl, S. *Anal. Chem. (Washington, DC, U. S.)* **2014**, *86*, 9533-9539.
(212) Han, B.; Wang, P.; Zhu, G.; Zhang, L.; Qu, F.; Deng, Y.; Zhang, Y. *J. Sep. Sci.* **2009**, *32*, 1211-1215.
(213) Jezierski, S.; Tehsmer, V.; Nagl, S.; Belder, D. *Chem. Commun.* **2013**, *49*, 11644-11646.
(214) Chartogne, A.; Tjaden, U. R.; Van der Greef, J. *Rapid Communications in Mass Spectrometry* **2000**, *14*, 1269-1274.
(215) Du, H.; Fuh, R.-C. A.; Li, J.; Corkan, L. A.; Lindsey, J. S. *Photochemistry and Photobiology* **1998**, *68*, 141-142.
(216) Dixon, J. M.; Taniguchi, M.; Lindsey, J. S. *Photochemistry and Photobiology* **2005**, *81*, 212-213.
(217) Landers, J. P. *Handbook of capillary electrophoresis*; CRC Press: Boca Raton, 1994, p 649 p.
(218) Allegrini, P. R.; Sigrist, H.; Schaller, J.; Zahler, P. *European Journal of Biochemistry* **1983**, *132*, 603-608.
(219) Ishida, A.; Fujisawa, H. *Journal of Biological Chemistry* **1995**, *270*, 2163-2170.
(220) Chan, K. C.; Veenstra, T. D.; Issaq, H. J. *Anal. Chem.* **2011**, *83*, 2394-2396.
(221) Pinto, D. M.; Arriaga, E. A.; Craig, D.; Angelova, J.; Sharma, N.; Ahmadzadeh, H.; Dovichi, N. J.; Boulet, C. A. *Anal. Chem.* **1997**, *69*, 3015-3021.
(222) Majumder, M.; Chopra, N.; Andrews, R.; Hinds, B. J. *Nature* **2005**, *438*, 44-44.
(223) Holt, J. K.; Park, H. G.; Wang, Y.; Stadermann, M.; Artyukhin, A. B.; Grigoropoulos, C. P.; Noy, A.; Bakajin, O. *Science* **2006**, *312*, 1034-1037.
(224) Thomas, J. A.; McGaughey, A. J. H. *Nano Letters* **2008**, *8*, 2788-2793.
(225) Qin, X.; Yuan, Q.; Zhao, Y.; Xie, S.; Liu, Z. *Nano Letters* **2011**, *11*, 2173-2177.
(226) Karan, S.; Samitsu, S.; Peng, X.; Kurashima, K.; Ichinose, I. *Science* **2012**, *335*, 444-447.

(227) Nair, R. R.; Wu, H. A.; Jayaram, P. N.; Grigorieva, I. V.; Geim, A. K. *Science* **2012**, *335*, 442-444.
(228) Sinha, S.; Rossi, M. P.; Mattia, D.; Gogotsi, Y.; Bau, H. H. *Physics of Fluids* **2007**, *19*, 013603.
(229) Whitby, M.; Cagnon, L.; Thanou, M.; Quirke, N. *Nano Letters* **2008**, *8*, 2632-2637.
(230) Zheng, S.; Ross, E.; Legg, M. A.; Wirth, M. J. *J Am Chem Soc* **2006**, *128*, 9016-9017.
(231) Wei, B.; Rogers, B. J.; Wirth, M. J. *J Am Chem Soc* **2012**, *134*, 10780-10782.
(232) Wei, B.; Malkin, D. S.; Wirth, M. J. *Anal. Chem.* **2010**, *82*, 10216-10221.
(233) Dulay, M. T.; Quirino, J. P.; Bennett, B. D.; Kato, M.; Zare, R. N. *Anal. Chem.* **2001**, *73*, 3921-3926.
(234) Malik, A. *Electrophoresis* **2002**, *23*, 3973-3992.
(235) Kato, M.; Sakai-Kato, K.; Jin; Kubota, K.; Miyano, H.; Toyo'oka, T.; Dulay, M. T.; Zare, R. N. *Anal. Chem.* **2004**, *76*, 1896-1902.